

UNIVERSITAT JAUME I

UNIVERSITAT JAUME I DOCTORAL SCHOOL

DOCTORAL PROGRAMME IN INDUSTRIAL TECHNOLOGIES AND  
MATERIALS



**UNIVERSITAT  
JAUME·I**

**IMPROVEMENT OF DIRECT ABSORPTION  
SOLAR COLLECTORS (DASCs)  
PERFORMANCE BY USING NANOFUIDS**

A dissertation presented by Jorge Burgos Rodríguez for the Degree of  
Doctor of Philosophy

Authored by:

Jorge Burgos Rodríguez

Supervised by:

Leonor Hernández López

Rosa Mondragón Cazorla

CASTELLÓ DE LA PLANA, OCTOBER 2023





UNIVERSITAT  
JAUME·I

DOCTORAL PROGRAMME IN INDUSTRIAL TECHNOLOGIES AND  
MATERIALS

UNIVERSITAT JAUME I DOCTORAL SCHOOL

**IMPROVEMENT OF DIRECT ABSORPTION  
SOLAR COLLECTORS (DASCs)  
PERFORMANCE BY USING NANOFUIDS**

A dissertation presented by Jorge Burgos Rodríguez for the Degree of  
Doctor of Philosophy

**Jorge Burgos Rodríguez**

Leonor Hernández López

Rosa Mondragón Cazorla

CASTELLÓ DE LA PLANA, OCTOBER 2023



# **Funding**

## **Pre-doctoral contract:**

- Funded by the *Generalitat Valenciana* through the Project PROMETEO/2020/029.

February 1<sup>st</sup>, 2021 – December 31<sup>st</sup>, 2023

## **Research stay:**

- University of Padova, Department of Industrial Systems Technology and Management, Vicenza, Italy.

September 5<sup>th</sup>, 2022 – December 16<sup>th</sup>, 2022

Funded by *Subvenciones para estancias de contratados predoctorales en centros de investigación fuera de la Comunitat Valenciana*. Grant Ref. CIBAFP/2021/10.



## **Compendium of publications**

- J. Burgos, R. Mondragón, E. Begum Elcioglu, F. Fabregat-Santiago and L. Hernández. Experimental characterization and statistical analysis of water-based gold nanofluids for solar applications: optical properties and photothermal conversion efficiency. *Solar RRL*. Vol. 6, no. 7, 2200104, pp.1-10. 2022.  
DOI: 10.1002/solr.202200104  
Impact factor: 7.9
- J. Burgos, R. Mondragón, R. Martínez-Cuenca, U. Nithiyantham, S. Barison, S. Mancin, F. Fabregat-Santiago and L. Hernández. Photothermal properties and performance of hybrid carbon-paraffin/water emulsions. *Journal of Energy Storage*. Vol. 73, no. 12, 109136, pp. 1-14. 2023.  
DOI: 10.1016/J.EST.2023.109136  
Impact factor: 9.4

*“This thesis has been accepted by the co-authors of the publications listed above that have waved the right to present them as a part of another PhD thesis.”*





*To my family  
and Laura*



## **Acknowledgments**

First, I would like to thank my supervisors Leonor and Rosa for giving me the opportunity to do my PhD and for helping me to achieve my goals as researcher. For their patience during these almost three years, teaching me how to manage in the lab, measuring and calculating, but mainly for their patience teaching me to write scientific papers (because it is not easy) and for the many corrections. It is not easy to start something new, and I appreciate all the support and help.

I would like to thank the entities that have participated in funding my research: the *Generalitat Valenciana* through the Project PROMETEO/2020/029 and the mobility grant for the research stay, *Subvenciones para estancias de contratados predoctorales en centros de investigación fuera de la Comunitat Valenciana*. Grant Ref. CIBAFP/2021/10.

Furthermore, thanks to Professor Simone Mancin from the University of Padova, and Simona Barison and Filippo Agresti from the National Research Council of Padova, for helping me and for receiving me in Italy. Also, to that group of Spanish speakers who made everything much easier for me at the Luzzatti.

In addition, I would like to thank the people of the Multiphase Fluids group for sharing meals, coffees, having good times and almost teach me Valencian unintentionally. Especially Salva, because without him, my short period as teacher would have been more difficult and for his help in the lab. I do not want to leave out Carlos, Josep, Luis, Sergio, Nithi, Marina and more, who also made all this time so far from home more enjoyable.

Por último, me gustaría agradecerlo enormemente a mi familia. Hablando de paciencia, son los que más la han tenido conmigo, gracias por no decirme nunca que no era capaz de hacer algo y animarme siempre a seguir adelante. También, de una manera muy muy especial a Laura, por siempre estar ahí, porque sé que no ha sido fácil y sin ti no hubiera sido posible. Gracias.



# Contents

Funding.....	I
Compendium of publications.....	III
Acknowledgments.....	VII
Contents.....	IX
Abstract .....	XIII
List of Figures .....	XVII
Nomenclature .....	XXIII
<b>1. Introduction .....</b>	<b>1</b>
<b>1.1. Solar collectors.....</b>	<b>2</b>
<b>1.2. Direct absorption solar collectors (DASCs) .....</b>	<b>4</b>
<b>1.3. Nanofluids .....</b>	<b>5</b>
<i>1.3.1. Solar applications.....</i>	<i>6</i>
<i>1.3.2. Thermal storage applications.....</i>	<i>10</i>
<i>1.3.3. Solar nanofluids and hybrid emulsions development.....</i>	<i>13</i>
<b>1.4. Objectives .....</b>	<b>19</b>
<b>2. Characterization techniques.....</b>	<b>25</b>
<b>2.1. Physical properties .....</b>	<b>25</b>
<i>2.1.1. Inductively Coupled Plasma Mass Spectroscopy .....</i>	<i>25</i>
<i>2.1.2. Transmission Electron Microscopy.....</i>	<i>27</i>
<i>2.1.3. Dynamic Light Scattering .....</i>	<i>28</i>
<b>2.2. Thermal properties.....</b>	<b>29</b>
<i>2.2.1. Transient Hot Wire .....</i>	<i>30</i>
<i>2.2.2. Differential scanning calorimetry .....</i>	<i>31</i>
<b>2.3. Optical properties.....</b>	<b>32</b>
<i>2.3.1. Spectrophotometry .....</i>	<i>33</i>

2.4.	<b>Photothermal conversion setups</b> .....	36
2.4.1.	<i>Simulated sunlight</i> .....	37
2.4.2.	<i>Natural sunlight</i> .....	39
3.	<b>Experimental characterization and statistical analysis of water-based gold nanofluids for solar applications: optical properties and photothermal conversion efficiency.</b> .....	45
3.1.	<b>Introduction</b> .....	46
3.2.	<b>Materials and Methods</b> .....	49
3.2.1.	<i>Nanofluids and experimental conditions</i> .....	49
3.2.2.	<i>Experimental Techniques</i> .....	51
3.3.	<b>Results and Discussion</b> .....	55
3.3.1.	<i>Nanoparticle size and colloidal stability</i> .....	55
3.3.2.	<i>Thermal conductivity</i> .....	58
3.3.3.	<i>Optical characterization</i> .....	58
3.3.4.	<i>Photothermal conversion efficiency</i> .....	61
3.3.5.	<i>PTE statistical analysis</i> .....	64
3.4.	<b>Conclusions</b> .....	66
4.	<b>Photothermal properties and performance of hybrid carbon-paraffin/water emulsions.</b> .....	71
4.1.	<b>Introduction</b> .....	72
4.2.	<b>Materials</b> .....	79
4.2.1.	<i>Raw materials</i> .....	79
4.2.2.	<i>Emulsions</i> .....	80
4.3.	<b>Experimental techniques</b> .....	80
4.4.	<b>Results and Discussion</b> .....	86
4.4.1.	<i>Stability</i> .....	86
4.4.2.	<i>Thermal characterization</i> .....	89

4.4.3. <i>Optical characterization</i> .....	93
4.4.4. <i>Photothermal conversion efficiency</i> .....	95
4.5. <b>Conclusions</b> .....	101
5. <b>General discussion and conclusions</b> .....	105
6. <b>Gaps and future research works</b> .....	111
7. <b>References</b> .....	115
8. <b>Annex</b> .....	135
8.1. <b>Uncertainty analysis</b> .....	135
8.2. <b>Scientific production</b> .....	137
8.2.1. <i>Experimental characterization and statistical analysis of water-based gold nanofluids for solar applications: optical properties and photothermal conversion efficiency.</i> .....	139
8.2.2. <i>Photothermal properties and performance of hybrid carbon-paraffin/water emulsions.</i> .....	143
8.2.3. <i>Contributions to international conferences</i> .....	147
8.3. <b>Co-authors letters</b> .....	159





## **Abstract**

This Thesis presents a set of experimental studies related to the application of solar nanofluids (NFs) and hybrid emulsions with phase change materials (PCMs) in direct absorption solar collectors (DASCs). The main objective is to develop novel materials capable of improving the absorption, storage and heat transfer properties of the conventional fluids used in direct absorption solar technologies.

Current technologies to produce energy from renewable energy sources allow climate change challenges to be faced to, thus, reduce greenhouse gas emissions from the production of fossil fuel-based energy. By paying attention to solar energy, the renewable energy transition helps to meet energy neutrality challenges, while also making these new technologies available worldwide.

Solar thermal energy is one of the most important renewable technologies used to deal with the transition of the energy system due to the unlimited and immense capacity of the energy provided by the Sun. Solar thermal collectors are capable of absorbing radiation from the Sun and converting it into heat for further uses. These systems use fluids, such as water, molten salts, thermal oils, etc., that are capable of transporting the heat transferred from an absorber surface. These fluids are known as heat transfer fluids (HTFs). However, conventional collector systems involve the drawback of heat losses during the absorption process in different stages, which is a disadvantage that can be solved by developing DASC systems. In this new solar collectors configuration, HTFs can be used to directly absorb solar radiation, and the resulting thermal energy can be transferred by HTFs, or even stored.

This Thesis focuses on developing new HTFs by incorporating nanoparticles (NPs), known as solar nanofluids and hybrid emulsions with PCMs. They present enhanced optical properties and higher thermal energy storage capacity than conventional fluids. To fulfill this purpose, in the present work water-based gold NFs (Au NFs) of different particle sizes (5 and 20 nm) and concentrations (5.1, 28.2 and 51.3 ppm), and hybrid carbon-paraffin/water emulsions with 5 wt. % of PCM (paraffin wax) and carbon black NPs at low concentrations (0.01 wt. %), were proposed and produced as enhanced HTFs for the DASC application.

The optical behavior of both HTFs was characterized by analyzing different optical parameters with the help of spectrophotometric techniques. For the Au solar NFs, the influence of particle size and concentration on the extinction coefficient was analyzed, and the surface plasmon resonance characteristic of metallic particles, such as Au, was observed. For hybrid emulsions, due to the opacity of samples, spectral reflectance and transmittance were measured and, thus, spectral absorptance was obtained. An improvement in the absorption capacity of both new HTFs was made thanks to the addition of Au and carbon black NPs, respectively.

Besides optical properties, thermal properties were measured to evaluate the effect of NPs and paraffin on storage and heat transfer capacity. The addition of NPs to the base fluid did not bring about a remarkable change in the final thermal conductivity or the specific heat capacity of both the new HTFs due to the low concentration of NPs. Notwithstanding, it was proven that the total thermal energy storage density of HTFs can be increased by using hybrid emulsions thanks to the contribution of the latent heat of the paraffin PCM.

Finally, new experimental facilities were developed using simulated and natural sunlight to study the photothermal conversion efficiency (*PTE*) of the new Au solar NFs and hybrid emulsions to evaluate their ability to convert solar radiation into thermal energy. For this purpose, facilities with and without sunlight concentration were developed, and differing scenarios were assumed to calculate *PTE*, including thermal losses and phase change. It was demonstrated that low concentrations of NPs in both HTFs, together with the latent heat contribution of paraffin in hybrid emulsions, increase *PTE* and enhance the performance of direct absorption solar technologies.

## **Resumen**

Esta tesis presenta una serie de estudios experimentales relacionados con la aplicación de nanofluidos (NFs) solares y emulsiones híbridas con materiales de cambio de fase (PCMs) en colectores solares de absorción directa (DASCs). El objetivo principal es el desarrollo de nuevos materiales capaces de mejorar las propiedades de absorción, almacenamiento y transferencia de calor con respecto a los fluidos convencionales utilizados en las tecnologías solares de absorción directa.

Las tecnologías actuales para producir energía a partir de fuentes de energía renovables permiten afrontar los retos del cambio climático para, de este modo, reducir las emisiones de gases de efecto invernadero procedentes de la producción de energía basada en combustibles fósiles. Atendiendo a la energía solar, la transición hacia las energías renovables contribuye a afrontar los retos de la neutralidad energética, al tiempo que permite disponer de estas nuevas tecnologías en todo el mundo.

La energía solar térmica es una de las tecnologías renovables más importantes utilizadas para abordar la transición del sistema energético debido a la ilimitada e inmensa capacidad de la energía que proporciona el Sol. Los colectores solares térmicos son capaces de absorber la radiación del Sol y convertirla en calor para usos posteriores. Estos sistemas utilizan fluidos, como agua, sales fundidas, aceites térmicos, etc., que son capaces de transportar el calor transferido desde una superficie absorbente. Estos fluidos se conocen como fluidos de transferencia de calor (HTFs). Sin embargo, los sistemas de colectores convencionales presentan el inconveniente de las pérdidas de calor durante el proceso de absorción en las diferentes etapas, lo cual es un inconveniente que puede solucionarse mediante el desarrollo de sistemas DASC. En esta nueva configuración de colectores solares, los HTFs pueden utilizarse para absorber directamente la radiación solar, y la energía térmica resultante puede transferirse mediante los HTFs, o incluso almacenarse.

Esta tesis se centra en el desarrollo de nuevos HTFs mediante la incorporación de nanopartículas (NPs), conocidos como nanofluidos solares y emulsiones híbridas con PCMs. Estos presentan propiedades ópticas mejoradas y una mayor capacidad de almacenamiento de energía térmica respecto a los fluidos convencionales. Para lograr este

propósito, en el presente trabajo se propusieron y produjeron NFs de oro en base acuosa con diferentes tamaños de partícula (5 y 20 nm) y concentraciones (5.1, 28.2 y 51.3 ppm), y emulsiones híbridas carbono-parafina/agua con un 5 % en peso de PCM (parafina) y NPs de carbon black (negro de humo) en pequeñas concentraciones (0.01 % en peso) para su aplicación en DASC.

Se caracterizó el comportamiento óptico de ambos HTFs, analizando diferentes parámetros ópticos con ayuda de técnicas de espectrofotometría. Para el caso de los NFs solares de oro, se analizó la influencia del tamaño de partícula y la concentración en el coeficiente de extinción, y se observó el plasmón de resonancia superficial característico de las partículas metálicas, como el oro. En el caso de las emulsiones híbridas, debido a la opacidad de las muestras, se midieron la reflectancia y la transmitancia espectral, con lo que se obtuvo la absorbancia espectral de las muestras. Se consiguió una mejora de la capacidad de absorción de los dos nuevos HTFs gracias a la adición de las NPs de oro y de carbon black, respectivamente.

Además de las propiedades ópticas, se midieron las propiedades térmicas para evaluar el efecto de las NPs y la parafina en la capacidad de almacenamiento y transferencia de calor. La adición de NPs al fluido base no produjo un cambio notable en la conductividad térmica final ni en la capacidad calorífica específica de los dos nuevos HTFs debido a la baja concentración de NPs. No obstante, se demostró que la densidad total de almacenamiento de energía térmica de los HTFs puede incrementarse mediante el uso de emulsiones híbridas gracias a la contribución del calor latente del PCM de parafina.

Por último, se desarrollaron nuevas instalaciones experimentales utilizando luz solar simulada y natural para estudiar la eficiencia de conversión fototérmica (*PTE*) de los nuevos NFs solares de oro y emulsiones híbridas para evaluar su capacidad de convertir la radiación solar en energía térmica. Para ello, se desarrollaron instalaciones con y sin concentración de luz solar, y se asumieron diferentes escenarios para el cálculo del *PTE*, incluyendo las pérdidas de calor y el cambio de fase. Se demostró que pequeñas concentraciones de NPs en ambos HTFs junto con la contribución de calor latente de la parafina en las emulsiones híbridas aumenta el *PTE* y mejora el rendimiento de las tecnologías solares de absorción directa.

# List of Figures

<b>Figure 1.1.</b> Global primary energy consumption by source <sup>[1]</sup> . .....	1
<b>Figure 1.2.</b> a) Conventional scheme of a non concentrating flat plate solar collector <sup>[10]</sup> and b) concentrating parabolic trough solar collector <sup>[11]</sup> .....	3
<b>Figure 1.3.</b> a) Scheme of surface and volumetric absorption in solar thermal collectors <sup>[13]</sup> and b) thermal resistance scheme comparison between surface (left) and volumetric (right) absorption configurations <sup>[14]</sup> .....	4
<b>Figure 1.4.</b> Classification of optical phenomena through a medium. ....	7
<b>Figure 1.5.</b> Sensible and latent heat storage processes. ....	12
<b>Figure 1.6.</b> PCM materials used according to their melting temperature and enthalpy <sup>[48]</sup> . .....	12
<b>Figure 1.7.</b> Two-step method for NFs synthesis.....	14
<b>Figure 2.1.</b> Inductively coupled plasma mass spectrometer instruments from Thermofisher Scientific. ....	27
<b>Figure 2.2.</b> Transmission electron microscope from JEOL.....	28
<b>Figure 2.3.</b> Zetasizer Nano ZS instrument from Malver Instruments Ltd.....	29
<b>Figure 2.4.</b> TEMPOS conductimeter from METER.....	31
<b>Figure 2.5.</b> Differential scanning calorimeter, DSC2, from Mettler Toledo.....	32
<b>Figure 2.6.</b> Spectrophotometer systems. a) Lambda 1050+ UV/Vis/NIR from PerkinElmer and b) V-780 from Jasco. ....	33
<b>Figure 2.7.</b> Different spectrophotometer configurations without integrating sphere a) <i>T</i> measurement and with integrating sphere b) <i>T+FS</i> , c) <i>FS</i> , d) <i>R+BS</i> and e) <i>BS</i> measurements. ....	35
<b>Figure 2.8.</b> a), c) solar simulator experimental setups and b), d) sample holders. ....	38
<b>Figure 2.9.</b> Natural solar spectrum (left axis) and simulated solar spectra (right axis). ....	38
<b>Figure 2.10.</b> Natural sunlight a) experimental setup and b) sample holder.....	39
<b>Figure 3.1.</b> Visual observation of the tested samples. ....	50
<b>Figure 3.2.</b> Experimental setup for the photothermal conversion efficiency tests. ....	53
<b>Figure 3.3.</b> Natural solar spectrum (left axis) and simulated solar spectrum (right axis). .....	54
<b>Figure 3.4.</b> Gold nanoparticles a) 5 nm and b) 20 nm. ....	56

<b>Figure 3.5.</b> Evolution of particle size distribution with temperature of the commercial NFs of 5 nm and 20 nm Au NPs.....	57
<b>Figure 3.6.</b> Extinction coefficient of the base fluid (water) and the water-based Au nanofluids. ....	59
<b>Figure 3.7.</b> Fraction of absorbed sunlight in relation to the penetration distance of the base fluid (water) and the water-based Au nanofluids. ....	60
<b>Figure 3.8.</b> Temperature evolution of the base fluid (water) and the water-based Au nanofluids in relation to irradiation time. ....	61
<b>Figure 3.9.</b> <i>PTE</i> enhancement of nanofluids in relation to water. ....	63
<b>Figure 3.10.</b> The statistical methodology of this study.....	64
<b>Figure 4.1.</b> TEM micrograph of the carbon black nanoparticles.....	79
<b>Figure 4.2.</b> Diagram of spectrophotometer configuration when measuring a) reflectance + backward scattered signal (R+BS) and b) transmittance + forward scattered signal (T+FS). ....	82
<b>Figure 4.3.</b> Solar simulator <i>PTE</i> a) experimental setup and b) custom-made sample holder. ....	84
<b>Figure 4.4.</b> Natural sunlight <i>PTE</i> a) experimental setup and b) quartz glass tube. ....	85
<b>Figure 4.5.</b> Particle size distribution of CBox-RT44HC/water emulsions with a) SDS and b) CTAB. ....	88
<b>Figure 4.6.</b> Images of RT44HC/water and CBox-RT44HC/water emulsions without and with SDS surfactant 3 days after fabrication. ....	89
<b>Figure 4.7.</b> DSC curves for bulk RT44H, RT44HC/water and CBox-RT44HC/water emulsions. ....	90
<b>Figure 4.8.</b> Experimental specific heat capacity ratio.....	91
<b>Figure 4.9.</b> Experimental thermal conductivity ratio.....	93
<b>Figure 4.10.</b> a) Absorptance and b) Reflectance of the base fluid (water), RT44HC/water and CBox-RT44HC/water emulsions. ....	94
<b>Figure 4.11.</b> Temperature increase evolution for the solar simulator experiments for a) water, b) RT44HC/water emulsion and c) CBox-RT44HC/water emulsion at different depths; d) for all samples at a constant depth of $z = 0.2$ cm. ....	96
<b>Figure 4.12.</b> Temperature increase evolution for the natural sunlight experiments at depth $z = 1.25$ cm for water, RT44HC/water and CBox-RT44HC/water emulsions.....	98
<b>Figure 4.13.</b> Photothermal conversion efficiency of samples for a) solar simulator at different depths and b) natural sunlight at depth $z = 1.25$ cm. ....	99

**Figure 4.14.** Relative photothermal efficiency of RT44HC/water and CBox-RT44HC/water emulsions with solar simulator and natural sunlight..... 100





# List of Tables

<b>Table 1.1.</b> Non concentrating and concentrating technologies for solar collectors. ....	2
<b>Table 1.2.</b> Summary of milestones achieved in this Thesis. ....	21
<b>Table 2.1.</b> Summary of the experimental techniques, measured properties and equipments used in this work. ....	41
<b>Table 3.1.</b> Review of the <i>PTE</i> results for water-based gold nanofluids. ....	48
<b>Table 3.2.</b> Tested samples: nomenclature and experimental conditions. ....	50
<b>Table 3.3.</b> Evolution of the mean particle size with temperature of the commercial NFs. ....	57
<b>Table 3.4.</b> Thermal conductivity enhancement at 25 °C and 60 °C. ....	58
Table 3.5. Values of $x_{50}$ for the different tested samples. ....	60
Table 3.6. Values of <i>PTE</i> for the different tested samples. ....	62
Table 3.7. Comparison of the means of the <i>PTE</i> values based on the NP size ( <i>D</i> ) groups. ....	65
<b>Table 3.8.</b> Comparison of the means of the <i>PTE</i> values based on the NP concentration [ <i>Au</i> ] groups. ....	65
<b>Table 3.9.</b> Correlation analysis between the independent ( <i>[Au]</i> , <i>D</i> ) and dependent ( <i>PTE</i> ) variables ( <i>p</i> : significance value, $\rho$ : correlation coefficient). ....	66
<b>Table 4.1.</b> Review of the characterization of carbon-PCM emulsions. ....	76
<b>Table 4.2.</b> Surfactants and comments about the VI and DLS tests for the different RT44HC/water-surfactant emulsions. ....	87
<b>Table 4.3.</b> Specific heat capacity data (theoretical and experimental) at 25 °C and 60 °C and melting phase change enthalpy. ....	91
<b>Table 4.4.</b> Thermal conductivity data (theoretical and experimental) at 25 °C and 60 °C. ....	92



# Nomenclature

$a(\lambda)$	[%]	Spectral absorptance
$\alpha$	[m <sup>2</sup> · s <sup>-1</sup> ]	Thermal diffusivity
$BS(\lambda)$	[%]	Spectral backward scattering
$\beta$	[kJ · s <sup>-1</sup> · K <sup>-1</sup> ]	Heat losses coefficient
$c_P$	[kJ · kg <sup>-1</sup> · K <sup>-1</sup> ]	Specific heat capacity
$D$	[nm]	Particle diameter
$D_{50}$	[nm]	Mean diameter
$D_t$	[m <sup>2</sup> · s <sup>-1</sup> ]	Translational diffusion coefficient
$\Delta H$	[kJ · kg <sup>-1</sup> ]	Phase change enthalpy
$\varepsilon$	[-]	Experimental error
$F$	[-]	Fraction of absorbed sunlight
$FS(\lambda)$	[%]	Spectral forward scattering
$I$	[W · m <sup>-2</sup> ]	Intensity
$k$	[W · m <sup>-1</sup> · K <sup>-1</sup> ]	Thermal conductivity
$k_B$	[J · K <sup>-1</sup> ]	Boltzmann constant
$\lambda$	[nm]	Wavelength
$m$	[kg]	Mass
$\mu_{abs}$	[cm <sup>-1</sup> ]	Absorption coefficient
$\mu_{ext}$	[cm <sup>-1</sup> ]	Extinction coefficient
$\mu_{sca}$	[cm <sup>-1</sup> ]	Scattering coefficient
$n$	[-]	Number of data
$\eta$	[Pa · s]	Absolute viscosity
$p$	[-]	Significance value
$Q$	[kJ]	Thermal energy
$R(\lambda)$	[%]	Spectral reflectance
$R_H$	[m]	Hydrodynamic radius
$\rho$	[-]	Correlation coefficient
$\sigma$	[-]	Standard deviation
$T$	[K]	Temperature
$T(\lambda)$	[%]	Spectral transmittance

$t$	[s]	Time
$\tau$	[-]	Correction factor
$W$	[W]	Power
$x$	[cm]	Penetration distance
$x_{50}$	[cm]	Distance at which 50 % incident radiation is absorbed
$z$	[cm]	Depth

### Subscripts

$0$	Incident
$a$	Absorbed
$amb$	Ambient
$c$	Crystallization
$em$	Emulsion
$i$	Initial
$latent$	Latent
$liq$	Liquid
$loss$	Losses
$m$	Melting
$max$	Maximum
$measured$	Measured
$min$	Minimum
$nf$	Nanofluid
$np$	Nanoparticles
$R$	Reflected
$S$	Scattered
$sample$	Sample
$sensible$	Sensible
$sol$	Solid
$solar$	Solar irradiance
$T$	Transmitted
$total$	Total
$w$	Water

## Abbreviations

BAC	Benzalkonium chloride
BS	Backward scattering
BZC	Benzethonium chloride
CBox	Oxidized carbon black
CNT	Carbon nanotubes
CTAB	Hexadecyltrimethylammonium bromide
CTPB	Methyltriphenylphosphonium bromide
DASC	Direct absorption solar collector
DI	Deionized
DLS	Dynamic light scattering
DS	Diphenyl sulphone
DSC	Differential scanning calorimetry
DTA	Differential thermal analysis
FS	Forward scattering
GNP	Graphene nanoplatelets
GO	Graphene oxide
HTF	Heat transfer fluid
ICP-MS	Inductively coupled plasma mass spectrometer
LHS	Latent heat storage
MWCNT	Multi-walled carbon nanotubes
NF	Nanofluid
NP	Nanoparticle
NS	Natural sunlight
PBS	Phosphate buffered saline
PCM	Phase change material
PEG	Polyethylene glycol
PTE	Photothermal conversion efficiency
PVA	Polyvinyl alcohol
PVP	Polyvinylpyrrolidone
R	Reflectance
SDBS	Sodium dodecylbenzene sulphonate

SDS	Sodium dodecyl sulphate
SHS	Sensible heat storage
SPR	Surface plasmon resonance
SS	Solar simulator
SWCNT	Single-walled carbon nanotubes
T	Transmittance
TcHS	Thermochemical heat storage
TEM	Transmission electron microscopy
TES	Thermal energy storage
TGA	Thermogravimetric analysis
THW	Transient hot wire
VI	Visual inspection

# **CHAPTER 1.**

## **Introduction**





# 1. Introduction

Since the Industrial Revolution, society's accelerated development has been associated with the exponential consumption of fossil fuels, such as coal, oil or natural gas since 1800 (Figure 1.1)<sup>[1]</sup>. This energy use has caused serious environmental damage, such as global warming, the pollution of natural systems and continued environmental degradation.

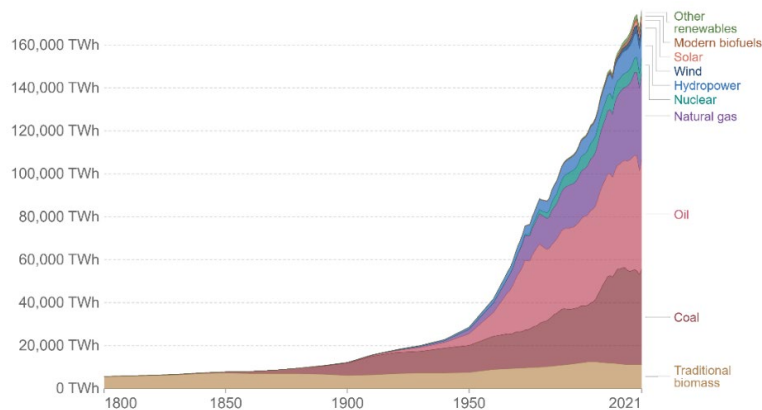


**Figure 1.1.** Global primary energy consumption by source<sup>[1]</sup>.

In 2015, the Paris Agreement was signed by 196 United Nation members during the 21<sup>st</sup> Conference of the Parties (COP21) on the Convention on Climate Change<sup>[2]</sup>. Almost all the world's economies committed themselves to adopt policies to reduce greenhouse gas emissions to curb global warming to below 2 °C, ideally to below 1.5 °C, compared to pre-industrial levels. More recently at COP26 in Glasgow<sup>[3]</sup>, the signatories to the previous treaties agreed to further strengthen their respective emission mitigation policies to enable them to become carbon-neutral in the future. In addition to this, in 2015 United Nations also adopted the Sustainable Development Goals (SDGs), “as a universal call to action to end poverty, protect the planet, and ensure that by 2030 all people enjoy peace and prosperity”<sup>[4]</sup>.

The possible replacement of conventional energy sources with renewable energy systems is one of the proposals to reduce contaminant emissions and to maintain the energy demand in a sustainable way.

In this context, the policies adopted to implement renewable energies have made Spain the second country in the European Union with the most renewable energy generation (116,583 GWh from photovoltaic, thermal solar, wind power and hydroelectric in 2022). It is worth noting that of all renewable energies, those from the Sun have generated more than 27 % of production. Both solar photovoltaic and solar thermal generation have grown, up to 239 % and 19 %, respectively, during the 2012-2022 period<sup>[5]</sup>.

### 1.1. Solar collectors

Solar thermal energy is a less extended technology in the Spanish electricity system, with an installed capacity of 3.5 GWh in 2022<sup>[6]</sup>. This technology is potentially exploitable thanks to the fact that the generation capacity of the Sun, as an energy source, exceeds any other source<sup>[7]</sup>.

Solar thermal collectors are an effective solution to the energy production problem because they transform solar radiation into thermal energy by heating a heat transfer fluid (HTF) that stores or transfers heat for later use. Depending on the application and the temperature that has to be reached by the HTF, solar collectors can be classified into low- (up to 120 °C), medium- (between 120 and 500 °C) and high- (above 500 °C) temperature. For each temperature range, it is necessary to use the most suitable HTF (i.e., water, glycols, molten salts, etc.) that allows its application, as well as the technology that enables these values to be obtained, divided into non concentrating and concentrating solar systems<sup>[8], [9]</sup>. Different solar thermal technologies are summarized in Table 1.1.

**Table 1.1.** Non concentrating and concentrating technologies for solar collectors.

Technology	System	Temperature working range [°C]
Non concentrating	Flat plate	30-80
	Compound parabolic	60-240
	Evacuated tube	50-230
Concentrating	Parabolic trough	50-400
	Linear Fresnel reflector	50-300
	Solar tower	300-2,000
	Parabolic dish	150-1,500

The operating principle of conventional solar collectors is based on the absorption of solar radiation by a dark surface that subsequently transfers heat to the HTF. Representative of conventional non concentrating collectors, flat plate collectors are the most widely used systems (Figure 1.2a) primarily for residential and commercial hot water applications. Radiation passes through a glass surface, which traps radiation and allows light to hit the dark absorber plate, which then transfers heat to the HTF that circulate inside the system. Systems with solar concentration use mirrors or reflectors to focus radiation on the collector (Figure 1.2b), which increases the temperature range reached with more applications during industrial processes.

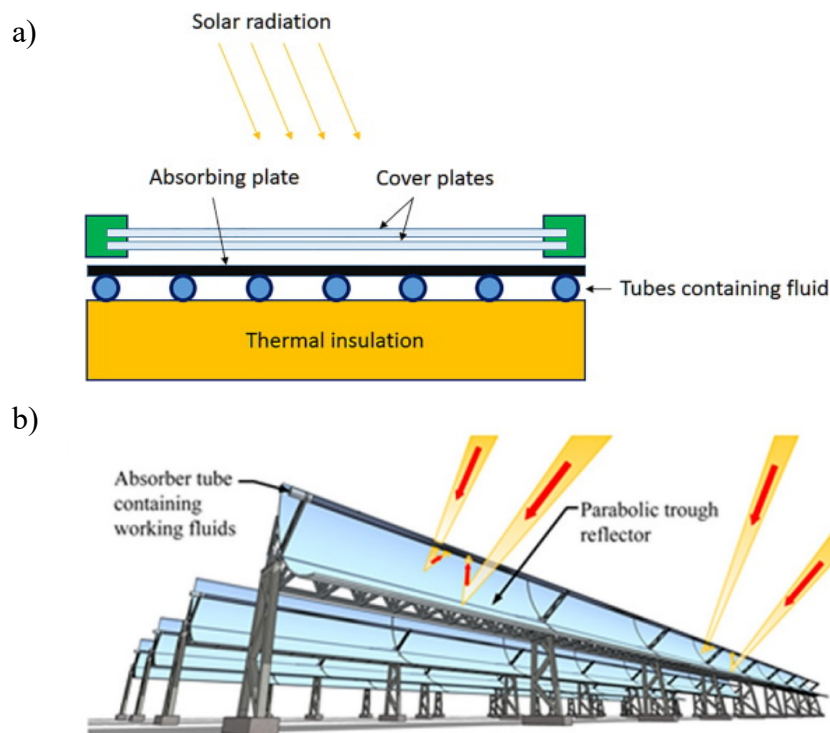


**Figure 1.2.** a) Conventional scheme of a non concentrating flat plate solar collector<sup>[10]</sup> and b) concentrating parabolic trough solar collector<sup>[11]</sup>.

However, both systems have the disadvantage of radiative and convective heat losses across the surface, which prevents these systems from reaching their full potential. To solve these drawbacks due to heat losses through the absorbing surface, a new technology has been proposed by developing systems that expose HTFs directly to solar radiation by switching to a volumetric absorption configuration. These systems are known as direct absorption solar collectors (DASCs).

## 1.2. Direct absorption solar collectors (DASCs)

DASC technology, in which the HTF directly absorbs radiation volumetrically through a transparent surface (Figure 1.3a), was developed in the 1970s. As shown in the thermal resistance scheme of Figure 1.3b, the volumetric absorption process in DASC reduces heat losses and, thus, the temperature drops by avoiding the stage in which heat is transferred by conduction/convection from the absorbance surface to the working fluid. The initial idea of the DASC systems developed by *Minardi and Chuang*<sup>[12]</sup> was to circulate a black liquid through transparent tubes that directly absorbed solar energy. In addition, the cost of installations was reduced because fewer components were required.

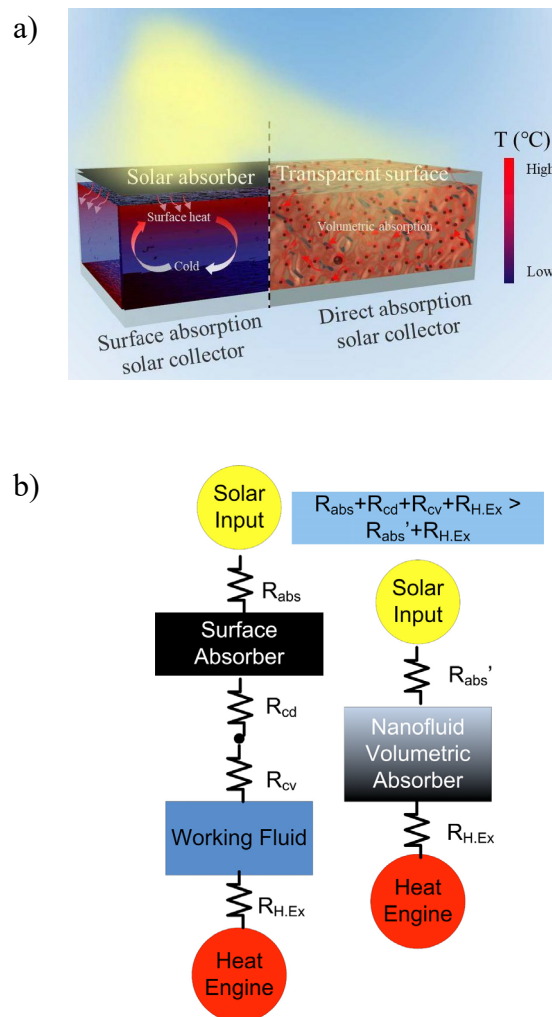


**Figure 1.3.** a) Scheme of surface and volumetric absorption in solar thermal collectors<sup>[13]</sup> and b) thermal resistance scheme comparison between surface (left) and volumetric (right) absorption configurations<sup>[14]</sup>.

Water is the most frequently used thermal fluid, but has a disadvantage: it can be employed only in solar collectors that work at low temperatures. Therefore, depending on the working temperature of collectors, other HTFs capable of operating at higher temperature ranges can be used. For example in linear Fresnel reflectors that work up to 300 °C, thermal oils can be utilized or molten salts are capable of working in power towers at higher temperatures<sup>[15],[16]</sup>. However, water and other conventional thermal fluids have very low solar radiation absorption capacities due to their transparent behavior to most of the solar spectrum. Fluids like molten salts or thermal oils also have lower specific heat capacity and thermal conductivity values compared to water, which result in low efficiencies in converting solar radiation into thermal energy. Efficiency in DASC systems can be quantitatively accomplished by photothermal conversion efficiency (*PTE*), which is defined as the ratio between the power of energy absorbed ( $W_a$ ) by the material and the power of incident radiation ( $W_0$ ) (Equation 1.1)<sup>[17],[18]</sup>. More details about the *PTE* calculation are included in Section 1.3.3.

$$PTE = \frac{W_a}{W_0} \quad (1.1)$$

During the last years, deep research was done to enhance thermal and optical properties of HTFs to be used in DASC systems. One of the most effective ways was introducing small particles in the HTFs, creating what is known as nanofluids, which has allowed to obtain improved DASC performances.

### 1.3. Nanofluids

It is known that solid particles, regardless of them being metallic, metal oxides, semiconductors or others, exhibit thermal conductivities higher than fluids. Therefore, the idea of enhancing heat transfer by adding solid particles to fluids has been extensively studied both theoretically and experimentally since Maxwell's publication in 1873<sup>[19]</sup>. However, all these initial works focused on using millimeter- or micrometer-sized particles, and showed certain disadvantages like sedimentation, erosion, clogging, etc., which has led to interest being shown in their application being lost. In 1995, *Choi and Eastman*<sup>[20]</sup> introduced the term nanofluid (NF), meaning a colloidal suspension of particles of sizes between 1-100 nm (nanoparticles, NPs) dispersed in a HTF. These

materials offered enhanced thermal properties, mainly thermal conductivity and convective heat transfer.

Long-term colloidal stability, referred to as the ability of particles to remain homogeneously suspended in a fluid for a certain time without sedimentation, is a key issue when thinking about practical NFs applications (see Section 1.3.3. for further discussion). Adding NPs to fluid has a major effect on its viscosity by increasing its resistance to deformation under shear or traction stresses.

As indicated in the previous section, conventional HTFs also exhibit poor optical performance to capture energy from solar radiation. Therefore, the ability to improve the light absorption of NFs has been investigated for more than a decade. In 2009, the research by *Otanicar et al.*<sup>[21]</sup> coined the term solar nanofluids for HTFs with improved optical properties due to the incorporation of low NP concentrations. These low concentrations for particle sizes within the nanometrical size range make it possible to assume an independent scattering regime under working conditions. Besides, problems related to colloidal stability and viscosity increase are avoided.

A wide variety of NPs of different natures has been investigated to improve thermal and solar absorption properties; for example, metallic particles (Ag, Au, Cu, Al, etc.), metal oxides (SiO<sub>2</sub>, Al<sub>2</sub>O<sub>3</sub>, TiO<sub>2</sub>, CuO, Fe<sub>2</sub>O<sub>3</sub>, etc.) and carbon-based materials (carbon nanotubes, graphene, graphene oxide, graphite, etc.)<sup>[22]–[28]</sup>.

The great versatility of NFs enables them to be employed in numerous applications to put their superior thermal and optical properties to good use. So, it is possible to incorporate them into solar thermal collectors.

### ***1.3.1. Solar applications***

In order to understand the behavior of solar NFs in direct absorption solar applications, one must comprehend their optical behavior. Multiple approaches have been used to study the absorption and scattering properties of light when a photon of light interacts with a colloidal solution that contains small nanometer-sized particles. Optical properties of solar NFs very much depend on factors like particle size and shape, volume fraction, material, base fluid, among others<sup>[29][30]</sup>. In spite of the influence of multiple parameters, according to *Brewster and Tiem*<sup>[31]</sup>, solar NFs working in an independent scattering regime require much simpler calculations of optical properties.

To design efficient solar collectors, it is necessary to know how light, defined as electromagnetic radiation within a range of wavelengths, behaves when it interacts with a fluid medium that contains solid NPs. As shown in Figure 1.4, when incident light ( $I_0$ ) passes through the optical medium, first part of it is reflected and returned to the original medium in the opposite direction ( $I_R$ ). Then part of incident light propagates through the optical medium in the same direction as incident light (transmitted intensity,  $I_T$ ). Finally, the light that propagates inside the optical medium and interacts with it can follow absorption ( $I_a$ ) and scattering ( $I_s$ ) phenomena all along the propagation distance. Scattered light can be scattered forwardly or backwardly. To evaluate materials' optical behavior, it is possible to measure and quantify these phenomena by certain techniques, such as spectrophotometry.

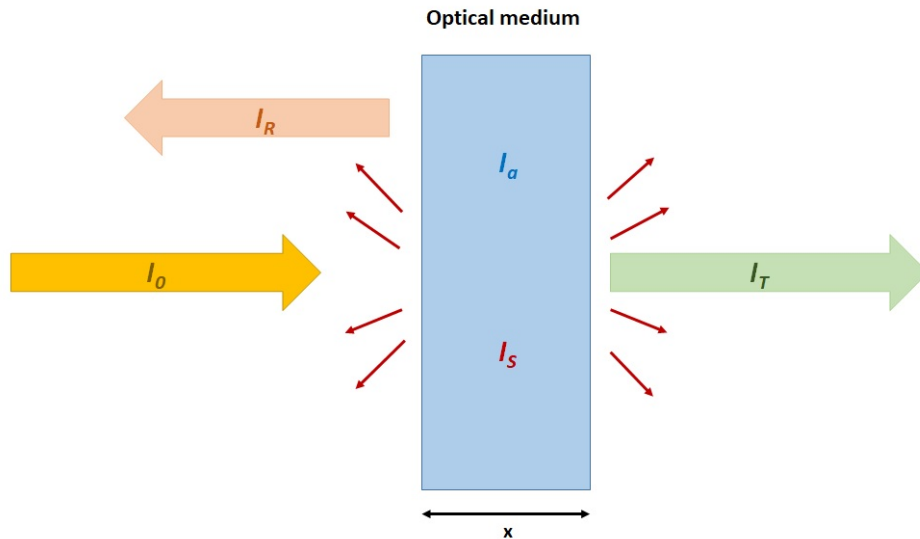


**Figure 1.4.** Classification of optical phenomena through a medium.

These properties are related to one another by means of Equation 1.2.

$$I_0 = I_T + I_R + I_a + I_s \quad (1.2)$$

where  $I_0$ ,  $I_T$ ,  $I_R$ ,  $I_a$  and  $I_s$  are the total incident light intensity and the transmitted, reflected, absorbed and scattered intensities, respectively. The above equation can be normalized to the incident signal to obtain:

$$\frac{I_0}{I_0} = \frac{I_T}{I_0} + \frac{I_R}{I_0} + \frac{I_a}{I_0} + \frac{I_S}{I_0} \quad (1.3)$$

Simplifying and correlating the optical parameters can obtain:

$$1 = T + R + a + S \quad (1.4)$$

where  $T$  is the direct transmittance defined as the ratio of the intensity of light passing through the sample and the total incident light,  $R$  is reflectance,  $a$  is absorptance and  $S$  is scattered light. This last phenomenon can be further dissociated into two terms depending on the angle at which light leaves after interacting with the sample: forward ( $FS$ ) or backward ( $BS$ ) scattering. The sum of the absorptance and the scattering produced by the medium can be defined as extinction.

The Beer-Lambert law establishes that the differential decrease in the transmitted intensity of light in a medium is, due to its extinction, proportional to the intensity and the penetration distance,  $x$ , traveled by light.

$$I_T(\lambda) = I_0(\lambda)e^{-\mu_{ext}(\lambda) \cdot x} \quad (1.5)$$

where  $\mu_{ext}$  is the extinction coefficient of the NF at the incident wavelength ( $\lambda$ ), which indicates that the intensity of transmitted light decreases exponentially with the increasing thickness of the optical medium.

The extinction coefficient can be defined as the sum of both the absorption and scattering coefficients (Equation 1.6). However, scattering phenomena in solar NFs can usually be considered negligible and, therefore, the value of the extinction coefficient equals the absorption coefficient ( $\mu_{abs}$ ).

$$\mu_{ext}(\lambda) = \mu_{abs}(\lambda) + \mu_{sca}(\lambda) \rightarrow \mu_{ext}(\lambda) \approx \mu_{abs}(\lambda) \quad (1.6)$$



By calculating these parameters, the optical analysis of solar NFs can be completed, which gives the fraction of absorbed incident light,  $F(x)$ . This key parameter can be used in direct absorption collectors' optimization to analyze a solar NF's ability to absorb a certain fraction of incident sunlight,  $I_{solar}(\lambda)$ , after a penetration distance,  $x$ , within a given wavelength range (normally associated with the solar spectrum).  $F(x)$  is calculated by Equation 1.7 [32]–[34]:

$$F(x) = 1 - \frac{\int_{\lambda_{min}}^{\lambda_{max}} I_{solar}(\lambda) \cdot e^{-\mu_{abs}(\lambda) \cdot x} d\lambda}{\int_{\lambda_{min}}^{\lambda_{max}} I_{solar}(\lambda) d\lambda} \quad (1.7)$$

where  $I_{solar}(\lambda)$  can be obtained from the American Society for Testing and Materials solar radiation [35].

Over time, many NPs have been synthesized and presented in solar NFs as potential materials to improve the efficiency of solar collectors by enhancing the absorption capacity of solar radiation. The optical properties and, therefore, the performance of solar collectors like DASCs depend on certain parameters (e.g., particle size and shape, volume fraction, material and base fluid), as previously mentioned [29][30].

In relation to the materials used throughout this work, special attention was paid to two classes of materials: metallic NPs, and carbon NPs and their allotropes. In the first group of selected materials, metallic materials are interesting because they exhibit surface plasmon resonance (SPR). This SPR is produced by the presence of free electrons on the conduction band of the surface of the metallic NPs that receive an incident beam of light, which induces a collective excitation of these free electrons. As a consequence, for certain frequencies of incident energy, coupling occurs between the frequencies of the incident wave and the oscillation of the so-called polariton of the surface plasmon. By this phenomenon, NPs like gold, silver or copper, are able to maximize light absorption at the specific wavelengths of 520, 400 and 740 nm, respectively. This SPR coupled to the solar radiation emission spectrum confers this phenomenon an advantage over conventional materials, such as semiconductors, organic molecules or pigments [36].

SPR originates when the NP size is smaller than the wavelength of incident radiation. Therefore, the resonance frequency and the width of the absorption band of the plasmon depend on the size and shape of the NPs. In addition, the intensity of absorption also depends on parameters, such as the aspect ratio, concentration, spatial distribution and

properties of the base fluid. *Chen et al.*<sup>[37]</sup> studied the effect of the size of Au NPs (25, 33 and 40 nm) dispersed in water on the absorbance of solar radiation at concentrations as low as ~0.08 ppm. They observed a red shift between 529 and 544 nm with increasing particle size. By also employing Au NPs, *Duan et al.*<sup>[38]</sup> demonstrated how different morphologies (nanospheres, nanorods and nanostars) presented maximum extinction coefficients at different wavelengths, produced by the different electron resonance modes along the distinct axes. This combination allows to expand the range of wavelengths within the visible spectrum to be extended, where the NF absorbs solar radiation. Other materials with SPR have also been studied as light absorbers with absorption peaks at different wavelengths such as Ag<sup>[39],[40]</sup>, Cu<sup>[17]</sup>, and even hybrid materials like Au/TiN<sup>[41]</sup>.

Regarding the second group, the optical absorption properties and solar radiation extinction capacity of carbon NPs have been extensively studied<sup>[42]</sup>, and promising results for their use in solar collectors have been obtained. By way of example, *Gimeno et al.*<sup>[43]</sup> obtained increases of 87 % and 3,200 % for the spectral transmittance and the absorption coefficient, respectively, in water-based NFs with low carbon black concentrations (33 ppm). *Karami et al.*<sup>[44]</sup> found that carbon nanotube (CNT) samples with a concentration of up to 150 ppm became completely opaque, which caused light transmittance to be almost zero within the UV range, and produced a linear increase in the extinction coefficient with the NP concentration by increasing light absorption by up to 2.5 times compared to the base fluid. *Ladjervardi et al.*<sup>[45]</sup> studied the effect of the diameter and concentration of graphite NPs on solar energy absorption. They showed a higher extinction coefficient when increasing the NP concentration with up to 50 % solar energy absorption for 0.5 ppm.

### ***1.3.2. Thermal storage applications***

Thermal energy storage (TES) systems are based on the ability of TES materials to store and release thermal energy thanks to their thermal properties. Three different mechanisms of TES can be found: sensible heat storage (SHS), latent heat storage (LHS) and thermochemical storage (TcHS). Of them, the most developed technology is that which uses sensible heat ( $Q_{sensible}$ ) to store thermal energy. Sensible heat is stored and released during the heating and cooling process of a TES material without undergoing a phase

change, as shown in Figure 1.5. The thermal energy stored during this process depends on the specific heat capacity ( $c_P$ ), the mass ( $m$ ) of the employed material, and also on the working temperature step ( $\Delta T$ ), as shown in Equation 1.8. Energy is absorbed during heating and is released during cooling processes. Regarding the use of NFs, dispersing NPs of solid materials with a lower  $c_P$  than the base fluids provides mixtures with lower specific heat capacity according to the mixture rule. This is the general trend observed for water- or oil-based NFs. However, in the particular case of using ionic liquids as the base fluid (i.e., molten salts), an abnormal increase in the specific heat capacity can occur<sup>[46]</sup>,  
[47].

$$Q_{sensible} = m \cdot c_P \cdot \Delta T \quad (1.8)$$

It is also possible to store higher thermal energy by storing latent heat ( $Q_{latent}$ ). Such heat is stored during the phase change process of a TES material and takes place at a constant temperature (Figure 1.5). Of all the possible phase changes, the solid-liquid phase change is preferable because its associated volume change is minor. For this purpose, phase change materials (PCMs) in TES systems are used because they have the ability to store and release energy during melting and crystallization processes, respectively, at a constant melting ( $T_m$ ) and crystallization ( $T_c$ ) temperature during phase changes. The thermal energy stored during this process depends on the melting enthalpy ( $\Delta H_m$ ), as seen in Equation 1.9. So the efficiency of the process depends on appropriate TES material selection.

$$Q_{latent} = m \cdot \Delta H_m \quad (1.9)$$

One possible phenomenon appears in the PCMs that undergo phase change: supercooling. This phenomenon is produced when the crystallization of the PCM takes place at a lower temperature than the melting process, as shown in Figure 1.5. This is an undesirable effect because charging and discharging processes occur at different temperatures and, thus, extend the range of operating temperatures and decrease the efficiency of TES systems.

Finally, PCMs can store thermal energy during heating and cooling processes by combining both sensible and latent mechanisms if a phase change takes place. The total

thermal energy storage density ( $Q_{total}$ ) is the contribution of the sensible heat stored in solid ( $c_{P,sol}$ ) and liquid ( $c_{P,liq}$ ) phases and the latent heat, as described Equation 1.10.

$$Q_{total} = m \cdot c_{P,sol} \cdot \Delta T_{sol} + m \cdot \Delta H_m + m \cdot c_{P,liq} \cdot \Delta T_{liq} \quad (1.10)$$

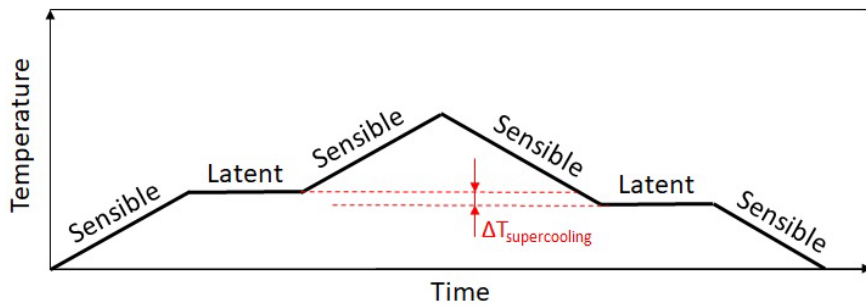


Figure 1.5. Sensible and latent heat storage processes.

A wide range of materials is available to develop efficient TES systems and, depending on their nature, PCMs can be classified into three categories: organic, inorganic and mixtures. As shown in Figure 1.6, depending on their melting temperature and enthalpy, it is possible to select different materials with organic materials, such as paraffins, which are the most widely used for low-temperature applications.

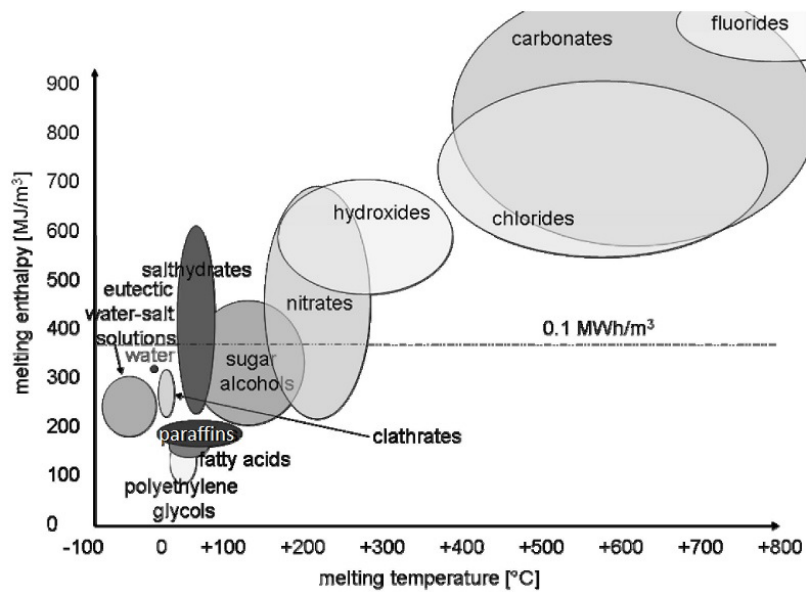


Figure 1.6. PCM materials used according to their melting temperature and enthalpy<sup>[48]</sup>.

Paraffin waxes, also known as paraffins, are a mixture of hydrocarbons, in particular linear n-alkane with chemical formula  $C_nH_{2n+2}$  and carbon number  $12 < n < 40$ . Some of the main characteristics offered by these materials are their high melting enthalpies (between  $100\text{-}200 \text{ kJ}\cdot\text{kg}^{-1}$ ) and specific heat capacities of  $2\text{-}2.9 \text{ J}\cdot\text{g}^{-1}\cdot\text{K}^{-1}$  within a wide temperature range from below  $0 \text{ }^\circ\text{C}$  to above  $100 \text{ }^\circ\text{C}$ . These two parameters increase with the carbon chain increment. They also withstand repeated thermal cycling, exhibit very low supercooling, and do not have wide variations in density between liquid and solid states, which means that volume changes do not exceed 10 % during phase transitions. Besides, they are odorless, tasteless and non-toxic materials which makes them good candidates to be used as PCMs for TES systems. However, they have low thermal conductivities,  $0.2\text{-}0.7 \text{ W}\cdot\text{m}^{-1}\cdot\text{K}^{-1}$  and, as non-polar liquids, paraffins do not mix with polar liquids like water.

Solar collector performance can be improved by combining the excellent radiation absorption properties of solar NFs with the thermal storage capacity of PCMs thanks to the use of those known as hybrid emulsions of PCMs. These emulsions are colloidal suspensions composed of a continuous phase, the HTF, NPs able to improve solar radiation absorption and the PCM capable of storing latent heat. These new fluids offer many advantages because they can be used for a triple function: solar absorption material, HTF and thermal storage media. However, PCM emulsions have certain challenges that need to be overcome, such as colloidal stability and the supercooling effect.

The supercooling effect is more pronounced in emulsions than in bulk PCMs, probably due to the purity and small size of the nuclei where crystal growth begins, which favors homogeneous crystallization. This type of crystallization requires more energy than heterogeneous crystallization, in which interfaces and heterogeneities act as nucleation points and, therefore, homogeneous crystallization occurs at a lower temperature than the melting temperature<sup>[49], [50]</sup>.

### ***1.3.3. Solar nanofluids and hybrid emulsions development***

The behavior of NFs and emulsions in practical applications very much depends on the preparation method due to the strong influence of the size and shape of particles on final properties, regardless of them being thermal, optical or physical. In addition, and as

previously mentioned, NFs and emulsions should show good stability over long periods of time and after multiple thermal cycles.

Several techniques have been applied over the years for the production and stabilization of these colloidal suspensions, and they have provided different results depending on the degree of particle agglomeration. Two types of production methods can be used:

- The single-step method. It combines the preparation of NPs with the synthesis of NFs and emulsions by producing NPs directly in the base fluid. In this method, it is possible to include physical vapor deposition techniques, the chemical method or the laser ablation of a material immersed in the base fluid. With these techniques, it is feasible to achieve a high degree of dispersion of the NPs in the fluids, which make them very stable. However, these methods normally use certain reagents that generate impurities and can be difficult to remove.
- The two-step method. In this method the NPs are first produced by a given technique, such as chemical vapor deposition, spray pyrolysis or others and are then dispersed in a base fluid during a subsequent manufacturing process, as seen in Figure 1.7. Therefore, the dispersion conditions determine both the size of the nanoparticles present in the NF and their stability. For the dispersion process in the second step, equipment like ultrasonic bath, ultrasonic probe, high-shear mixer, magnetic stirrer or ball mills can be employed. Both treatment time and the applied energy influence the final dispersion state. The ultrasonic probe technique, used in the present work, is the most effective dispersion system thanks to its higher energy density, which breaks agglomerates more easily than other mechanisms, and also requires shorter times to obtain well-dispersed suspensions.

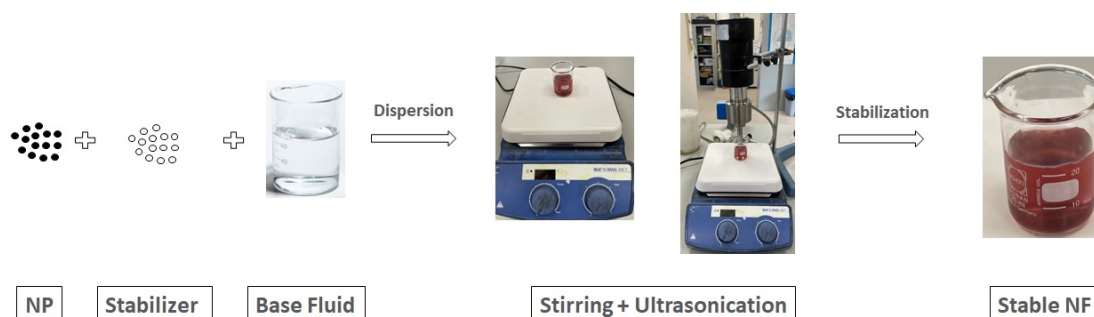


**Figure 1.7.** Two-step method for NFs synthesis.

After production by dispersing NPs in the base fluid, they tend to agglomerate again due to the presence of interparticle forces. With NFs, as the surface-to-volume ratio of particles is very high, all interactions are controlled by short-range forces, such as Van der Waals attraction forces and surface forces. When NPs interact due to Brownian motion, they agglomerate because of Van der Waals attractive forces, unless a higher repulsive force prevents this. According to the classic DVLO (Derjaguin-Landau-Verwey-Overbeek) theory, only electrostatic repulsion forces are taken into account, but steric and electrosteric repulsion forces must also be considered.

Electrostatic repulsion between particles is due to the presence of surface charges that appear when inorganic particles are suspended in water and the acquired surface charge depends on the pH of the medium. For each system and chemical substance, there is a pH value at which the surface charge on the shear plane surrounding the particle is zero. It is known as the isoelectric point. When NFs have different pH values from this isoelectric point, they result in charged particles and stable suspensions. This keeps some particles separated from others due to electrostatic repulsion, and this prevents the formation of agglomerates. So by modifying pH, it is possible to achieve good stabilization.

In non-aqueous media or dispersions of non-polar solids in aqueous media, steric repulsion is necessary. With this mechanism, repulsion is achieved by polymeric chains or surfactant adsorption on the particle surface that extends into the surrounding medium. As particles approach one another, polymeric layers begin to compress and, thus, generate steric repulsion that prevents particle agglomeration. Therefore, NPs stabilization is achieved by adding non-ionic surfactants. However, the preferred and most effective stabilization mechanism is electrosteric repulsion, in which electrostatic and steric repulsions are combined with the help of adding charged polymeric chains. Stabilization is achieved by adding ionic surfactants (cationic or anionic), which generate a charged medium surrounding the polymer chains adsorbed on the surface of particles. Widely used surfactants are sodium dodecyl sulphate (SDS), sodium dodecylbenzene sulphonate (SDBS), hexadecyltrimethylammonium bromide (CTAB), benzethonium chloride (BZC), benzalkonium chloride (BAC), polyethylene glycols (Triton TM X-100), among others<sup>[51]</sup>.

NFs and emulsions are stable if particles and droplets do not increase in size (due to agglomerations) and there is no phase separation. In thermal applications, in which they may need to be pumped, NPs interact strongly and PCM droplets undergo several solid-

liquid phase changes. Therefore, stability must be tested over time under static and dynamic conditions, after several heating-cooling cycles, under mechanical shear stresses, etc.<sup>[52], [53]</sup>.

Colloidal stability is normally studied by measuring particle size by the dynamic light scattering (DLS) technique. A particle size analysis allows to study the agglomerates formation and its evolution over time, and the suspension is considered stable when particle size distribution remains unchanged with time and temperature. This analysis can be complemented to study the evolution of thermophysical properties. In this regard, NFs and emulsions can be assumed stable if their optical or thermal properties are stable under similar working conditions to those found in real industrial applications.

Finally, one of the most important parameters to be considered for implementing solar NFs and emulsions in DASC installations is photothermal conversion efficiency (*PTE*), defined previously in Equation 1.1. To evaluate *PTE*, three scenarios were considered in this doctoral Thesis: 1) without PCM (no phase change) and not considering heat losses; 2) without PCM but including heat losses; 3) including PCM phase change but not considering heat losses.

In the first scenario, where there are no heat losses and no phase change occurs during the heating process, from Equation 1.1 and 1.8 *PTE* can be calculated as:

$$PTE = \frac{Q_{sensible, sample}}{W_{measured} \cdot \Delta t} = \frac{m_{sample} \cdot c_{p, sample}}{W_{measured}} \cdot \frac{\Delta T}{\Delta t} \quad (1.11)$$

where  $W_{measured}$  is the measured light power in the sample position with the potentiometer and  $\Delta T$  is the temperature rise within a time interval  $\Delta t$ .

When taking into account heat losses, but still with no phase change happening in the sample (second scenario), a balance between the power energy stored by the sample,  $W_{sample}$ , and the power associated with heat losses,  $W_{loss}$ , is applied, as defined in Equation 1.12.

$$W_{sample} = W_a - W_{loss} \quad (1.12)$$



$$m_{sample} \cdot c_{P,sample} \cdot \frac{dT}{dt} = W_a - \beta(T - T_{amb}) \quad (1.13)$$

where  $T$  is the sample temperature,  $T_{amb}$  is the ambient temperature and  $\beta$  is the heat losses coefficient. By operating and applying the experiment's boundary conditions, the equation of the heating process can be obtained (Equation 1.14):

$$T = \left[ \frac{W_a}{\beta} + T_{amb} \right] + \left[ T_i - T_{amb} - \frac{W_a}{\beta} \right] e^{-\frac{\beta}{m_{sample} \cdot c_{P,sample}} \cdot t} \quad (1.14)$$

where  $T_i$  is the initial temperature and  $t$  is the measured time. By fitting the experimental temperature-time data to the theoretical exponential curve,  $W_a$  is obtained and then the  $PTE$  from Equation 1.1 is calculated.

Finally for the third scenario, in which the phase change of the PCM must be considered and no heat losses occur,  $PTE$  can be calculated by including in  $W_a$  the contribution of sensible and latent heat, previously presented in Equation 1.10. Therefore, from Equations 1.1 and 1.10,  $PTE$  can be calculated as follows:

$$PTE = \frac{Q_{total,sample}}{W_{measured} \cdot \Delta t} = \frac{m \cdot c_{P,sol} \cdot \Delta T_{sol} + m \cdot \Delta H_m + m \cdot c_{P,liq} \cdot \Delta T_{liq}}{W_{measured} \cdot \Delta t} \quad (1.15)$$

From this previous analysis and equations, it can be concluded that several parameters must be controlled and optimized to develop solar NFs and hybrid emulsions for DASC applications. First, it is necessary to achieve a small particle/agglomerate size during the preparation method to ensure colloidal stability. Then the NPs that maximize solar absorption radiation must be selected. Finally, to maximize the thermal energy storage capacity, PCMs with high phase change enthalpy are needed so that the possible decrease in SHS can be overcome by the contribution of latent heat.



#### 1.4. Objectives

The objective of this Thesis was to contribute profounder knowledge on the use of solar NFs and hybrid emulsions with PCMs to be employed in DASCs. Thanks to these new heat transfer fluids with improved optical and thermal properties, these systems are provided with materials capable of transporting and storing the heat absorbed through the same medium. This triple function allows heat losses to be reduced compared to conventional collectors during the absorption, transport and storage process. This new solar collector approach, based on direct solar radiation absorption with no need for an absorber surface, requires fluids with improved optical and thermal properties for solar applications.

The partial objectives of this Thesis, which allow to evaluate, control and optimize the photothermal behavior of water-based solar NFs and hybrid emulsions with PCMs for their use in DASCs, are to:

- Select optimal heat transfer fluids, nanoparticles and phase change materials for DASC systems.
- Evaluate the suitability of water-based Au NFs as potential solar NFs thanks to the presence of SPR.
- Determine statistically the influence of the size and concentration of NPs on photothermal behavior to produce optimal NFs with enhanced efficiency in DASC applications.
- Assess the possible implementation of hybrid emulsions with carbon NPs and PCMs to simultaneously maximize solar radiation absorption and thermal energy storage capacity.
- Produce colloidally stable hybrid emulsions by correctly selecting surfactants and by the optimization of the fabrication process using the two-step method.
- Evaluate the colloidal stability of water-based Au NFs and hybrid emulsions with time and thermal cycling.
- Evaluate experimentally optical properties, such as extinction coefficient, transmittance, reflectance and absorptance of water-based Au NFs and hybrid emulsions using different spectrophotometer configurations depending on samples' response to incident light.

- Measure the thermal energy storage capacity of hybrid emulsions to evaluate the latent heat contribution of the PCM to *PTE*.
- Measure the thermal conductivity of water-based Au NFs and hybrid emulsions to characterize the charging and discharging rates during TES processes.
- Develop experimental facilities for the *PTE* characterization of the produced fluids under simulated and natural sunlight conditions, with and without light concentration.
- Measure and evaluate the *PTE* of water-based Au NFs and hybrid emulsions with the different developed facilities under different experimental conditions.
- Obtain a *PTE* database for the different designed fluids.

A summary of the main milestones of this Thesis together with the chapter in which these milestones were fulfilled, is presented in Table 1.2.

**Table 1.2.** Summary of milestones fulfilled in this Thesis.

Milestone	Chapter 3	Chapter 4
Formulation and production of solar nanofluids and hybrid emulsions		
Heat transfer fluid, nanoparticle and/or PCM selection	✓	✓
Experimental and statistical analysis of $D$ and $[Au]$ influence	✓	
Optimal surfactant selection		✓
Colloidal stability study	✓	✓
Thermophysical characterization of solar nanofluids and hybrid emulsions		
Optical properties measurement and analysis	✓	✓
Thermal conductivity measurement and analysis	✓	✓
Thermal energy storage capacity measurement and analysis		✓
Photothermal conversion efficiency in DASC applications		
Development of a simulated sunlight testing facility without concentration	✓	
Development of a simulated sunlight testing facility with concentration		✓
Development of a natural sunlight testing facility with concentration		✓
Photothermal conversion efficiency measurement and analysis	✓	✓



# **CHAPTER 2.**

## **Characterization Techniques**





## **2. Characterization techniques**

In order to characterize samples, different techniques were used depending on the property under study. In this work, physical, thermal, optical and photothermal characterization techniques were employed. The first group of techniques includes the analysis of the particle concentration in the NFs under study, morphological structure and NP size distribution. The second group comprises the experiments carried out to analyze thermal properties: thermal conductivity, specific heat capacity and phase change enthalpy. The third group deals with the optical analysis, and includes the tests done with a spectrophotometer to determine optical parameters, such as absorbance and transmittance. Finally, the last techniques concern the experiments performed under simulated or natural sunlight conditions to study the *PTE* of NFs and emulsions.

In the next subsections, a detailed explanation of the techniques and experimental conditions applied according to the aforementioned classification, is presented.

### **2.1. Physical properties**

The optical and thermal behavior of solar NFs and hybrid emulsions in real applications very much depends on the concentration, size and shape of NPs. Besides, these characteristics of samples influence the colloidal stability of NFs and hybrid emulsions, which is a key parameter because stable suspensions are required. Hence these three physical properties (concentration, size and shape of NPs) were experimentally measured by the following techniques.

#### ***2.1.1. Inductively Coupled Plasma Mass Spectroscopy***

The concentration of NPs in NFs was measured by the inductively coupled plasma mass spectroscopy (ICP-MS) technique. ICP-MS is a typical trace element analysis technique for the identification and quantification of elements within a wide range of samples. It is

a technique with high sensitivity and specificity and is typically used in applications in which low limits of detection are required.

ICP-MS quantitatively determines almost all the elements with an ionization potential lower than the ionization potential of argon (Ar) at very low concentrations, right down to parts per trillion. It is based on the coupling of a method for generating ions (inductively coupled plasma) and on a method for separating and detecting ions (mass spectrometer). The sample, in a liquid form, is transported by a pump to the nebulizer system where it is transformed into an aerosol by the action of Ar gas. This aerosol is conducted to the ionization zone, which consists of plasma generated by subjecting a flow of Ar gas to the action of an oscillating magnetic field induced by a high-frequency current. Under these conditions, the atoms in the sample are ionized. Ions pass into the quadrupole filter through an interface of increasing vacuum, where they are separated according to their charge/mass ratio. Each tuned mass arrives at the detector, where it evaluates its abundance in the sample.

This technique was applied to measure the NPs concentration in Au solar NFs. An ICAP-RQ (ThermoFisher Scientific) device was employed in this study (Figure 2.1). Ar was used as the carrier gas and helium (He) to eliminate possible interferences. The initial NFs were diluted to fit the equipment detection requirements (under 1 ppm) and the concentration was obtained with the help of a gold standard. The Au concentration of the initial NFs under study was calculated from the ICP-MS results for the diluted samples by knowing the previously carried out dilution. To do tests, three individual samples with a volume of 10-15 ml of the Au NF were tested for each NF concentration to obtain an average value. This technique was used in Chapter 3.



**Figure 2.1.** Inductively coupled plasma mass spectrometer instruments from Thermofisher Scientific.

### ***2.1.2. Transmission Electron Microscopy***

The morphological analysis of NPs was carried out by electron microscopy techniques because they allow resolution on the nanometer scale. Transmission electron microscopy (TEM) was used to obtain a detailed image of the shape and size of the primary NPs present in NF. The principle of operation of a TEM microscope is based on the fact that an electron cannon fires a beam of electrons. Electrons are then accelerated to high speeds by electromagnetic coils and voltages of up to several million volts in the gun. A condenser lens, with a large aperture that excludes high-angle electron, focuses the electron beam on a narrow beam. Electrons rush through the specimen, and then an objective lens group forms an image from the fraction of the beam emitted by the sample. The whole system operates under vacuum conditions to prevent electrons and gas atoms from colliding.

In Chapters 3 and 4, different NPs were observed by a TEM (JEM-1010, JEOL) system (Figure 2.2). This TEM operates at an accelerating voltage of 100 kV and a resolution of 0.45 nm. It includes a MAT RX80 (8 Mpx) digital camera. A droplet of the water-based NF was placed onto a carbon-coated copper-based grid. The liquid content was then evaporated to leave solid dry particles on the grid surface. Both morphology and primary particle size were analyzed with the acquired images.



**Figure 2.2.** Transmission electron microscope from JEOL.

### ***2.1.3. Dynamic Light Scattering***

It is essential to know the colloidal stability of NFs for their application in DASC systems because the presence of aggregates and the sedimentation of NPs can reduce efficiency or damage the installations in which NFs are used.

The dynamic light scattering (DLS) technique provides information about the particle size distribution of the NPs suspended in a base fluid. In the experimental DLS system, a NF sample is irradiated with a monochromatic laser light beam at a certain wavelength. As a consequence of the Brownian motion of particles, the relative positions of particles constantly vary among themselves, which also causes changes in not only the interference conditions, but also in the scattering intensity itself. The speed of particles movement depends on their size: the smaller the particles, the faster their speed. Therefore, a photon detector examines the light fluctuations produced by NPs, and a value of the measured diffusion coefficient is obtained that provides information about particle size by using the Stokes-Einstein equation:

$$R_H = \frac{k_B T}{6\pi\eta D_t} \quad (2.1)$$

where  $R_H$  is the hydrodynamic radius,  $D_t$  is the translational diffusion coefficient,  $k_B$  is the Boltzmann constant,  $\eta$  is the absolute viscosity and  $T$  is temperature.

The colloidal stability of the NFs and emulsions in Chapters 3 and 4 was studied by analyzing particle size distribution with a Zetasizer Nano ZS (Malver Instruments Ltd.) instrument (Figure 2.3). A 1-ml volume sample was placed inside a quartz cuvette, held in a sample holder inside the instrument, which was illuminated by a monochromatic laser light source centered at 532 nm. A detector collects the light scattered by particles at an angle of  $173^\circ$  to, thus, obtain the hydrodynamic radius. The equipment contains a Peltier system that is able to heat samples up to  $90^\circ\text{C}$  by allowing the evaluation of particle size distribution and stability according to temperature. At least three runs were carried out per sample to analyze the repeatability of measurements, which is directly influenced by colloidal stability, and to obtain an average value of the distribution mean diameter ( $D_{50}$ ).



**Figure 2.3.** Zetasizer Nano ZS instrument from Malver Instruments Ltd.

## 2.2. Thermal properties

The efficiency of TES processes depends on the thermal properties of TES materials. The heat transfer rate and the charging and discharging times are influenced by thermal conductivity, while the amount of stored and released energy depends on the specific heat capacity (SHS) and phase change enthalpy (LHS). Therefore, these properties need to be

experimentally measured to evaluate systems' TES performance. The techniques followed to experimentally measure these properties are described in the next subsections.

### 2.2.1. *Transient Hot Wire*

Thermal conductivity was measured by the transient hot wire (THW) method, in which a thin metal wire is used as both a heat source and temperature sensor. The wire is submerged in the sample and a certain voltage is applied through the wire by heating it. Heat is then transferred to the surrounding liquid at a rate that depends on the thermal conductivity of the liquid. The resistance variations measured in the wire can correlate with temperature variations and, therefore, thermal conductivity is calculated.

The thermal conductivity in Chapters 3 and 4 was measured by a TEMPOS (METER) conductimeter (Figure 2.4). To do so, a 40-ml sample volume was placed inside a sealed glass tube into which the wire was vertically inserted. To take measurements at a given temperature, the tube was immersed in a thermostatic bath while controlling temperature up to 140 °C. To obtain reliable results, the thermostatic bath was switched off while measurements were taken to avoid errors that could result from natural convection. Sample temperature evolution with time over a 60-second period was recorded. The  $\Delta T(t)$  values were fitted to Equation 2.2 to obtain the experimental thermal conductivity ( $k$ ) value.

$$\Delta T = \left( \frac{W}{4\pi k} \right) \ln t + C \quad (2.2)$$

where  $W$  is the applied power,  $\Delta T$  is the temperature increase at a certain measurement time  $t$  and  $C$  is a fitting constant.

A standard glycerin sample provided by the manufacturer was used to calibrate the equipment before taking measurements. Finally, a minimum of six measurements was taken for each sample to obtain an average thermal conductivity value for each tested temperature.



**Figure 2.4.** TEMPOS conductimeter from METER.

### **2.2.2. Differential Scanning Calorimetry**

Differential scanning calorimetry (DSC) is a common analytical technique used to measure the amount of heat released or absorbed by a sample during the heating or cooling process over a temperature range. This technique is applied to characterize the thermal properties of a material, such as specific heat capacity and phase change enthalpy, and to determine the temperature at which phase transitions occur, including melting and crystallization events during thermal cycling.

The measurement principle of this technique is based on the variation of the heat flux absorbed or released by the sample due to a phase change or variation in the structure of the material. The equipment registers the supplied heat flow to keep the sample under study and a reference sample (empty crucible) at the same temperature during a given temperature cycle. From the heat flow *versus* the temperature curves, it is possible to not only quantify in detail the amount of thermal energy stored and/or released, but to also know the melting and crystallization enthalpies. From the heat flow measured in a temperature step far from the phase change, the specific heat capacity in the solid and liquid phases can also be determined. For this purpose, a standard sapphire is used to calibrate equipment before taking each measurement. A correction factor that considers equipment deviations is obtained and applied to calculate the specific heat capacity of samples.

This technique was used in Chapter 4 to characterize the  $c_p$ ,  $\Delta H_m$  and  $T_m$  of the materials for energy storage by employing a differential scanning calorimeter (DSC2, Mettler Toledo), as shown in Figure 2.5. The areas method was applied to study the specific heat capacity in the solid and liquid phases. Temperature steps of 1 °C were applied, with isothermal steps of 5 minutes before and after a step. To obtain information on the melting and crystallization process, samples were thermally cycled within a temperature range that comprised the phase change temperatures, with specific heating and cooling rates (5 K·min<sup>-1</sup>) and isotherms at the maximum and minimum temperatures. All the measurements were taken at a constant flow rate of 25 ml·min<sup>-1</sup> of N<sub>2</sub> and aluminum crucibles with a 40 µl volume capacity were used. For each fluid under study, at least three crucibles were prepared, in which 17 mg of sample were placed and two cycles were carried out to corroborate the repeatability of the measurements and to obtain an average value for each thermal property.



**Figure 2.5.** Differential scanning calorimeter, DSC2, from Mettler Toledo.

### 2.3. Optical properties

The efficiency of solar absorption radiation processes depends on the optical properties of the employed fluids. The optical absorptance of samples is the most important parameter for DASC design and needs to be experimentally evaluated to enhance the photothermal conversion performance of systems. Depending on samples, other optical



parameters, such as scattering or reflectance, can be also important. The spectroscopy technique used to measure all these properties is described in detail in the next subsection.

### 2.3.1. Spectrophotometry

In this doctoral Thesis, two different spectrophotometers were used to analyze the optical features of samples. In Chapter 3, a Lambda 1050+ UV/Vis/NIR (PerkinElmer) spectrophotometer was employed to analyze the water-based Au solar NFs, as shown in Figure 2.6a. The system includes two lamps, tungsten-halogen and deuterium, as light sources, which allow it to perform tests within a broad wavelength range, and light was collected through two InGaAs photodiodes. In Chapter 4, a V-780 (Jasco) spectrophotometer was used to analyze hybrid emulsions, as shown in Figure 2.6b. The equipment has a halogen-deuterium light source, which also allows measurements to be taken within the wide wavelength range, and it incorporates an InGaAs photodiode as a detector. An integrating sphere can be attached to both spectrophotometers, which enables measurements of the different spectral optical properties of samples to be taken.

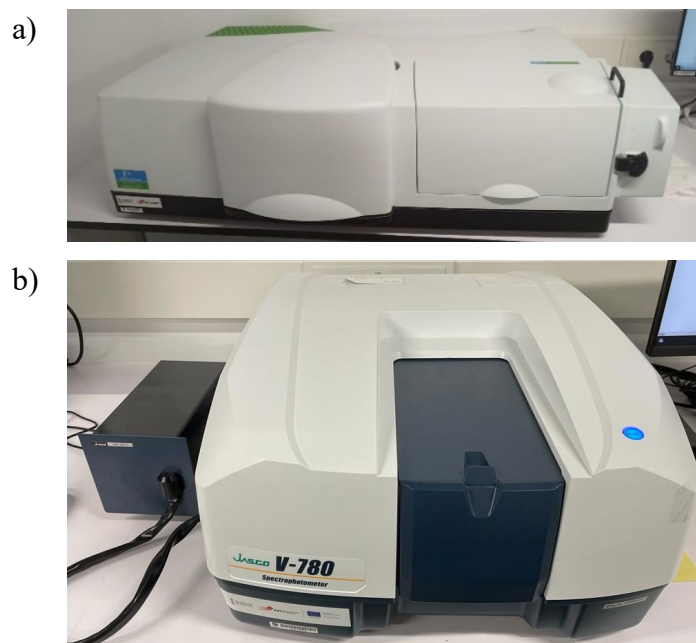


**Figure 2.6.** Spectrophotometer systems. a) Lambda 1050+ UV/Vis/NIR from PerkinElmer and b) V-780 from Jasco.

Both systems are based on the same operating principle: a mirror creates a double beam from the light source, which passes through the sample to be studied and through a reference to, thus, collect two signals with different intensities. The light passing through the reference position arrives with intensity  $I_0$  at a detector corresponding to the total intensity of the lamp. Another signal that passes through the sample reaches another detector with its corresponding intensity.

Both instruments can work with different configurations to obtain distinct optical parameters:  $I_T$ ,  $I_R$ ,  $I_a$  and  $I_S$ , as defined in Section 1.3.1. During standard operation when the light beam passed through the sample and the signal is collected by the detector, the direct transmitted light signal ( $T$ ) was obtained (Figure 2.7a). When employing the integrating sphere, it is possible to place the sample in different positions, so that the detector measures distinct optical properties. In Figure 2.7b, the sample was placed before the integrating sphere, and a tilted white cap was placed opposite the sample, to allow the detector to measure a combination of transmitted and forward scattered light ( $T + FS$ ). If as shown in Figure 2.7c, the white cap is removed, the direct transmitted light is not measured by the detector, and the optical property measured in this configuration is only forward scattering ( $FS$ ). By placing sample on the rear part of the integrating sphere in a tilted position using a black cap, the detector measures the combination of the reflected signal and the backward scattered ( $R + BS$ ) (Figure 2.7d). As shown in Figure 2.7e, by removing the tilt in the previous configuration, the measured property is only the backward scattered ( $BS$ ) light. By combining the results obtained with the different configurations, the distinct optical properties can be estimated.

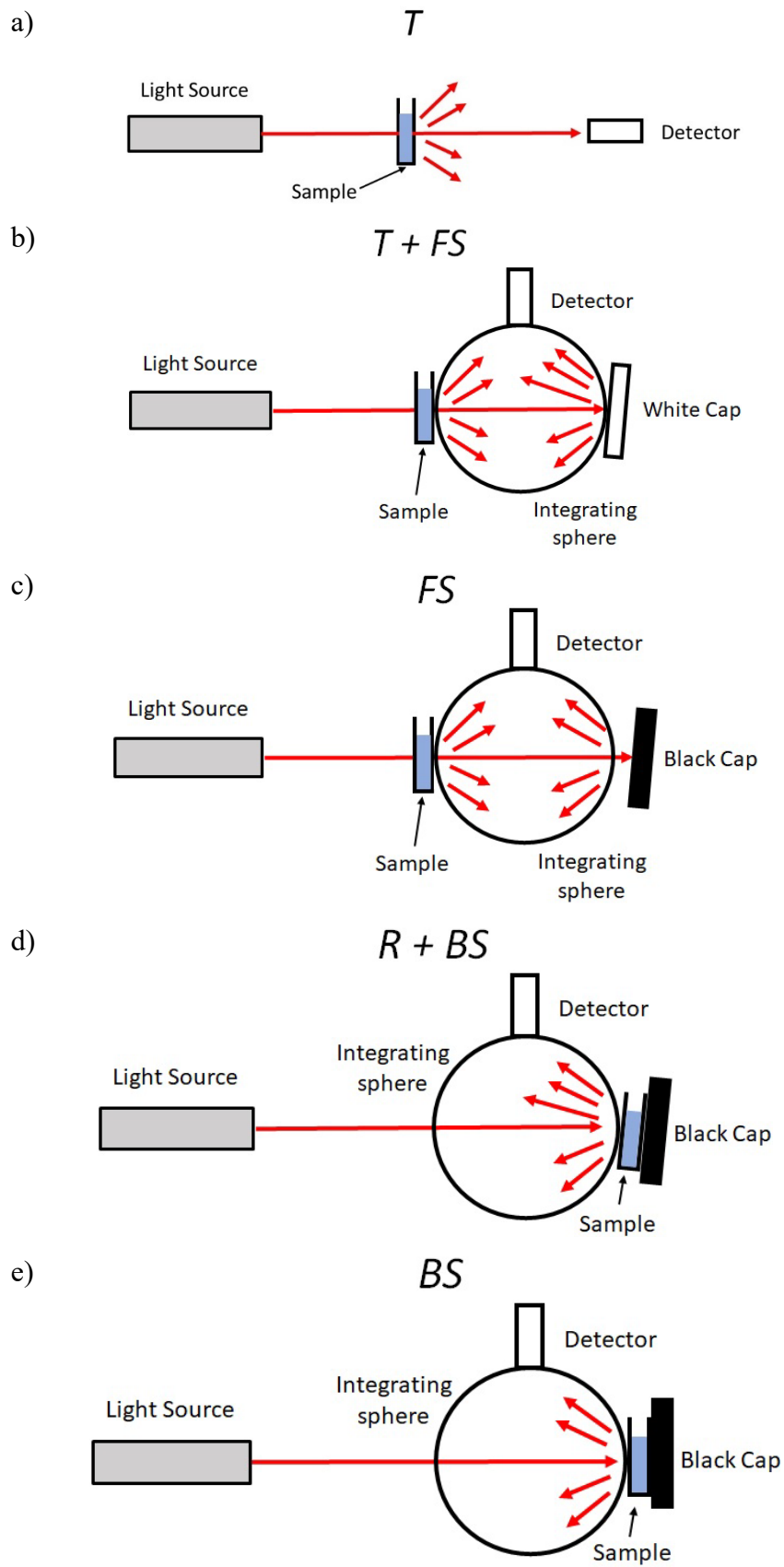


**Figure 2.7.** Different spectrophotometer configurations without integrating sphere a)  $T$  measurement and with integrating sphere b)  $T+FS$ , c)  $FS$ , d)  $R+BS$  and e)  $BS$  measurements.

In Chapter 3, the water-based Au NFs placed inside a 10 mm quartz cuvette were characterized by a Lambda 1050+ spectrophotometer without integrating a sphere (Figure 2.7a). In this case, by taking the direct transmittance measurement, it was possible to calculate the extinction coefficient following Equation 2.3. As NPs were highly dispersed in the NF, multiple scattering was considered a phenomenon that could be neglected. Hence this made the extinction coefficient equal the absorption coefficient.

$$\mu_{ext}(\lambda) = -\frac{\log[T(\lambda)]}{x} \quad (2.3)$$

In Chapter 4, the hybrid emulsions placed inside a 1 mm quartz cuvette were characterized by a Jasco V-780 spectrophotometer with an integrating sphere (Figure 2.7b-d). Due to the high opacity of the samples produced by the NPs and paraffin in the emulsion, it was necessary to obtain reflectance and scattering information in addition to transmittance. In this case, the optical data from two different spectrophotometer configurations were measured. The intensities obtained from the configurations in Figure 2.7b (to directly measure  $T$  and  $FS$  light) and Figure 2.7d (to directly measure  $R$  and  $BS$  light) were combined. With these parameters, the spectral absorptance,  $a(\lambda)$ , of samples could be calculated according to Equation 2.4:

$$a(\lambda) = 1 - [T(\lambda) + FS(\lambda)] - [R(\lambda) + BS(\lambda)] \quad (2.4)$$

#### 2.4. Photothermal conversion setups

How HTFs convert solar radiation into thermal energy is a key factor in the design and implementation of DASC systems. Therefore, the  $PTEs$  of the different NFs and emulsions researched in this Thesis were evaluated. Distinct experimental setups, including simulated and natural sunlight, were developed to measure the  $PTE$  performance of the fluids being evaluated.

For the experimental setups described below, incident radiation intensity was evaluated by a potentiometer (Ophir 1Z01500, Nova Display) at the position of samples. The

temperature evolution of samples was recorded by a data acquisition system that consisted of a data logger (Agilent 34970 A) connected to a computer.

### 2.4.1. Simulated sunlight

The *PTE* of the solar NFs under the simulated sunlight conditions was evaluated by various experimental systems.

In Chapter 3, an Oriel solar simulator (6263 75 W Xe OZONE FREE) was used, as shown in Figure 2.8a, which is equipped with a xenon arc lamp. In addition, a high-temperature custom-made quartz glass tube, which contains a vacuum interlayer to avoid convective heat loss to the environment, was utilized in the experimental system to contain samples (Figure 2.8b). Fluids were located in the inner tube part (25 mm diameter), whose outer diameter was 50 mm and vertical total length was 150 mm. Samples were illuminated with an intensity of 4.7 suns and a k-type thermocouple (RS PRO K-228-7451, with  $\pm 1.5$  °C measurement uncertainty) was placed inside the quartz glass tube to obtain the temperature evolution of samples. Another k-type thermocouple was placed outside to evaluate the ambient temperature during the heating process.

In Chapter 4, a collimated irradiation source NEWPORT (91195A-1000 Class A solar simulator & SPECTRA-PHYSICS 69920 Universal Arc Lamp Power Supply ORIEL) was used, as shown in Figure 2.8c. The samples under study were placed inside a custom-made Teflon cylindrical container, whose internal diameter was 18.2 mm and height was 11 mm (Figure 2.8d). The sample holder was insulated with an expanded polystyrene container to reduce heat losses. To obtain temperature distribution, three k-type thermocouples were inserted 3 mm from the inner wall at different depths (top:  $z = 0.2$  cm, medium:  $z = 0.5$  cm; bottom:  $z = 0.7$  cm) and another k-type thermocouple was used to record ambient temperature evolution. Samples were irradiated under initial illumination conditions of  $1,000 \text{ W}\cdot\text{m}^{-2}$ , which was concentrated by a Fresnel lens and a filter to reach an intensity of 3.5 suns.

The spectrum of both sources is depicted in Figure 2.9, which shows that, to a certain extent, the simulated sunlight spectrums (right axis) reproduced the spectral behavior of solar irradiance at the ground level,  $I_{solar}(\lambda)$ , (left axis).

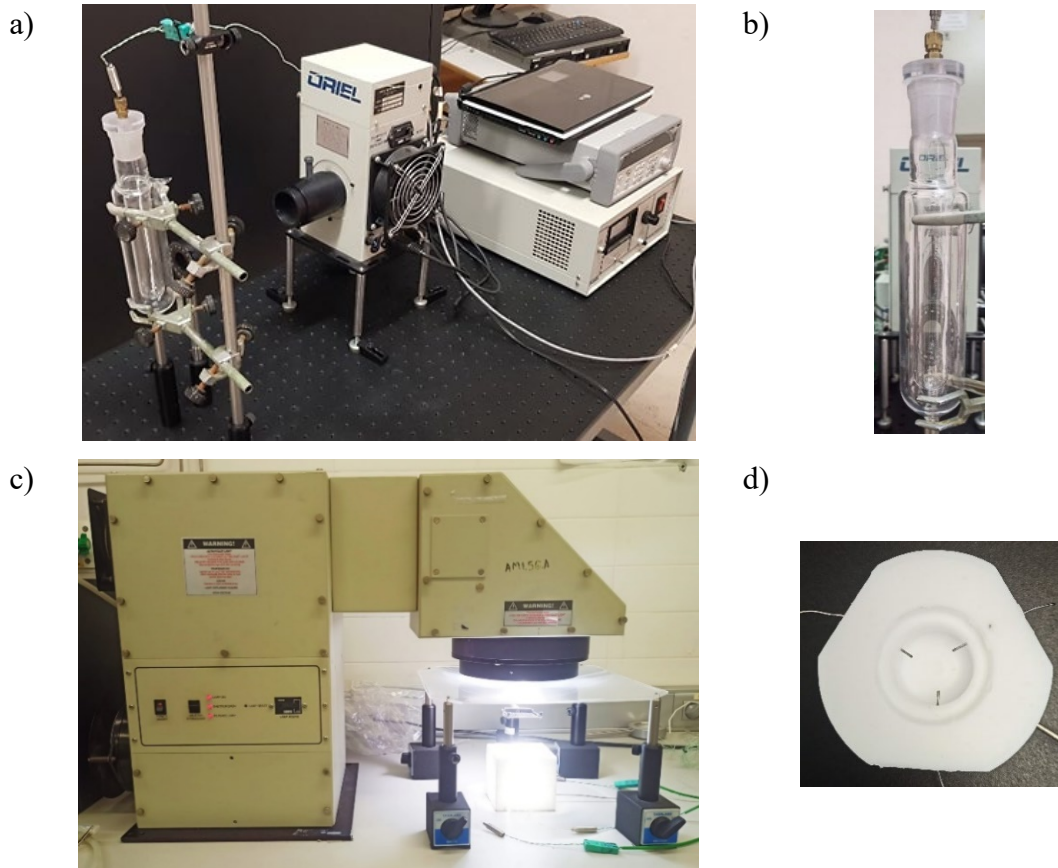


**Figure 2.8.** Solar simulator a), c) experimental setups and b), d) sample holders.

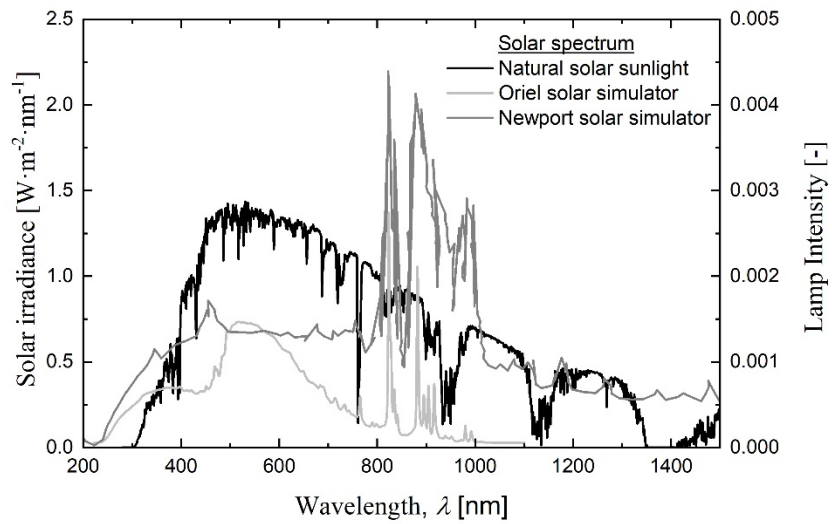


**Figure 2.9.** Natural solar spectrum (left axis) and simulated solar spectra (right axis).

### 2.4.2. Natural sunlight

In order to evaluate *PTE* under the natural sunlight conditions in Chapter 4, a custom-made adjustable aluminum structure with four Fresnel lenses (Orafol SC 213-600) to concentrate natural sunlight at an intensity of 136 suns was used, as shown in Figure 2.10a. This structure allows the position of the Sun to be tracked to always keep its rays perpendicular to the surface of lenses and the quartz glass tubes. Samples were placed inside four quartz glass tubes (see Figure 2.10b), similarly to those employed in Figure 2.8b. A k-type thermocouple (Inconel 600 with  $\pm 2.5$  °C measurement uncertainty) was immersed in the radial center position of the tube ( $z = 1.25$  cm depth from the illuminated surface) and in the center of spotlight. Another k-type thermocouple was left outside the experimental system to know ambient temperature evolution. During the measurement process, a pyranometer (MS-102; irradiance range of 0-4,000  $\text{W}\cdot\text{m}^{-2}$ ) was used to measure the incident solar radiation that reached the position of the Fresnel lenses.

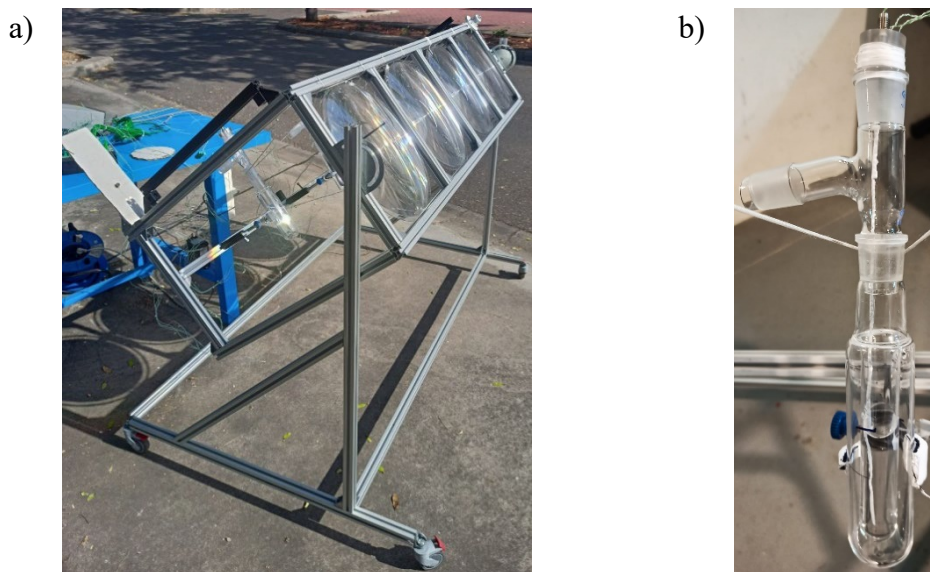


**Figure 2.10.** Natural sunlight a) experimental setup and b) sample holder.

A summary of all the techniques followed in this doctoral Thesis for measuring the different thermophysical properties is presented in Table 2.1, including the employed equipment and the chapters of this Thesis book in which they were applied and further information can also be found.





**Table 2.1.** Summary of the experimental techniques, measured properties and equipments used in this work.

Technique	Property	Equipment	Chapter 3	Chapter 4
ICP-MS	Nanoparticle concentration	ICAP-RQ ThermoFisher Scientific	✓	
TEM	Nanoparticle size and shape	JEM-1010 JEOL	✓	✓
DLS	Nanoparticle size distribution	Zetasizer Nano ZS Malver Instruments Ltd	✓	✓
DSC	Specific heat capacity, phase change enthalpy and temperature	DSC2 Mettler Toledo		✓
THW	Thermal conductivity	TEMPOS METER	✓	✓
Spectrophotometry	Transmittance, reflectance, absorptance, scattering and extinction coefficient	Lambda 1050+ UV/Vis/NIR PerkinElmer  V-780 Jasco	✓	✓
Photothermal Conversion	<i>PTE</i>	Oriel (6263 75 W Xe OZONE FREE) NEWPORT (91195A-1000 Class A)	✓	✓
		Fresnel lenses (Orafol SC 213- 600)		✓



**CHAPTER 3.**  
**Experimental Characterization and**  
**Statistical Analysis of Water-Based**  
**Gold Nanofluids for Solar**  
**Applications: Optical Properties and**  
**Photothermal Conversion Efficiency**



### **3. Experimental characterization and statistical analysis of water-based gold nanofluids for solar applications: optical properties and photothermal conversion efficiency**

Optimizing optical and photothermal properties of the solar nanofluids to be used in direct absorption solar collectors is a key issue to maximize efficiencies in these collector types. This work both experimentally and statistically analyzes the influence of the size (5 and 20 nm) and concentration (5.1, 28.2 and 51.3 ppm) of gold nanoparticles on several important variables for collector performance: nanofluid stability, extinction coefficient, photothermal efficiency, etc. The research work shows that the addition of small amounts of gold nanoparticles, whose surface plasmon resonance has wavelengths close to 520 nm, greatly improves the light absorption capacity of the base fluid (water). The statistical analysis confirms the influence of nanoparticle size and concentration on photothermal conversion efficiency, which lead to an increase of up to 121 % for the smallest-sized nanofluid with the highest concentration.

### 3.1. Introduction

The 2015 Paris Agreement was motivated to obtain a global response to climate change by keeping the rise in global temperature well below 2 °C and pursuing efforts to limit it to 1.5 °C<sup>[2]</sup>. European Union and United Nations Member States intend to address different strategies in relation to the energy system: improving energy efficiency and decarbonizing energy production systems by implementing renewable energy sources. While recent trends indicate that the implementation of environment-conscious energy systems is an accompanist to alternative fossil fuel use, it is becoming increasingly clear that a paradigm change is required to make clean energy processes dominant to not exceed the global warming limit.

In recent decades, solar energy has been regarded as the most promising source of inexhaustible clean energy. The two main ways of collecting and transforming solar energy are photovoltaic solar energy and solar thermal energy<sup>[54]</sup>, of which the latter is the basis of this work. In solar thermal energy, solar radiation is collected by an absorption material and transferred as heat energy to a transfer medium, usually a heat transfer fluid (HTF). Solar collectors are the devices used for solar-to-thermal energy conversion. They can be classified as concentrating and non concentrating solar collectors. Non concentrating solar collectors are used at low-to-medium temperatures, while the concentrating collectors that employ mirrors to concentrate incident solar energy are employed at higher temperatures.

The absorption material in conventional collectors is a dark surface that heats up and transfers heat to the HTF flowing through pipes. Although these collectors offer good energy conversion efficiency, a series of thermal losses appear to lower the possible maximum efficiency limit. In the 1970s, directly exposing HTF to incident radiation was proposed as an alternative to avoid such losses in conventional collectors<sup>[12]</sup>. This concept, in which heat is absorbed volumetrically by the working fluid instead of the surface, is known as direct absorption solar collectors (DASC). However, commonly used HTFs (water, oils, molten salts, etc.) are transparent in most of the solar spectrum, and possess low solar radiation absorption capacity and, hence, offer low solar-to-thermal conversion efficiency. To overcome this issue, nanofluids (NFs) used as HTFs have been proposed in the literature<sup>[21][55]</sup>.

NFs were first postulated by *Choi and Eastman* in 1995<sup>[20]</sup> as suspensions of nanoparticles (NPs, with sizes ranging from 1-100 nm) homogeneously dispersed in a base fluid to achieve improved thermal properties, mainly thermal conductivity and heat transfer performance. A wide variety of materials of different natures can be employed in these NFs to improve thermal characteristics. Some examples are metals (Ag, Au, Cu, Al, etc.), metal oxides (SiO<sub>2</sub>, Al<sub>2</sub>O<sub>3</sub>, TiO<sub>2</sub>, CuO, Fe<sub>2</sub>O<sub>3</sub>, etc.) and carbon-based materials (carbon nanotubes, graphene, graphene oxide, graphite, etc.)<sup>[23], [56], [57]</sup>.

The term solar nanofluids was later proposed in 2009 by *Otanicar et al.*<sup>[21]</sup>. It refers to those NFs with better solar radiation absorption capacity thanks to the addition of NPs, even at very low concentrations<sup>[32], [58]</sup>. Since then, many works have studied the optical properties and photothermal conversion efficiency of solar NFs. This consists of different NPs like metals<sup>[17], [18], [64], [24], [37], [39], [59]–[63]</sup>, metal oxides<sup>[25], [65], [66]</sup>, carbon-based materials<sup>[26], [67]–[69]</sup> and hybrid composites<sup>[27], [41], [70]</sup>. The NFs from coffee waste or black Chinese ink<sup>[28], [71], [72]</sup> have been investigated as possible NFs for being cheap and also biodegradable. Hence, they can reduce waste production.

Metal NPs include a special group of metals of much interest as solar NFs because they exhibit surface plasmon resonance (SPR) at certain wavelengths when exposed to sunlight. They also have the potential to enhance absorption characteristics<sup>[73]</sup>. This plasmonic response is a collective oscillation of electrons, stimulated by incident light absorption. It is an effective way of increasing solar energy in thermal energy conversion. Therefore, these NPs are interesting candidates for the photothermal conversion processes required in DASCs. The metal NPs that present SPR include Au, Ag, Cu, Al and Li. Of these, Ag, Cu and Al are easily oxidized, and Li is difficult to handle given its reactivity. Au NPs exhibit good colloidal and thermal stability, high electrical and thermal conductivity and strong SPR over a wide wavelength range within the sunlight spectrum, all of which make it a good candidate as an NP in solar NFs for DASC.

A parameter-based review literature is presented in Table 3.1. It summarizes the results obtained in previous works for photothermal conversion efficiency (*PTE*). *PTE* is defined as the ratio between the energy absorbed by the NF to the incident radiation for pure water and water-based Au NFs with different NP sizes and concentrations.

**Table 3.1.** Review of the *PTE* results for water-based gold nanofluids.

Author (year) [Ref]	Size [nm]	Nanoparticle concentration [ppm]	Energy source* [W·m <sup>-2</sup> ]	<i>PTE<sub>w</sub></i> [%]	<i>PTE<sub>nf</sub></i> [%]
Zhang <i>et al.</i> (2014, 2015) <sup>[60]</sup> [24]	10-20	0.28-11.2	SS: 1,000	45	54-78
Chen <i>et al.</i> (2016) <sup>[37]</sup>	25, 33 and 40	0.08	SS: 450	Cube: 71 Flat: 65	Cube: 83.5- 86.5 Flat: 72-85
Chen <i>et al.</i> (2016) <sup>[39]</sup>	10	0.5-2.5	SS:10,000	N/A	15-35
Jin <i>et al.</i> (2016) <sup>[18]</sup>	20	0.36-5.8	NS:600-950	35(@600) 17.3(@950)	56-80 (@600) 45.5-73.6 (@950)
Jin <i>et al.</i> (2016) <sup>[61]</sup>	20	1.02-12.75	NS: Fresnel lens 220,000	13	45-80.3
Chen <i>et al.</i> (2017) <sup>[62]</sup>	10	0.5-2.5	SS: 10,000	N/A	48-70
Wang <i>et al.</i> (2017) <sup>[63]</sup>	13	5-178	SS: 10,000	8	19-25
Zeiny <i>et al.</i> (2018) <sup>[17]</sup>	3-6	30-150	SS:1,000	23	28-44
He <i>et al.</i> (2018) <sup>[64]</sup>	10	5.1	SS: 1,000	33.8	71.7

\*SS: Solar Simulator; NS: Natural sunlight

Table 3.1 reveals how *PTE* values differ depending on the energy source, radiation conditions and NF characteristics, with values ranging from 8 % to 71 % for pure water. *PTE* is always enhanced when Au NPs are added, even at very low concentrations. Enhancements from 11 %<sup>[37]</sup> to 518 %<sup>[61]</sup> have been reported for different tested



conditions. These findings reflect the high potential of Au NPs for solar-to-thermal conversion processes under optimal conditions.

A statistical analysis is an important and rather recently appreciated requirement for the NFs productization path for enabling: (i) evaluations of parameter (e.g., nanoparticle concentration and morphology, temperature, NF type) effects on performance (e.g., thermal efficiency); (ii) evaluations of associations (correlations) between parameters (e.g., between nanoparticle agglomeration and viscosity); (iii) performance predictions (e.g., Nusselt number correlations, figures of merit); and all quantitatively<sup>[74]</sup>. Accordingly, this work employs statistical analyses to quantify: (i) whether a dependent variable changes significantly as an independent variable changes; (ii) how parameters are associated with or correlate to one another.

In this article, the optical and photothermal properties of NFs were studied in-depth for aqueous Au NFs. The results were compared to pure water. The morphology and colloidal stability of NPs in fluid were analyzed by transmission electron microscopy (TEM) and the dynamic light scattering (DLS) technique. The influence of both NP size (5 and 20 nm) and concentration (51.3, 28.2 and 5.1 ppm) on optical and photothermal properties (i.e., extinction coefficient, fraction of absorbed sunlight, temperature increase and photothermal conversion efficiency) was experimentally studied. The experimental data were processed by rigorous statistical analyses to quantitatively interpret the results and to shed light on statistically significant variations and associations.

## **3.2. Materials and Methods**

### ***3.2.1. Nanofluids and experimental conditions***

The two selected commercial Au NFs (particle sizes 5 and 20 nm) were supplied by Sigma-Aldrich. Both were stabilized in 0.1 mM PBS (Phosphate buffered saline). Micrographs of both the 5 nm and 20 nm nanoparticles appear in Section 3.3.1 (Figure 3.4). Their optical density was 1 and they were free of reactants. Both commercial NFs were initially tested by inductively coupled plasma mass spectrometry (ICP-MS). The Au concentrations of 63.8 and 51.3 ppm for the 5 and 20 nm NFs were respectively obtained.

Table 3.2 and Figure 3.1 include the nomenclature and conditions of the different samples tested in this study. The two independent variables of this experiment are NP diameter ( $D$ ) and concentration ( $[Au]$ ), respectively, at two and three levels. Concentrations were set at 51.3, 28.2 and 5.1 ppm for each NP size by diluting the initial commercial samples with distilled water. These two inputs were used to study their effect on the three following output (performance) variables: temperature variation ( $\Delta T$ ); photothermal conversion efficiency ( $PTE$ ); distance at which 50 % of incident solar radiation is absorbed ( $x_{50}$ ).

**Table 3.2.** Tested samples: nomenclature and experimental conditions.

ID	$D$ [nm]	$[Au]$ [ppm]
Water	0	0
5_5	5	5.1
5_28	5	28.2
5_51	5	51.3
20_5	20	5.1
20_28	20	28.2
20_51	20	51.3

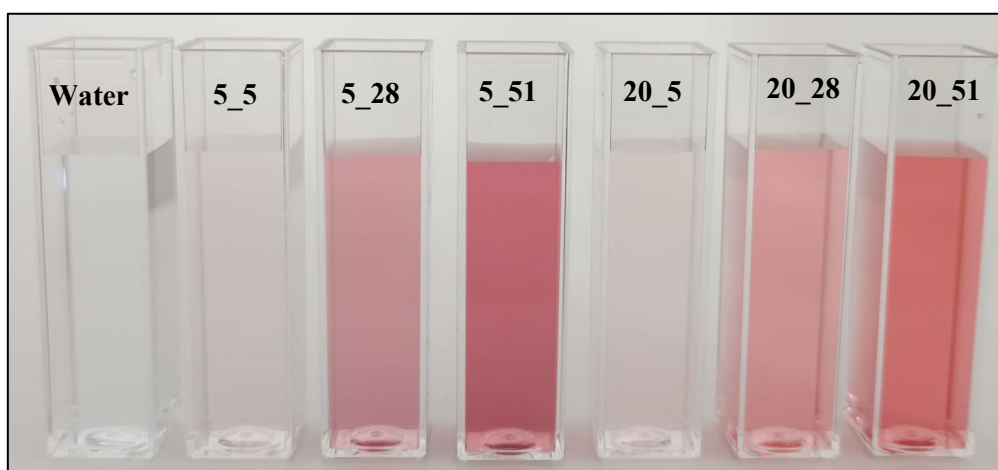


**Figure 3.1.** Visual observation of the tested samples.

### 3.2.2. *Experimental Techniques*

#### Nanoparticle concentration

The concentration of the NPs contained in NFs was measured by ICP-MS with an ICAP-RQ (ThermoFisher Scientific) device. Argon was the carrier gas. Helium was used to eliminate possible interferences. The sample volume was 10-15 ml and a gold standard was employed.

#### Nanoparticle morphology and size, $D$

The Au NPs were observed under a transmission electron microscope (TEM, JEM-1010, JEOL) operating at an accelerating voltage of 100 KV, a resolution of 0.45 nm and an AMT RX80 (8 Mpx) digital camera. A droplet of the NF was dispersed on a carbon-coated copper-based grid. The liquid content was removed with the help of absorbent paper to leave solid particles on the grid surface. Both morphology and primary particle size were studied with the acquired images.

The size distribution of the NPs in NF was analyzed by the DLS technique with a Zetasizer Nano ZS instrument (Malvern Instruments Ltd.). Size can be known from the light scattered by particles due to their Brownian motion and signal intensity. The equipment comprises a laser centered at 532 nm and a detector that acquires the intensity of the light scattered by suspended particles. Both the laser and detector are enclosed in the device. The hydrodynamic diameter is calculated based on the intensity of scattered light at 173°. It also contains a Peltier heating system that can heat samples up to 90 °C.

#### Thermal conductivity, $k$

Samples' thermal conductivity was measured by the transient hot wire technique using a TEMPOS conductimeter (Meter). The sample was placed inside a sealed glass tube (40 ml) where the sensor was vertically inserted. To run the test at a specific temperature, the tube was immersed in a thermostatic bath at a controlled temperature. Measurements were taken at 25 °C and 60 °C. Six tests were run for all the samples to obtain an average value per temperature. The experimental error was obtained from the standard deviation by means of Equation A.2 in the Section 8.1 Uncertainty analysis, with an average value of 2.64 %.

Extinction coefficient,  $\mu_{ext}(\lambda)$

The extinction coefficient was estimated from optical measurements with a Lambda 1050+ UV/Vis/NIR (PerkinElmer) spectrophotometer. The system consists of a lamp as a light source, a mirror to produce a double beam and two photodetectors located once light has crossed the reference and sample cuvettes. The wavelength range of measurements spanned 220-1,100 nm, which covers 83.5 % of total solar radiation.

The spectral extinction coefficient ( $\mu_{ext}(\lambda)$ ) was obtained according to the Beer-Lambert law, given by Equation 3.1.

$$\mu_{ext}(\lambda) = -\frac{\log[T(\lambda)]}{x} \quad (3.1)$$

where  $T(\lambda)$  is spectral transmittance (the ratio between transmitted light and incident radiation) and  $x$  is the penetration distance that equals sample thickness (namely 10 mm).

Sunlight-absorbed fraction,  $F(x)$

The solar absorption ability of NFs is important in volumetric solar collectors and is evaluated by the sunlight-absorbed fraction  $F(x)$ . This parameter calculates the fraction of incident sunlight,  $I_{Solar}(\lambda)$ , which is absorbed by fluid after a penetration distance,  $x$ , within the specified wavelength range. The  $F(x)$  value is obtained by Equation 3.2<sup>[32]–[34]</sup>:

$$F(x) = 1 - \frac{\int_{\lambda_{min}}^{\lambda_{max}} I_{Solar}(\lambda) \cdot e^{-\mu_{ext}(\lambda) \cdot x} d\lambda}{\int_{\lambda_{min}}^{\lambda_{max}} I_{Solar}(\lambda) d\lambda} \quad (3.2)$$

where  $I_{Solar}(\lambda)$  was obtained from ASTM solar radiation<sup>[35]</sup>, the extinction coefficient was calculated by Equation 3.1 and the spectral range was determined by optical measurements (within  $\lambda_{min} = 220$  nm and  $\lambda_{max} = 1,100$  nm). As a characteristic value for each sample, the penetration distance at which 50 % of the incident radiation was absorbed ( $x_{50}$ ) was determined.

Photothermal conversion efficiency, PTE

The measurements to determine the efficiency of fluids to transform solar energy into thermal energy were taken according to the experimental setup shown in Figure 3.2. It

consisted of a quartz glass tube in which a 10 ml sample volume was placed per measurement. The quartz glass tube in the experiment was custom-made for high-temperature resistance purposes. The tube contained a vacuum interlayer to reduce heat losses by convection to ambient air. Fluids were placed inside the inner-tube (25 mm diameter, 150 mm length). The outer-tube diameter was 50 mm. Samples' temperature evolution was recorded by a data acquisition system that comprised a data logger (Agilent 34970 A) linked to a PC. As shown in Figure 3.2, a k-type thermocouple (RS PRO K-228-7451) with  $\pm 1.5$  °C measurement uncertainty was placed inside fluid. This position remained constant in relation to the light source while taking all the measurements. Another thermocouple was employed to measure ambient temperature.

Samples were illuminated using a collimated radiation source from an artificial sunlight simulator (Oriel 6263 75 W Xe OZONE FREE). The spectrum of the source is depicted in Figure 3.3, which shows that the sunlight simulator reproduced to a certain extent the spectral behavior of solar irradiance at ground level,  $I_{Solar}(\lambda)$ . A potentiometer (Ophir 1Z01500, Nova Display) was used to measure the solar simulator power in the quartz glass tube position ( $W_{measured}$ ).

Experiments were performed in a closed insulated room to avoid thermal effects from the environment and to work under controlled conditions. Up to four repetitions of measurements were taken per sample to perform the statistical analysis.

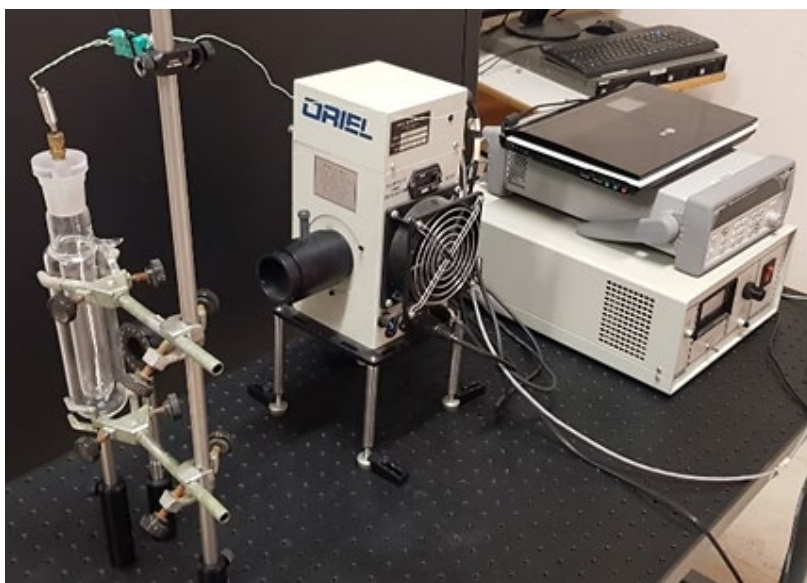


**Figure 3.2.** Experimental setup for the photothermal conversion efficiency tests.

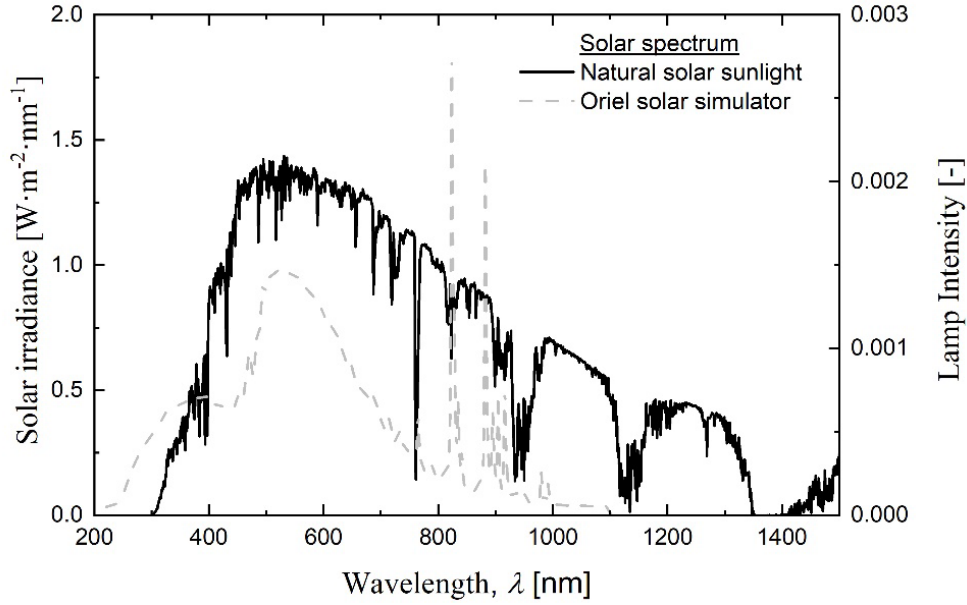


**Figure 3.3.** Natural solar spectrum (left axis) and simulated solar spectrum (right axis).

Photothermal conversion efficiency ( $PTE$ ), as defined in Equation 3.3, was calculated as the ratio between the power of energy absorbed by fluid ( $W_a$ ) and the power of the incident radiation on the sample ( $W_0$ ):

$$PTE = \frac{W_a}{W_0} = \frac{W_a}{W_{measured} \cdot \tau} \quad (3.3)$$

where  $W_0$  was calculated by applying a correction factor,  $\tau$ , to the potentiometer measurement ( $W_{measured}$ ). This factor considers the losses brought about by light propagating through media with different refractive indexes, including air, quartz, vacuum and fluid. In this work, its value was 0.86<sup>[43]</sup>.

Two different methods were followed to estimate  $PTE$ . The first method (Equation 3.4), evaluates  $W_a$  as the energy stored in fluid and does not take heat losses into account:

$$PTE_1 = \frac{W_a}{W_{measured} \cdot \tau} = \frac{(m_w \cdot c_{P,w} + m_{np} \cdot c_{P,np}) \cdot \Delta T}{W_{measured} \cdot \tau \cdot \Delta t} \sim \frac{(m_w \cdot c_{P,w}) \cdot \Delta T}{W_{measured} \cdot \tau \cdot \Delta t} \quad (3.4)$$

where  $c_{P,w}$ ,  $m_w$  and  $c_{P,np}$ ,  $m_{np}$  are respectively the specific heat, mass of water and the NP.  $\Delta T$  is the temperature increase within a time interval  $\Delta t$ . As the NP concentration of the

nanofluid was very low, term  $(m_{np} \cdot c_{P,np})$  was disregarded<sup>[18], [24], [62]</sup>. Enough time was left for the experimental temperature to stabilize. So  $PTE_1$  was calculated for 5,400 s.

To calculate the power absorbed by fluid in the second method,  $W_a$ , a balance was struck between the power measured directly in fluid,  $W_{sample}$ , and the power associated with heat losses due to convection and heat radiation effects,  $W_{loss}$ , by these equations:

$$W_{sample} = W_a - W_{loss} \quad (3.5)$$

$$m_w \cdot c_{P,w} \cdot \frac{dT}{dt} = W_a - \beta(T - T_{amb}) \quad (3.6)$$

where  $T$  is fluid temperature,  $T_{amb}$  is ambient temperature and  $\beta$  is the heat losses coefficient. In this case, the NP contribution to the  $W_{sample}$  term was neglected. By operating and applying the experiment's boundary conditions, the equation of the heating process can be obtained:

$$T = \left[ \frac{W_a}{\beta} + T_{amb} \right] + \left[ T_i - T_{amb} - \frac{W_a}{\beta} \right] e^{-\frac{\beta}{m_w \cdot c_{P,w}} t} \quad (3.7)$$

where  $T_i$  is the initial NF temperature and  $t$  is time (also 5,400 s in this case). By fitting the measured temperature to the theoretical exponential curve in Equation 3.7,  $W_a$  was obtained. Therefore,  $PTE_2$  was calculated using Equation 3.3.

### 3.3. Results and Discussion

#### 3.3.1. Nanoparticle size and colloidal stability

The morphology and size of the primary NPs dispersed in the commercial NFs were observed by TEM as received. The micrographs of both materials are shown in Figure 3.4. It depicts how particles were almost spherical in shape. The primary particle size well agreed with the values provided by the manufacturer.

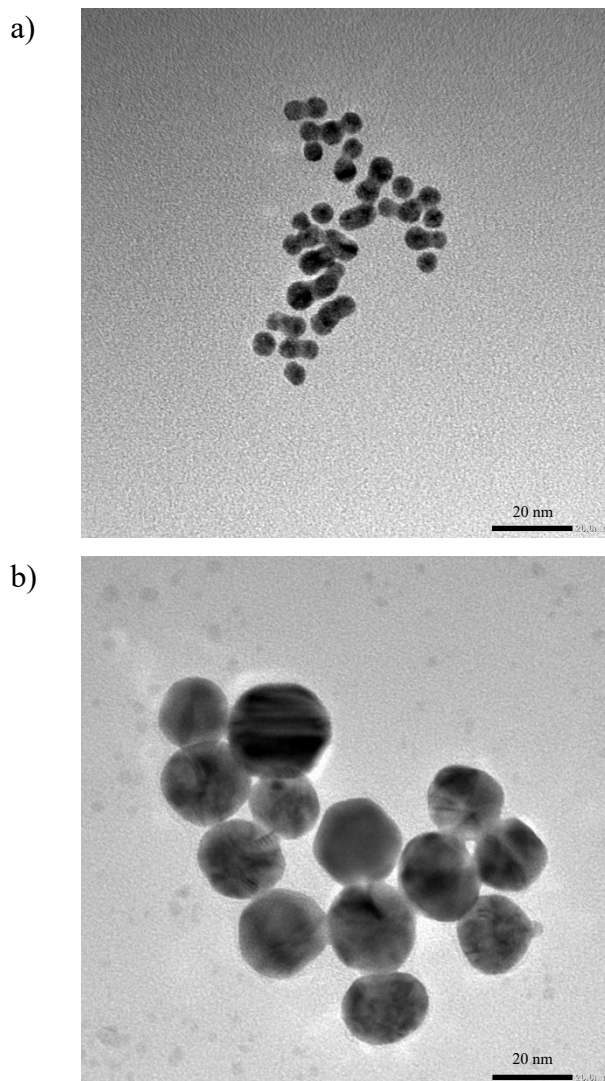


**Figure 3.4.** Gold nanoparticles a) 5 nm and b) 20 nm.

To analyze the degree of dispersion of the NPs in the base fluid and its colloidal stability with temperature increase, DLS measurements of the two commercial NFs were taken between 25 °C and 60 °C. Tests were run for the highest NP concentration after checking that the influence of the solid content on particle size distribution was negligible. The study of colloidal stability with temperature was then performed with the commercial NFs for being the most concentrated. As their stability was confirmed, further dilutions at lower concentrations were assumed stable.

The evolution of the particle size distributions obtained for both NFs with temperature appears in Figure 3.5. All the samples exhibited mono-modal distributions, and no large agglomerates formed in fluid. The mean diameter ( $D_{50}$ ) values of the NPs for each temperature are included in Table 3.3. The results showed that the mean particle sizes



came close to those of the manufacturer, and to those observed for the primary particles in the TEM images, which corroborated NPs' high degree of dispersion. With rising temperature, NPs remained mono-modal with a similar mean particle size, and displayed slight differences that could be attributed to the experimental error. These results indicate good colloidal stability with temperature for NFs with both NPs.

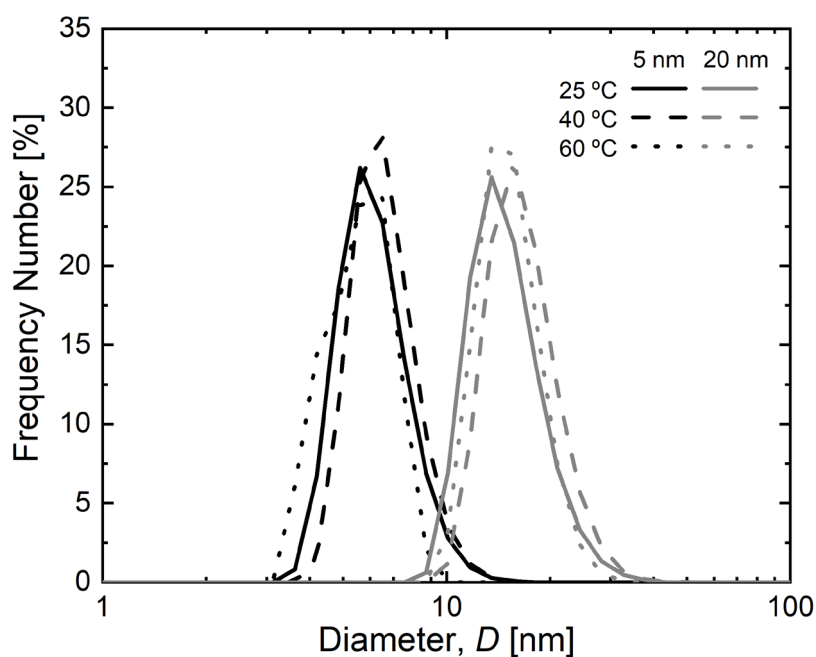


**Figure 3.5.** Evolution of particle size distribution with temperature of the commercial NFs of 5 nm and 20 nm Au NPs.

**Table 3.3.** Evolution of the mean particle size with temperature of the commercial NFs.

Temperature [°C]	$D_{50}$ [nm]	
	5 nm	20 nm
25	6.0	16.2
40	7.3	18.9
60	5.8	16.5

### 3.3.2. Thermal conductivity

This section evaluates the thermal conductivity enhancement caused by adding solid particles to water. However, it should be noted that the NFs herein studied have very low particle concentrations. So limited increments were expected in this case. The results of the enhancements in relation to the base fluid are shown in Table 3.4 for the six samples at 25 °C and 60 °C. In all cases, thermal conductivity increased when the Au NPs were present in the base fluid. The average enhancement was 2.08 %. However, the obtained results indicate experimental uncertainty, and their difficult interpretation increases insofar as NP size or concentration are not feasible.

**Table 3.4.** Thermal conductivity enhancement at 25 °C and 60 °C.

Sample	$\Delta k$ [%]	
	25 °C	60 °C
5_5	1.7	3.9
5_28	3.2	3.3
5_51	3.2	2.4
20_5	0.5	3.7
20_28	1.0	1.3
20_51	0.4	0.3

### 3.3.3. Optical characterization

Figure 3.6 shows the extinction coefficients of the base fluid (water) and the water-based Au NFs with different nanoparticle sizes and concentrations. Water remained almost transparent over the entire studied wavelength range, and only a small amount of near-infrared light was absorbed. The extinction properties of NFs were enhanced given the presence of Au NPs. The peaks associated with the SPR of the Au NPs were located at 516 nm and 520 nm for the 5 nm and 20 nm samples, respectively, regardless of NP concentration. The peak wavelengths and the slight shift to longer wavelengths with particle size agreed with the values expected for the spherical Au NPs within this size range<sup>[17], [37], [60]</sup>. Higher extinction coefficient magnitudes were obtained for the Au NFs

with increasing concentrations. This means that as the sample became more concentrated, its absorption capability improved. The extinction coefficient for wavelengths below 450 nm lowered with increasing particle size, while within SPR wavelength ranges an increase is observed with particle size.

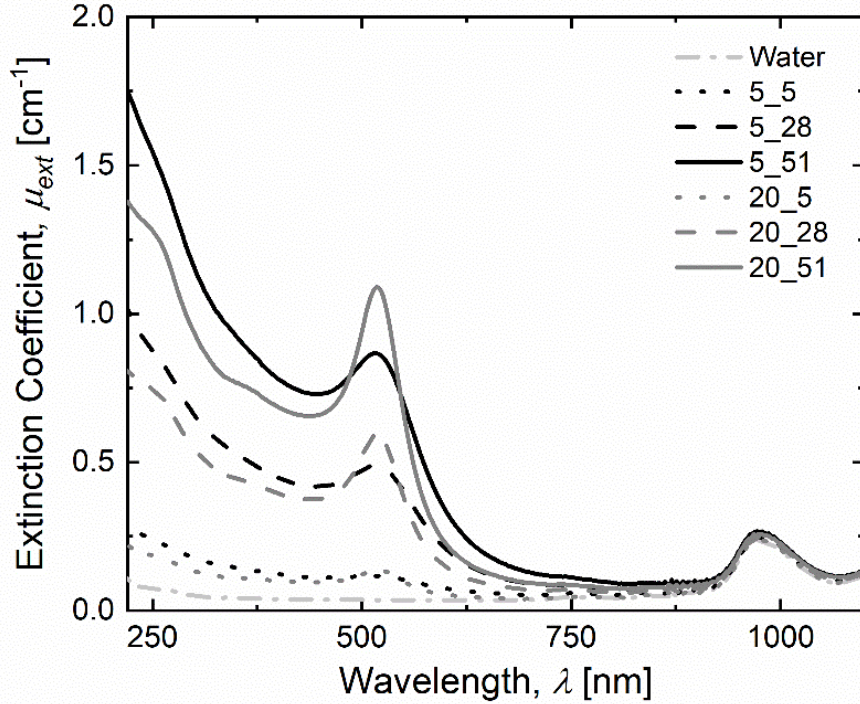


**Figure 3.6.** Extinction coefficient of the base fluid (water) and the water-based Au NFs.

Figure 3.7 compares the fraction of sunlight absorbed by the tested samples ( $F(x)$ ), as calculated with Equation 3.2. The obtained results clearly showed that using water-based Au NFs for a solar collector allowed sunlight to be fully absorbed at a shorter penetration distance compared to the base fluid alone. Therefore, implementing NFs in a solar collector is expected to improve its compactness by reducing both the volume of required liquid and the system's cost. To quantitatively evaluate the differences in Figure 3.7, the values of the penetration distance at which the tested fluids absorbed 50 % of the incident radiation ( $x_{50}$ ) are shown in Table 3.5. The base fluid absorbed 50 % of the incident radiation at a distance of 17.14 cm. The measured water-based Au NF with the highest concentration and the smallest NP size significantly cut this distance to 1.55 cm. This confirmed the positive effect of NPs' optical characteristics for efficient solar energy absorption.

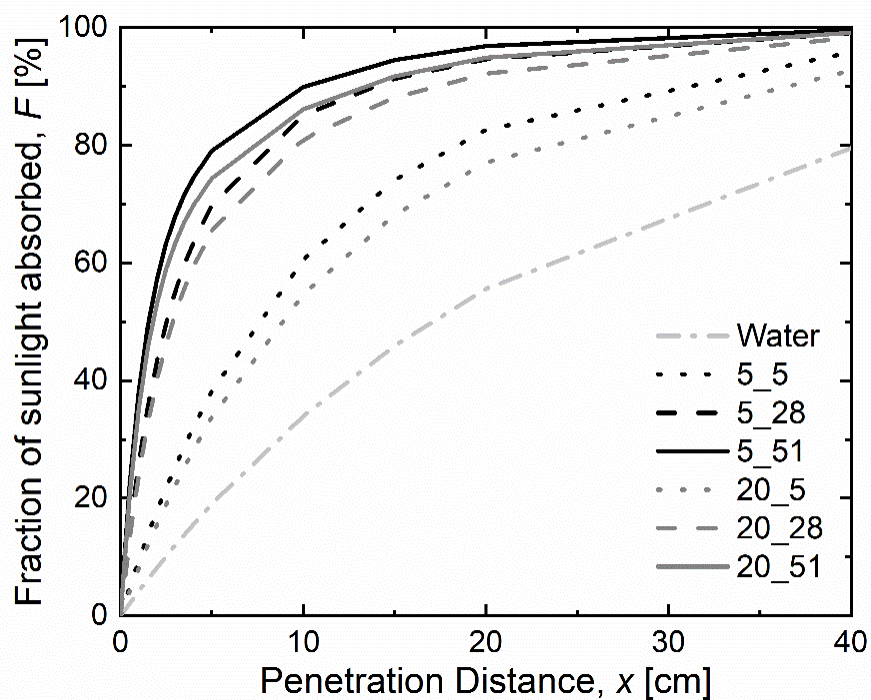


**Figure 3.7.** Fraction of absorbed sunlight in relation to the penetration distance of the base fluid (water) and the water-based Au NFs.

**Table 3.5.** Values of  $x_{50}$  for the different tested samples.

Sample ID	$x_{50}$ [cm]
water	17.14
5_5	7.60
5_28	2.50
5_51	1.55
20_5	8.90
20_28	2.85
20_51	1.78

Although optical properties are a key factor for evaluating solar NFs, detailed studies into photothermal conversion are necessary to better evaluate their applicability in DASC.

### 3.3.4. Photothermal conversion efficiency

To evaluate the efficiency to transform radiation from the solar simulator into heat, the temperature evolution with time in the different samples was measured from the experimental setup shown in Figure 3.2. After an initial rapid increase in temperature, a balance between heat losses and the energy of incident radiation was achieved and provided a maximum temperature increase (see Figure 3.8). The water-based Au NFs showed a more marked temperature rise than pure water, which was expected given their corresponding extinction coefficients. For each NP size,  $\Delta T$  increased as NP concentration rose. The maximum temperature increase obtained for water was 5.45 °C, while after adding gold NPs went up to 11.41 °C.

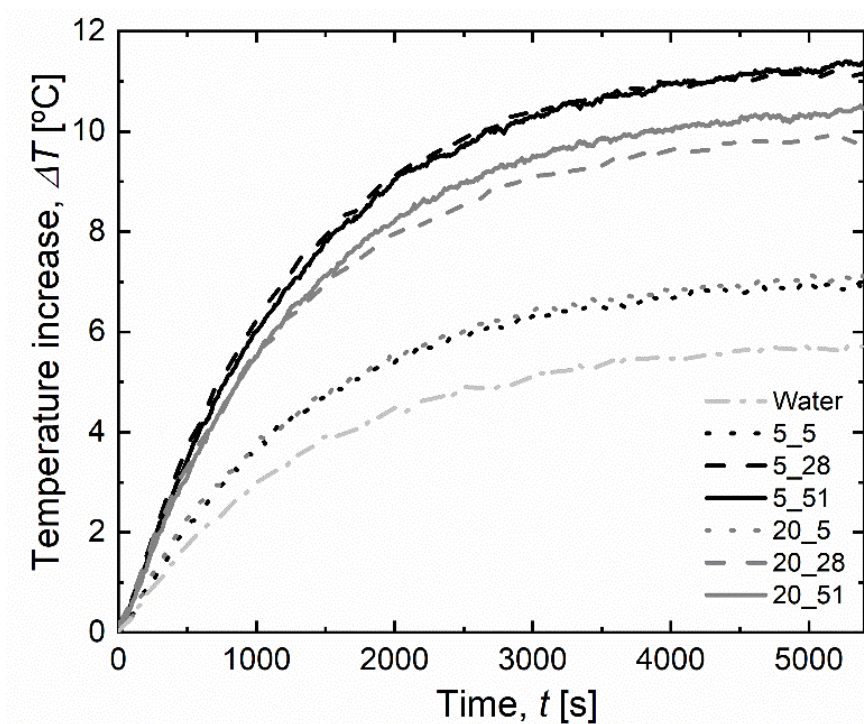


**Figure 3.8.** Temperature evolution of the base fluid (water) and the water-based Au NFs in relation to irradiation time.

Both experimental *PTEs* were obtained from the measured temperature evolutions. Table 3.6 shows the experimental *PTE* values obtained by both methods ( $PTE_1$  and  $PTE_2$ ). The average values of all the repetitions for each sample are shown.

**Table 3.6.** Values of *PTE* for the different tested samples.

Sample ID	$PTE_1$ [%]	$PTE_2$ [%]
water	5.25	22.39
5_5	7.09	28.46
5_28	10.98	48.59
5_51	11.15	49.44
20_5	7.18	28.19
20_28	9.72	41.04
20_51	10.59	44.49

Comparing the obtained *PTE* results to previous studies is not straightforward. Even for water, differences in experimental setups, selecting times for *PTE* calculations (5,400 s in this study, but 300 s for *Jin et al.*<sup>[61]</sup> and 60 s for *Zhang et al.*<sup>[60]</sup>) and the *PTE* equations, can lead to a wide range of *PTE* values. Table 3.1 shows the *PTE* values for water within the 8-71 % range. In this study, and depending on the *PTE* equations, the photothermal conversion efficiency value for water was 5.25 % when heat losses were not contemplated and was 22.39 % when they were.

By comparing the *PTE* values in Table 3.6 for all the samples, and as expected from the power balance equation, the photothermal conversion efficiencies that considered heat losses in the system ( $PTE_2$ ) were higher than those that lacked them ( $PTE_1$ ). According to Equation 3.4, as the sample mass remained constant in all the experiments,  $PTE_1$  was directly proportional to the maximum temperature increase ( $\Delta T$ ) (see Figure 3.8). It is noteworthy that remarkable *PTE* values for the Au NFs were obtained even for very low NP concentrations.

A wide range of results has been reported by different studies for absolute *PTE* values. Thus, to remove the influence of factors other from NP, it is better to analyze improvements in NFs in relation to the base fluid. Figure 3.9 includes the *PTE* enhancements provided by the NFs in Table 3.6 in relation to water, as calculated by Equation 3.8:

$$Enhancement = \frac{PTE_{nf} - PTE_w}{PTE_w} \cdot 100 \quad (3.8)$$

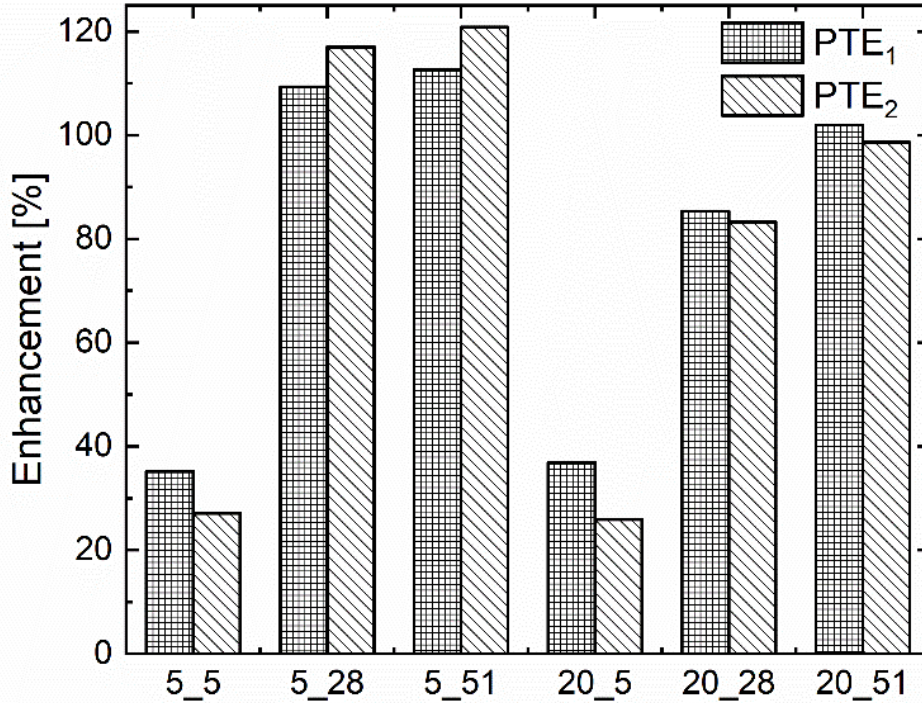


**Figure 3.9.** *PTE* enhancement of NFs in relation to water.

Although the absolute values obtained for both *PTE* definitions differed, the enhancements provided by both equations indicated similar trends. As observed in Figure 3.9 for both experimental *PTE*s, the higher the NP concentration, the greater the photothermal conversion efficiency. Although this relation was not linear, a rapid increase was noted for both NP sizes when changing from 5.1 to 28.2 ppm, with somewhat asymptotic behavior when moving to the highest concentration. This could be related to the fluid thickness effect, where the absorption efficiency of an NP may vary with fluid depth<sup>[37], [60], [63]</sup>. The maximum enhancement was around 121 % for the sample with the smallest particle size and the highest NP concentration. Similarly, to the water case, comparing these results to the *PTE* enhancements for the water-based Au NFs obtained in previous studies is a difficult task. The references in Table 3.1, which also cover different experimental setups, calculation procedures, light sources, and NP sizes and concentrations, provide a wide range of enhancement variations (from 11 % to 518 %). To help to advance the potential ability of solar NFs for DASC, it is necessary to do

away with the inconsistencies in these *PTE* enhancement results. Round robin tests have been used in the past to overcome the high dispersion of results in other NFs variables, such as: thermal conductivity<sup>[75], [76]</sup>, specific heat capacity<sup>[77]</sup>, contact angle<sup>[78]</sup>, numerical simulation<sup>[79]</sup>, etc. They might help in this case.

### 3.3.5. *PTE* statistical analysis

The experimental data collected for *PTE* were statistically analyzed. The methodology followed for the statistical analyses is depicted in Figure 3.10. The analyses started with an initial normality check by the Shapiro Wilk test<sup>[80]</sup>, along with the homogeneity of variances assumptions and some descriptive data statistics. Parametric tests are used if data exhibit normal distribution, and non-parametric tests otherwise. A comparison of the differences between the mean ranks of the independent groups of the normally distributed variables was performed by independent samples, with T-tests and ANOVAs when there were two groups or more, respectively<sup>[81]</sup>. The Kruskal-Wallis test was employed when the normal distribution assumption was not valid<sup>[82]</sup>.

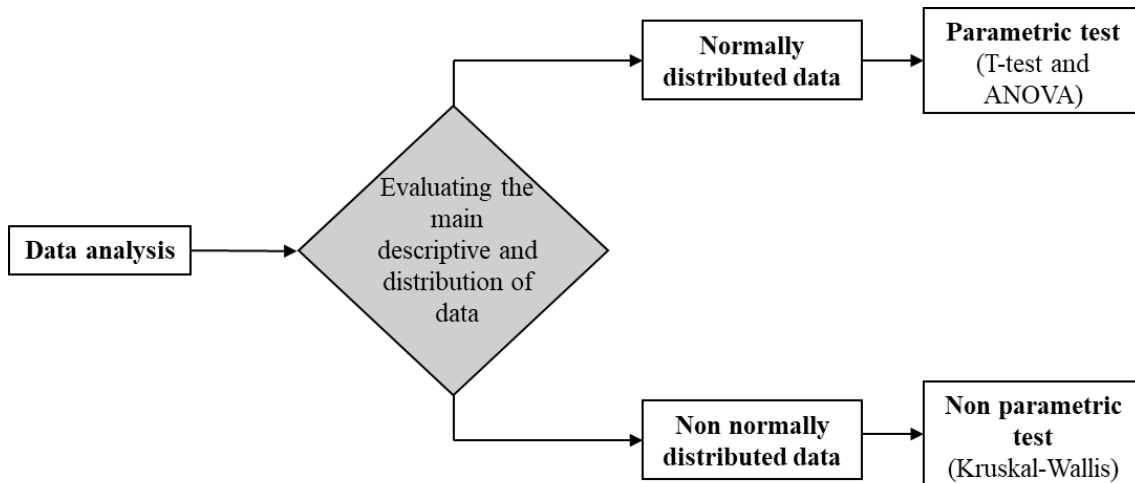


**Figure 3.10.** The statistical methodology of this study.

The statistical analyses were followed with the *PTE* variation based on the independent variables (Au NP concentration,  $[Au]$  and NP size,  $D$ ). As the normal distribution assumption was not valid in this case, the Kruskal-Wallis test was run to investigate the



differences between the means of the *PTE* trends based on the *D* groups. The results are provided in Table 3.7.

**Table 3.7.** Comparison of the means of the *PTE* values based on the NP size (*D*) groups.

	<i>D</i> [nm]	<i>n</i>	Mean	Standard deviation	Mean Rank	Test statistics	<i>p</i>
<i>PTE</i> [%]	0	4	22.390	1.181	2.50	11.312**	0.003*
	5	8	43.983	9.967	13.44		
	20	6	37.903	7.695	8.92		

\*  $p < 0.05$ ; \*\* Kruskal-Wallis test.

The mean rank values of the *PTE* measurements were statistically different based on the *D* groups ( $p < 0.05$ ). For the different *D* values (0, 5, 20 nm), the *PTE* values significantly changed. A *post hoc* Bonferroni analysis was run to determine the group/groups of *D* that brought about this difference. The results showed that the difference between the mean rank values of *PTE* was statistically significant for the *D* = 0 nm (water) and *D* = 5 nm groups ( $p = 0.002$ ). The *D* = 5 nm group obtaining higher *PTE* mean values than those of *D* = 0 nm (water). All the other comparisons were statistically insignificant (i.e., between *D* = 5 nm and *D* = 20 nm, and between *D* = 0 nm and *D* = 20 nm).

To determine the differences between the means of the *PTE* trends based on the [*Au*] groups, the ANOVA test was used because data exhibited normal distribution and more than two groups were present. The results are provided in Table 3.8.

**Table 3.8.** Comparison of the means of the *PTE* values based on the NP concentration [*Au*] groups.

	[ <i>Au</i> ] [ppm]	<i>n</i>	Mean	Standard Deviation	Test Statistics	<i>p</i>
<i>PTE</i> [%]	0	4	22.390	1.181	66.701**	0.000*
	5.1	4	28.323	0.236		
	28.2	4	44.813	4.684		
	51.3	6	47.790	3.913		

\*  $p < 0.05$ ; \*\* ANOVA test.

The results in Table 3.8 revealed that the difference in the mean *PTE* measurement values was statistically significant based on the  $[Au]$  groups ( $p < 0.05$ ). The *post hoc* Bonferroni analysis showed that the  $[Au] = 0$  ppm (water) group's *PTE* mean statistically differed from those of the  $[Au] = 28.2$  ppm and  $[Au] = 51.3$  ppm groups ( $p = 0.000$ ,  $p = 0.000$ ).  $[Au] = 0$  ppm gave a lower *PTE* mean value than the  $[Au] = 28.2$  ppm and  $[Au] = 51.3$  ppm groups. The differences between the mean *PTE* values of  $[Au] = 5.1$  ppm and  $[Au] = 28.2$  ppm, and  $[Au] = 5.1$  ppm and  $[Au] = 51.3$  ppm were statistically significant ( $p = 0.000$ ,  $p = 0.000$ ).  $[Au] = 51.3$  ppm gave the highest *PTE* mean value.

The correlation between the  $[Au]$  and *D* (ordinal) categorical and the *PTE* continuous variables was studied by Kendal's Tau correlation, applied for normally distributed data. The results in Table 3.9 indicate that the correlations between *D-PTE* were not statistically significant ( $p > 0.05$ ). This implies that these variable pairs were not statistically associated with one another. The correlation between  $[Au]$ -*PTE* was statistically significant ( $p < 0.05$ ), with a correlation coefficient between those two variables of 0.770 ( $> 0.60$ ), indicating a positive strong correlation<sup>[83]</sup>.

**Table 3.9.** Correlation analysis between the independent ( $[Au]$ , *D*) and dependent (*PTE*) variables ( $p$ : significance value,  $\rho$ : correlation coefficient).

		<i>PTE</i>
<i>D</i>	$p$	0.305
	$\rho$	0.199
$[Au]$	$p$	0.000*
	$\rho$	0.770

\* $p < 0.05$

### 3.4. Conclusions

Gold, one of the metallic materials that presents SPR, is a good candidate to improve the solar radiation absorption capacity of solar NFs using this property. The suitability of water-based Au NFs to be used in DASC was herein studied. Different particle sizes of 5 nm and 20 nm, and Au concentrations of 5.1, 28.2 and 51.3 ppm, were applied to evaluate the effect of these variables on the study of several properties related to DASC photothermal performance. Some important conclusions can be drawn:

- Commercial Au NFs of both sizes showed good colloidal stability at the maximum temperatures reached during the *PTE* experiments (below 40 °C).
- The extinction coefficient measurements reveal that NFs have an advantage over water for absorbing solar radiation at wavelengths within the visible radiation spectrum.
- For the employed Au NP sizes, NFs presented a plasmon resonance wavelength at 516 and 520 nm for 5 and 20 nm, respectively. This wavelength was independent of the concentration and increases with NP size.
- The influence of particle size on the extinction coefficient was not relevant compared to the Au concentration. The best result was obtained for the NFs at the 51.3 ppm concentration.
- A positive effect on the fraction of absorbed sunlight with the addition of NPs appears, and the penetration distance at which light is absorbed significantly reduces. All this is important for reducing dimensions and costs when designing DASC.
- Two methods were used to calculate photothermal conversion efficiency. The first one does not consider heat losses, but the second calculation method does. Although the absolute values of both *PTE* calculations differ, *PTE* enhancements in relation to water showed similar trends in both cases.
- Enhanced photothermal conversion efficiency takes place for all the tested NFs. The maximum 121 % *PTE* enhancement in relation to the base fluid was obtained for the NF with 5 nm NPs at the 51.3 ppm concentration.
- A statistical analysis can be used to evaluate the influence of the input variables on the *PTE* results. It confirms that NP size ( $D$ ) and Au concentration ( $[Au]$ ) statistically and significantly influence *PTE*.
- For the entire dataset, the correlations between  $D$ -*PTE* were not statistically significant. So, these variable pairs were not statistically associated with one another, while the correlations between  $[Au]$ -*PTE* were statistically significant, positive and strong.
- Although the Au concentration positively impacts *PTE*, the increase in *PTE* within the measured concentration range was not linear. A threshold was obtained beyond which no further improvement can be achieved.
- Given the high dispersion of the photothermal conversion efficiency present in the literature, comparing the results to previous works is not easy. A round robin

test might be interesting to overcome this high dispersion and to help to advance in the potential application of solar NFs in DASC.

From the future DASC industrial application point of view, the results in this paper highlight the advantage of using smaller sized NPs (thanks to the lower Au concentration improving the *PTE* results) and the reduction in the required NF volume to reduce collector depth. Both have a positive effect on the DASC cost.

**CHAPTER 4.**

**Photothermal Properties and  
Performance of Hybrid Carbon-  
Paraffin/Water Emulsions**



## **4. Photothermal properties and performance of hybrid carbon-paraffin/water emulsions**

Solar thermal energy has attracted renewed research interest for its excellent energy efficiency among different types of solar technologies. However, the limiting factor of them all is the intermittent nature of solar radiation. To overcome this drawback, it is possible to store absorbed light in form of heat using emulsions with phase change materials (PCMs) dispersed in solar nanofluids by combining the advantage of solar thermal storage characteristics of PCMs and the higher light absorption capacity of solar nanofluids. In this study, paraffin/water and hybrid carbon-paraffin/water emulsions with 5 wt. % paraffin wax RT44HC as PCM are proposed. Low-cost emulsions with proven colloidal stability were successfully produced, with and without small amounts of oxidized carbon black nanoparticles (0.01 wt. %) dispersed in the emulsion. Thermal energy storage capacity improved up to 16 %, while maintaining good thermal conductivity properties. Optical properties were evaluated by means of a spectrophotometer with an integrating sphere, including both spectral absorptance and reflectance of the samples. Two experimental setups were developed with concentrated light, to evaluate the photothermal conversion efficiency under simulated and natural sunlight. The improvement of the light to heat conversion properties provided by the oxidized carbon black nanoparticles was confirmed, with *PTE* values of 1.5- and 2.7-fold better than the base fluid (water) using a solar simulator and natural sunlight, respectively.

#### 4.1. Introduction

The global climate emergency has forced society to look for alternatives to produce sustainable clean energy. A variety of renewable energy sources is being proposed to replace or minimize the use of fossil fuels, including biomass, geothermal, hydropower, solar and wind<sup>[84]</sup>. Of them, solar energy has become an effective and potential way to achieve sustainable human development. Taking the leap from conventional fossil fuel energy production to renewable energy sources, such as solar, also implies an imbalance between production and demand. For this reason, thermal energy storage (TES) is one of the most promising ways to improve the efficiency and energy demand faced by society mainly due to industrial revolution<sup>[85], [86]</sup>.

Solar collectors in which solar radiation is absorbed directly on a dark surface and then thermal energy is transferred to a heat transfer fluid (HTF) are the commonest technology used to convert solar radiation into heat. This collector type offers good efficiencies. However, during the process of transferring heat from the surface to fluid, losses that limit systems' efficiency occur. To improve this collector type, in the 1970s<sup>[12]</sup> the alternative of exposing HTF directly to incident radiation to, thus, absorb heat volumetrically, but not superficially, was proposed. These systems are now known as direct absorption solar collectors (DASC). In DASC systems, the possible effect of heat losses by conduction and convection processes is neglected compared to conventional collectors through direct absorption. However, the HTFs traditionally used in these systems (i.e. water, alcohols, oils, molten salts, etc.)<sup>[15]</sup> are mostly transparent over most of the solar spectrum, which makes them inefficient in absorbing light and, thus, reduces the heat conversion efficiency ability of light<sup>[55]</sup>.

To solve the issue raised by these HTFs, employing nanofluids (NFs), consisting of the dispersion of nanoparticles (NPs) with a size range from 1 to 100 nm in a base fluid, was proposed. These NFs, capable of improving solar radiation absorption with very low concentrations of NPs in the base fluid, were named solar nanofluids by *Otanicar et al.* in 2009<sup>[21]</sup>. Many NPs of different natures have since then been studied to improve not only optical and thermal properties, but also photothermal conversion efficiency (*PTE*) of these solar NFs, including metals<sup>[17], [24], [37], [59], [60]</sup>, metal oxides<sup>[25], [87]</sup>, carbon-based materials<sup>[34], [67]</sup>, hybrid with composites different NPs<sup>[27], [41], [70]</sup>, and even biodegradable and more sustainable materials<sup>[28], [71], [72]</sup>. Of them, carbon-based NFs are considered an



interesting potential candidate for their highlighted thermal and optical properties. DASC efficiency depends on the several solar NFs factors, such as nanoparticles type, size, shape, concentration, etc.<sup>[42]</sup>. In particular, spectral optical properties (i.e. absorptance and reflectance) play a key role in photothermal conversion applications<sup>[32], [88], [89]</sup>.

In addition to the photothermal conversion process, the solar NFs used in DASC can store absorbed thermal energy. Thermal energy storage technologies can be classified into three main categories: sensible heat storage (SHS)<sup>[90]</sup>; latent heat storage (LHS)<sup>[91]</sup>; thermochemical heat storage (TcHS)<sup>[92]</sup>. The highest energy value commonly stored in SHS is (10-50 kWh·t<sup>-1</sup>), (50-150 kWh·t<sup>-1</sup>) in LHS and (200 kWh·t<sup>-1</sup>) in TcHS<sup>[93]</sup>. Compared to TcHS, the technology of both SHS and LHS is more advanced for commercial TES applications. In this regard, solar NFs commonly store thermal energy through the sensible heat of fluid in the liquid phase, which depends on temperature variation and the material's specific heat capacity, with no phase change taking place<sup>[94], [95]</sup>. Water is the most commonly used base fluid for its availability, low-cost, high specific heat capacity and safety.

Another method by which thermal energy can be stored or released is in the form of latent heat via phase change materials (PCMs), which is exploited at a constant temperature during phase change processes (melting and crystallization) and provides a high thermal energy storage density over a narrow temperature range. These materials are capable of storing and releasing large amounts of energy in the form of latent heat during the phase change process, of which the commonest is solid-liquid phase change<sup>[96]</sup>. Different types of organic and inorganic phase change materials are available, with paraffin (saturated hydrocarbons of C5-C15 in liquid and > C15 in the solid state) being the most widely used organic compound for solar-thermal energy storage<sup>[97]</sup>. These organic PCMs possess interesting properties, such as the possibility of being used over a wide range of temperatures, and having high phase change enthalpy, high heat capacity, non-corrosive nature, low vapor pressure, no phase segregation, negligible supercooling and good stability<sup>[98]</sup>. However, the thermal conductivity of PCMs is poor, which affects effective heat transfer properties.

Subsequently, addition of PCMs to solar NFs to produce an emulsion, combines the advantage of the thermal storage characteristics of PCMs with the increased light absorption capability of solar NFs<sup>[99]-[101]</sup>. Increased thermal conductivity can also be achieved compared to bulk PCMs by, thus, enhancing the photothermal conversion and

heat storage in DASC systems<sup>[102]–[104]</sup>. These emulsions are characterized by their simple preparation process, a wide range of commercial applications, low-temperature resistance and low cost. However, one of the main issues is colloidal instability, which is generally due to several thermodynamic reasons such as coalescence or Ostwald ripening, creaming, flocculation, etc.<sup>[50], [105], [106]</sup>. Stable emulsions must be formed in such a way that paraffin droplets do not increase in size and phase separation does not occur.

It is for all these reasons that the thermal and optical properties, as well as the colloidal stability of PCM emulsions have been extensively studied in recent years<sup>[107]–[111]</sup>. Several works have investigated their stability by different encapsulation methods, the preparation of low/high energy techniques, the selection of surfactants and their synthesis methods<sup>[101], [112]</sup>.

In thermal energy storage applications, such as DASC systems, PCM emulsions need to be pumped and droplets are subjected to continuous solid-liquid phase change. Therefore, stability must be tested over time after many cycles of thermal changes, where other processes like shear stress also occur<sup>[50], [113]</sup>. A commonly used stabilization method consists in the addition of surfactants, which are organic molecules containing two opposing halves: a polar part of hydrophilic nature and a non-polar hydrophobic part. Due to this difference in affinities, surfactants tend to be mostly located at interfaces or on surfaces, which, thus, orientates the polar part of the molecule in the direction of water and its non-polar part in the opposite direction, e.g., in the paraffin phase. Based on the nature of the hydrophilic part, surfactants can be classified into two main categories: ionic and non-ionic. Many studies have been carried out applying these surfactants (i.e. SDS, CTAB, Span, Tween, etc.)<sup>[114]–[116]</sup> to paraffins with different melting. The stability of the emulsions was studied by analyzing particle sizes using different techniques, observing the separation of phases with the time of stored samples, carrying out tests by applying thermal cycles, etc.<sup>[50], [117]–[119]</sup>.

Addition of NPs and paraffin to water to produce emulsions with enhanced solar absorption capacity, thermal energy storage, thermal conductivity and *PTE* has been explored in recent years. The excellent combination of properties provided by the mixture of solar NPs and PCM makes it possible to use this type of material in a wide range of applications such as DASC systems based on parabolic trough collectors in solar thermal systems. Such systems can be used in desalination functions, drying processes, heating and cooling loops and power generation plants<sup>[99], [120]</sup>. For low and medium temperatures,

the most common applications for these types of systems include solar water heaters, solar air heaters, solar stoves and solar photovoltaic-thermal systems, among others<sup>[121]</sup>,<sup>[122]</sup>. Table 4.1 summarizes previous works that have incorporated PCMs with different types of carbon-based NPs, in which important properties for understanding the behavior of emulsions like HTFs and TES material in DASC systems are described. In all the cases, the energy source was a solar simulator.

Table 4.1. Review of the characterization of carbon-PCM emulsions.

Author (Year) [Ref]	Base fluid/surfactant	PCM: Type/ Concentration [wt.%]/ $T_m$ [°C]	NPs: Type/ Concentration [wt.%]	Colloidal stability measurement technique*	Thermal properties	Optical properties	Photothermal performance: Max $T$ [°C]/ Max $PTE$ [%]
<i>Yuan et al.</i> 2015 <sup>[123]</sup>	DI water/ Span80- Tween80, SDS	Paraffin/ 7.5/ 50.1	GO-(SiO <sub>2</sub> )/ 0.005	N/A	$c_p$ , $\Delta H$ , $k$ and thermal cycling	Absorbance and transmittance	80/ 85
<i>Wang et al.</i> 2016 <sup>[124]</sup>	Water/ PVA and PEG-600	Paraffin/ 20/ 48.9	Graphite/ 0.05-0.1	DLS and VI	$c_p$ , $\Delta H$ and $k$	N/A	80.1/ 91.5
<i>Liu et al.</i> 2017 <sup>[125]</sup>	Ionic liquid ([BMIM][BF <sub>4</sub> ])/ SMA1000HNa	Paraffin/ 0-2.67/ 49.4	Graphite/ ~ 0.05	VI	$c_p$ , $\Delta H$ , $k$ and thermal cycling	Absorbance	113.2/ N/A
<i>Wang et al.</i> 2018 <sup>[126]</sup>	Water/ PVA and PEG-600	Paraffin/ 15-25/ 62-64	GNP/ 0.04-0.1	N/A	$c_p$ , $\Delta H$ , $k$ and thermal cycling	Absorbance	80.5/ N/A
<i>Yuan et al.</i> 2018 <sup>[127]</sup>	DI water/ SDS	Paraffin/ 8/ 49.4	GO/ N/A	N/A	$c_p$ , $\Delta H$ , $k$ and thermal cycling	N/A	77/ 80
<i>Liu et al.</i> 2019 <sup>[128]</sup>	DI water/ SDS	Dodecanol/ 43/ 26	GO and CNT/ 1.2	$\zeta$ -potential	TGA, $\Delta H$ , $k$ and thermal cycling	Transmittance	79/ N/A

<i>Wang et al.</i> 2019 <sup>[129]</sup>	Water-Ethanol/ N/A	Paraffin@melamine/ 5-15/ 49.8	MWCNT/ 0.005	DLS and VI	$\Delta H$	Transmittance	79.8/ N/A
<i>Latibari et al.</i> 2019 <sup>[130]</sup>	DI water/ PVA	Cr60 wax/ 11.5/ 61.9	GNP/ 0.04-0.1	DLS	$c_p$ , $\Delta H$ and TGA	Transmittance	85/ N/A
<i>Zhao et al.</i> 2019 <sup>[131]</sup>	DI water/ PVA, PEG- 600, SMA	Paraffin/ 11/ 42-44	GO / 0.1-0.3	DLS and VI	$\Delta H$ , $k$ and thermal cycling	N/A	51.31/ N/A
<i>Agresti et al.</i> 2019 <sup>[132]</sup>	DI water/ SDS	RT55HC and RT70HC/ 2-10/ 55 and 70	SWCNT/ 0.002-0.01	DLS, $\zeta$ - potential and VI tests	$c_p$ , $\Delta H$ , $k$ and $\alpha$	Mass extinction coefficient	N/A
<i>Zhang et al.</i> 2020 <sup>[133]</sup>	DI water/ SDS	n-octadecane/ 10 and 20/ 30.9	MWCNT/ 0-1	DLS	$\Delta H$ and $k$	N/A	N/A
<i>Gao et al.</i> 2020 <sup>[134]</sup>	DI water/ SDS	MPCM octadecane with Fe <sub>3</sub> O <sub>4</sub> / 5-20/ 29.06	MWCNT/ 0.005-0.02	N/A	$c_p$ , $\Delta H$ , $k$ , TGA and DTA	Transmittance	37.5/ N/A
<i>Barison et al.</i> 2021 <sup>[135]</sup>	Water/ SDS	RT21HC and RT55HC/ 5/ 21 and 55	GO / 0.05-0.2	DLS (time)	$\Delta H$ , $k$ and $\alpha$	Mass extinction coefficient	N/A

\*VI: Visual Inspection

Table 4.1 reveals how thermal properties of emulsions with phase change materials were extensively studied experimentally. However, less deep analysis was performed on the optical and photothermal properties. Emulsions with a dispersion of PCMs, that maximize the thermal energy storage capacity, and carbon-based NPs, that improve optical behavior, in the base fluid require a detailed analysis of the optical parameters. In the previous studies presented in Table 4.1 optical properties of these materials were studied by direct measure of absorbance and transmittance, but as they are generally opaque materials with high light scattering, it is necessary to analyze the effect of light reflectance to know its effect on the global absorption capacity of solar radiation. Also, as can be seen, the photothermal conversion performances made in the reviewed research were done in all cases by measuring temperature increments of the samples when exposed to simulated sunlight. Furthermore, it can be concluded from Table 4.1 that less attention was paid to the colloidal stability. Stabilization was generally done by the addition of surfactants, being SDS widely used in most research, together with PVA or PEG-600. In this work a deeper analysis was carried out by testing the effect of different surfactants on the colloidal stability of the emulsions also when submitted to thermal cycling. Finally, from the point of view of the materials, multiple types of carbon-based nanoparticles were analyzed with different concentrations, from 0.002 to 1.2 wt. %. GO and CNT were the most widely used allotropes in the literature, synthesized through different methods but no studies using carbon black NPs were available.

In this article, the thermal, optical and photothermal properties of carbon-paraffin/water emulsions were studied in-depth. Paraffin RT44HC (5 wt. % in relation to water) and oxidized carbon black (CBox) NPs (0.01 wt. %) were dispersed in distilled water. The step forward in the present work was the fabrication of the emulsions choosing SDS from a large set of surfactants as it provided the best colloidal stability for the resulting emulsions. Also, CBox nanoparticles were used for the first time in this type of carbon hybrid emulsions. This carbon material present excellent light absorption properties<sup>[136]–[138]</sup>, are easily available and economical, therefore being promising for DASC applications. The specific heat capacity, phase change enthalpy and thermal conductivity of DI water, pure paraffin emulsion (RT44HC/water, pure emulsion) and hybrid carbon-paraffin emulsion (CBox-RT44HC/water, hybrid emulsion) were experimentally measured to analyze the influence of carbon black and paraffin. Furthermore, experimental thermal properties were compared with the theoretical calculated results. To

deeply understand the light-sample interactions and in addition to the absorbance measurement, reflectance was analyzed using an integrating sphere spectrophotometry system capable to investigate the high effect of the scattering in emulsions absorbance. *PTE* tests were carried out under two new developed facilities for different conditions to obtain a better approach to emulsions' behavior in real practical applications: one using a solar simulator and another exposing samples to natural sunlight.

## 4.2. Materials

### 4.2.1. Raw materials

In order to prepare pure and hybrid emulsions, paraffin wax RT44HC (Rubitherm Technologies GmbH) was used. According to the manufacturer, RT44HC exhibits a melting temperature between 41 - 44 °C (main peak at 43 °C), a specific heat capacity of  $2 \text{ kJ}\cdot\text{kg}^{-1}\cdot\text{K}^{-1}$  and a heat storage capacity of  $250 \text{ kJ}\cdot\text{kg}^{-1}$  (combination of latent and sensible heat over a range of 15 °C). As reported in *Burgos et al.* [139], this paraffin was selected from among three commercial paraffin waxes of this brand within the temperature range of the water applications, because it provided the highest thermal energy storage capacity.

For the carbon NPs, spherical carbon black NPs, were supplied by Cabot Corporation. Commercial NPs ELFTEX 570 consist of clusters of amorphous carbon with a primary particle size of 10 nm (see Figure 4.1). To ensure compatibility with the base fluid and stability, carbon black was oxidized (CBox) with hydrogen peroxide at 120 °C with magnetic stirring following the method reported in *Han et al.*[67].

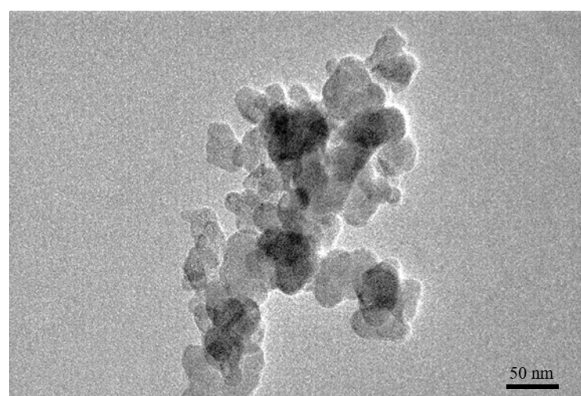


**Figure 4.1.** TEM micrograph of the carbon black nanoparticles.

To improve the stability of hybrid emulsions, a surfactant was needed. Different commercial surfactants (provided by Sigma Aldrich, Ltd.) were used as stabilizers to evaluate their effect on the stability of emulsions. The tested ionic surfactants included sodium dodecylbenzene sulphonate (SDBS), sodium dodecyl sulphate (SDS), benzalkonium chloride (BAC), hexadecyltrimethylammonium bromide (CTAB) and methyltriphenylphosphonium bromide (CTPB). The non-ionic surfactants were polyvinylpyrrolidone (PVP), Triton X-100 (Triton) and diphenyl sulphone (DS).

#### **4.2.2. Emulsions**

Initially, to prepare the pure emulsion (RT44HC/water), the corresponding amount of the surfactant was dissolved in distilled water with magnetic stirring. Then paraffin was added to the dissolution and sonicated for 3 minutes at 50 % input energy with an ultrasound probe (Sonopuls, HD2200, Bandelin, 200 W). During the sonication process, the sample was heated up to a temperature higher than the paraffin melting temperature. Then, emulsions were cooled down after sonication.

To prepare the hybrid emulsion (CBox-RT44HC/water), CBox was first dispersed in distilled water with the ultrasound probe for 2 minutes. Then the surfactant was dissolved in the carbon-water NF with magnetic stirring. Finally, paraffin was added to the NF and sonicated for 3 minutes at 50 % input energy with the ultrasound probe. Emulsions were also heated up during the sonication process and then cooled down.

The paraffin:water ratio for all the samples was kept at 5:95 per weight, while the selected surfactant:paraffin ratio was 1:8 per weight. This surfactant:paraffin ratio was chosen following previous studies with similar paraffin waxes and carbon NPs<sup>[132], [135]</sup>. The CBox concentration was set at 0.01 wt. % in relation to the total emulsion.

### **4.3. Experimental techniques**

#### Particle diameter, $D$

The size distribution of the solid particles in emulsions was analyzed by the dynamic light scattering (DLS) technique with a Zetasizer Nano ZS instrument (Malvern Instruments



Ltd.). Size can be known from the light scattered by particles due to their Brownian motion and signal intensity. The equipment comprises a laser centered at 532 nm and a detector that acquires the intensity of the light scattered by suspended particles. The hydrodynamic diameter is calculated based on the intensity of the scattered light at 173°. It also contains a Peltier heating system that can heat samples. Measurements were taken at 25 °C and 70 °C, and at 25 °C again to evaluate the degree of dispersion of particles at different temperatures and the stability of samples with thermal cycling, including the paraffin phase change.

Several measurements were carried out for each sample at the temperatures tested and the experimental error was obtained from the standard deviation by means of Equation A.2 in Section 8.1 Uncertainty analysis. The average values were 2.7 % and 7.6 % for SDS and CTAB samples, respectively.

#### Specific heat capacity, $c_p$ , and phase change enthalpy, $\Delta H$

Both the SHS and LHS of samples were studied by differential scanning calorimetry (DSC, DSC2 Mettler Toledo). Two different thermal cycles were run to measure specific heat capacity and phase change enthalpy. The areas method was applied to study specific heat at 25 °C (solid phase) and 60 °C (liquid phase). A 1 °C-temperature step was applied at each temperature, with 5 minutes isothermal stabilizations before and after each step. To obtain information about the melting and crystallization process, samples were submitted to a thermal cycle from 15 °C to 65 °C, with 5 K·min<sup>-1</sup> heating and cooling rates, and 5-minute isothermal stabilization at the maximum and minimum temperatures. All the tests were carried out at a constant 25 ml·min<sup>-1</sup> N<sub>2</sub> flow rate. An aluminum crucible (40 µl) was used. Three samples of each fluid (17 mg) were prepared and two cycles were run to obtain an average value. The experimental error was statistically obtained from the standard deviation by means of Equation A.2 in Section 8.1 Uncertainty analysis, with average values of 3.5 % and 6.9 % for  $c_p$  and  $\Delta H$ , respectively.

#### Thermal conductivity, $k$

Thermal conductivity was measured by the transient hot wire technique using a TEMPOS conductimeter (Meter). The device was calibrated following the manufacturer's recommendations with a glycerin verification standard before measurements. Samples were placed inside a sealed glass tube (40 ml) where the sensor was vertically inserted. To run the test at a specific temperature, the tube was immersed in a thermostatic bath at

a controlled temperature. Measurements were taken at 25 °C and 60 °C. Five tests were run for all the samples to obtain an average value. The experimental error was statistically obtained from the standard deviation by means of Equation A.2 in Section 8.1 Uncertainty analysis, with an average value of 1.9 %.

### Optical properties

Optical properties were measured at room temperature with a V-780 UV/Vis/NIR (Jasco) (wavelength accuracy of  $\pm 0.3$  nm at 656.1 nm and  $\pm 1$  nm at 1,312.2 nm) spectrophotometer equipped with an integrating sphere. The span of the wavelength range of measurements was 300-1,400 nm, which covers 92.8 % of total solar radiation. Due to samples' high opacity, a 1 mm-thick cuvette was used.

$$a(\lambda) = 100 - R(\lambda) - T(\lambda) \quad (4.1)$$

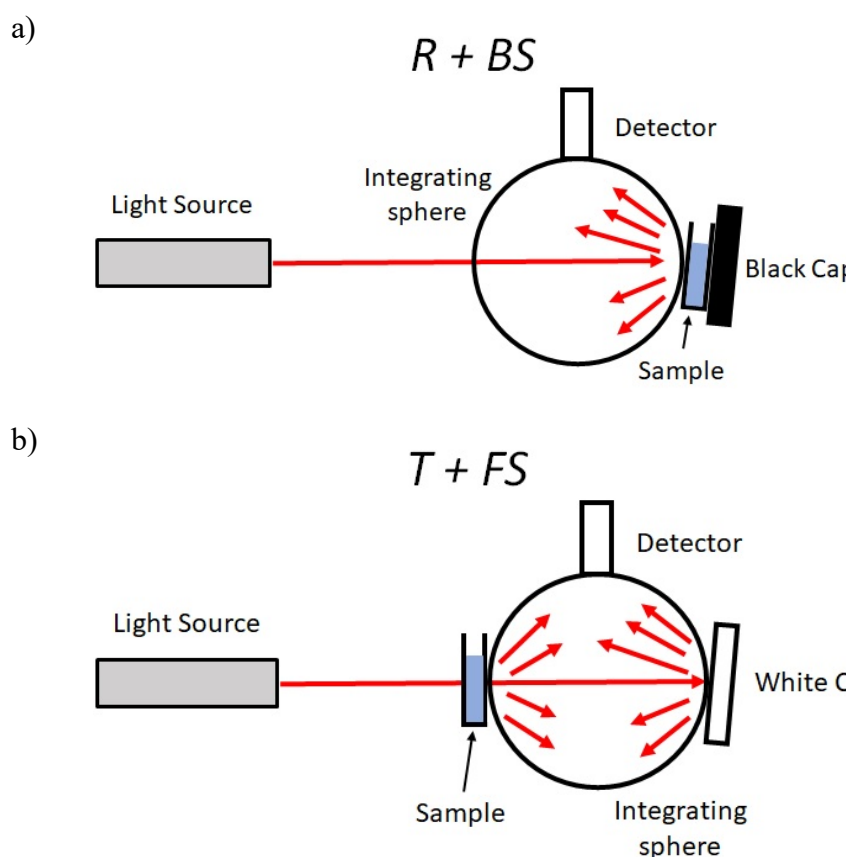


**Figure 4.2.** Diagram of spectrophotometer configuration when measuring a) reflectance + backward scattered signal (R+BS) and b) transmittance + forward scattered signal (T+FS).

Spectral absorptance ( $a(\lambda)$ ) was calculated from spectral reflectance ( $R(\lambda)$ ) and the transmittance ( $T(\lambda)$ ) measurements. For reflectance, signal intensity included both the light directly reflected by the sample, together with that scattered backward. For transmittance, signal intensity included both the light directly transmitted through the sample, together with the forward scattered intensity. Figure 4.2 illustrates the measuring configuration for both these optical measurements. Having acquired the experimental data, the different samples' spectral absorptance was calculated using the following equation:

Photothermal conversion efficiency, PTE

The measurements to determine the efficiency of fluids to transform solar energy into thermal energy were obtained in two different experimental setups: one using a solar simulator (SS) (Figure 4.3a) and a second one employing natural sunlight (NS) (Figure 4.4a). The first experimental setup involves a cylindrical custom-made sample holder made of Teflon with an inner diameter of 18.2 mm and 11 mm high (Figure 4.3b). The sample holder was insulated with an expanded polystyrene container to minimize heat losses. To evaluate the sample's temperature distribution, three k-type thermocouples (RS PRO K-228-7451 with  $\pm 1.5$  °C measurement uncertainty) were inserted 3 mm from the inner wall at different depths (top:  $z = 0.2$  cm, medium:  $z = 0.5$  cm and bottom:  $z = 0.7$  cm). Another thermocouple was used to record the ambient temperature evolution. Samples (3 g) were illuminated by a collimated radiation source from a solar simulator (NEWPORT 91195A-1000 class A solar simulator & SPECTRA-PHYSICS 69920 Universal Arc Lamp Power Supply ORIEL), under an illuminated condition of  $1,000 \text{ W}\cdot\text{m}^{-2}$ , which was concentrated by means of a Fresnel lens and a filter. A potentiometer (Ophir 1Z01500, Nova Display) was used to evaluate the power that resulted from the incident radiation at the sample position, measured as 3.5 suns.



**Figure 4.3.** Solar simulator *PTE* a) experimental setup and b) custom-made sample holder.

The second experimental setup (Figure 4.4a) consisted of a custom-made adjustable aluminum structure including four Fresnel lenses (Orafol SC 213-600) to concentrate the NS. The concentrated intensity in experiments was 136 suns. The structure allowed manual sun tracking so that the sun's rays were always perpendicular to the surface of lenses and quartz glass tubes. Samples (42 g) were placed inside four cylindrical tubes (Figure 4.4b). The quartz glass tubes (25 mm inner diameter, 50 outer diameter, 150 mm long) were custom-made for high-temperature resistance purposes and contained a vacuum interlayer to reduce heat losses by convection to ambient air. To obtain samples' temperature distribution, one k-type thermocouple (Inconel 600 with  $\pm 2.5$  °C measurement uncertainty) was immersed in the central radial tube position ( $z = 1.25$  cm depth from the illuminated surface) and in the center of the focused spot. Another k-type thermocouple outside the setup was used to measure the ambient air temperature. A pyranometer (MS-102; irradiance range of 0-4,000  $\text{W}\cdot\text{m}^{-2}$ ) was utilized to measure solar radiation during the process.

In both experimental setups, temperature evolution was recorded by a data acquisition system comprising a data logger (Agilent 34970 A) linked to a computer. For each sample, experiments were repeated up to 8 times, and the average temperature rise values were taken into account for further analyses.

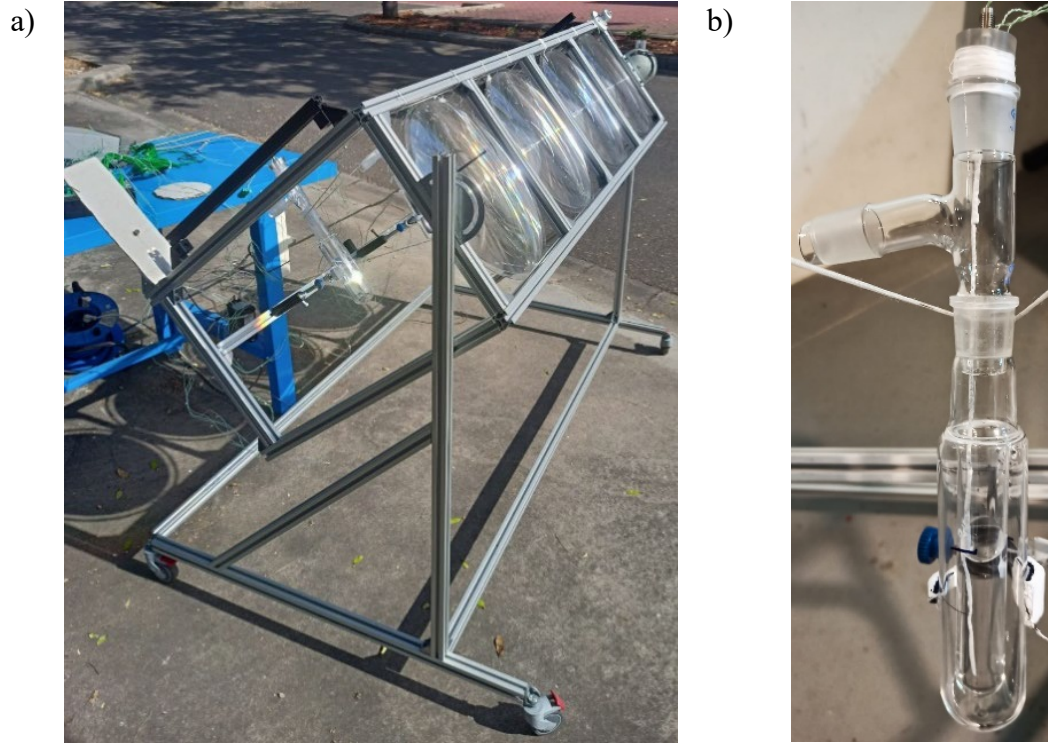


**Figure 4.4.** Natural sunlight *PTE* a) experimental setup and b) quartz glass tube.

To quantify *PTE*, it was calculated as the ratio between the power energy absorbed ( $W_a$ ) in relation to the power of incident radiation ( $W_0$ ) on the sample<sup>[17], [18], [140]</sup>.

$$PTE = \frac{W_a}{W_0} = \frac{Q_{total,sample}}{W_{measured} \cdot \Delta t} \quad (4.2)$$

where  $Q_{total,sample}$  is the total thermal energy stored,  $W_{measured}$  is the power measured in the sample position with the potentiometer and  $\Delta t$  is the time interval associated with the temperature step ( $\Delta T$ ).  $Q_{total,sample}$  was calculated by including both the SHS of samples (within the measured temperature range) and LHS due to paraffin melting:

$$Q_{total,sample} = m \cdot c_{P,sol} \cdot \Delta T_{sol} + m \cdot \Delta H_m + m \cdot c_{P,liq} \cdot \Delta T_{liq} \quad (4.3)$$

where  $m$  is the sample mass,  $c_P$  is samples' specific heat capacity for either the solid or liquid state, and  $\Delta H_m$  is the sample's melting phase change enthalpy. The experimental datasets presented in Table 4.3 were used for these calculations. The experimental error

was statistically obtained from the standard deviation by means of Equation A.2 in Section 8.1 Uncertainty analysis, with an average value of 5.2 % and 13.9 % for solar simulator and natural sunlight setups, respectively.

## 4.4. Results and Discussion

### 4.4.1. Stability

To analyze the degree of dispersion of PCM and the CBox NPs in the base fluid and its colloidal stability with thermal cycling between 25 and 70 °C, a visual inspection of emulsions was first carried out. Then samples' particle size distribution with the best visual results was analyzed by means of DLS measurements.

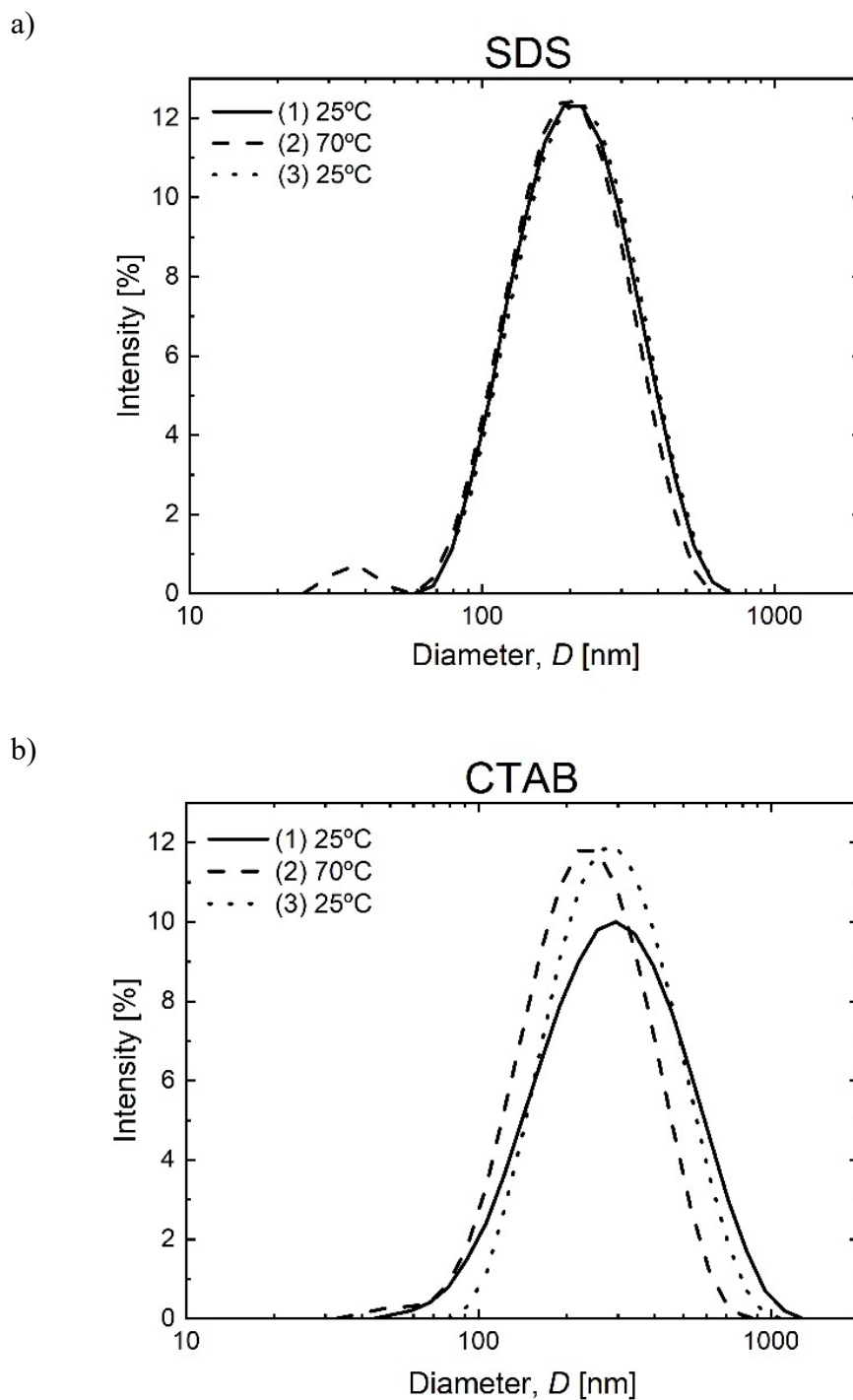
Initially, the stability (with both time and thermal cycling) of the RT44HC/water samples using different surfactant types was evaluated. Samples were left inside a refrigerator (7 °C) for 1 h immediately after fabrication. Then they were heated at 70 °C in an oven for 1 h and finally left at room temperature.

Table 4.2 summarizes the results of the initial visual inspection of the pure emulsions with the different surfactants 3 days after fabrication. The samples containing PVP, Triton, DS and CTPB were discarded for the different problems reported in Table 4.2. Next the samples that showed a good degree of stability were measured by DLS at different temperatures (first at 25 °C, next at 70 °C, and then again at 25 °C). Emulsions, including SDBS and BAC, were discarded due to wider particle size variations with the applied temperature cycle. Finally, SDS and CTAB were chosen as the best stabilizers according to the DLS results with thermal cycling. Taking into account the DLS measurements, samples were submitted to a total number of two thermal cycles.

**Table 4.2.** Surfactants and comments about the VI and DLS tests for the different RT44HC/water-surfactant emulsions.

Sample	Surfactant	Comments (VI: Visual inspection; DLS: particle size)
RT44HC/water	PVP	VI: Solid PCM at the top
	Triton	VI: Stable, but highly viscous
	DS	VI: Phase separation
	CTPB	VI: Phase separation
	SDBS	VI: Stable DLS: Not stable with thermal cycling
	BAC	VI: Stable DLS: Not stable with thermal cycling
	SDS	VI: Stable DLS: Stable with thermal cycling
	CTAB	VI: Stable DLS: Stable with thermal cycling

Having proved that SDS and CTAB provided the best stability for the pure emulsions, hybrid emulsions stability with these surfactants was also checked after adding CBox. Figure 4.5 shows the DLS measurements for both hybrid emulsions, including the results for thermal cycling (25 °C – 70 °C – 25 °C). The obtained average particle sizes for the different temperatures were 208 – 195 – 207 nm for the hybrid emulsion using SDS and 286 – 232 – 284 nm for that using CTAB. It can be concluded that the hybrid emulsion with SDS provided better stability results and a smaller droplet size than that with CTAB and was, therefore, used for the final synthesis of emulsions.



**Figure 4.5.** Particle size distribution of CBox-RT44HC/water emulsions with a) SDS and b) CTAB.

Figure 4.6 presents different images of samples 3 days after their synthesis, including or not the optimal surfactant and the CBox NPs. As the images depict, addition of SDS provided homogeneous samples, and avoided phase separation and NP sedimentation.





**Figure 4.6.** Images of RT44HC/water and CBox-RT44HC/water emulsions without and with SDS surfactant 3 days after fabrication.

#### 4.4.2. Thermal characterization

Figure 4.7 shows the heat flux curves obtained for pure paraffin (left *Y*-axis) and both emulsions (right *Y*-axis), and both without and with CBox NPs, and thermally characterized with DSC. It can be observed that the melting temperature of bulk paraffin and emulsions well agrees with the value given by the manufacturer (main peak at 43 °C). However, the crystallization temperature dropped when paraffin was dispersed in the

emulsion, which led to greater supercooling than the bulk material due to the smaller nucleation interface<sup>[49], [141], [142]</sup>.

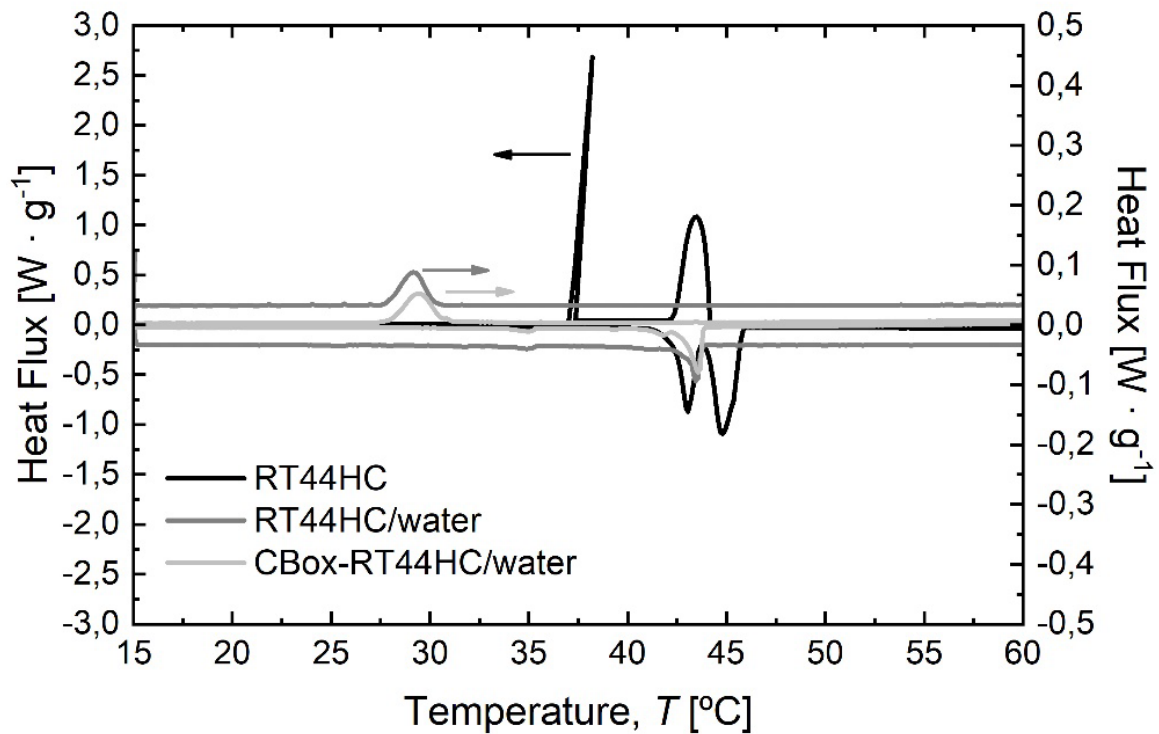


**Figure 4.7.** DSC curves for bulk RT44H, RT44HC/water and CBox-RT44HC/water emulsions.

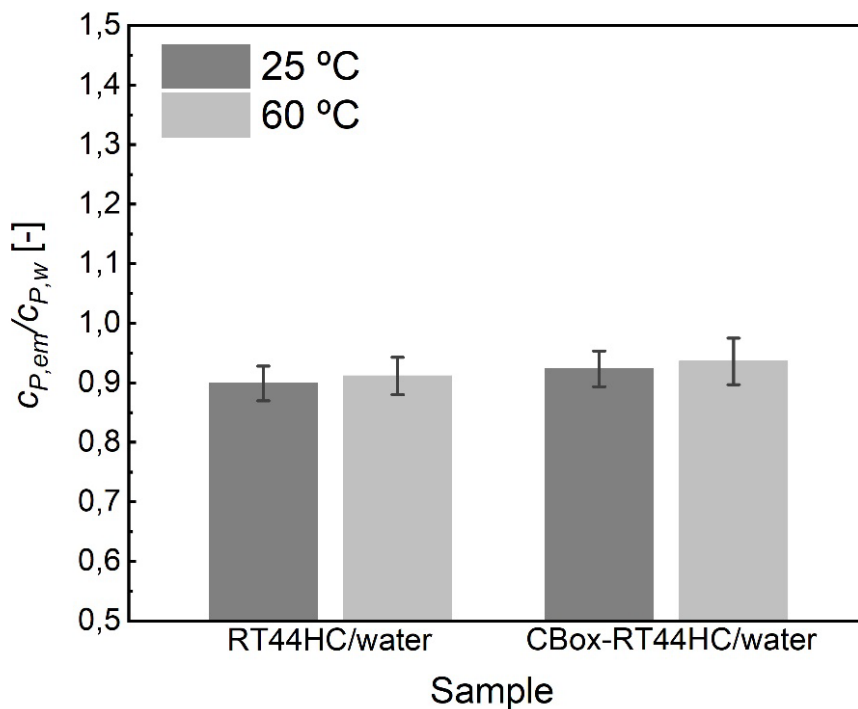
Table 4.3 shows the experimental DSC results, and also the theoretical values (from the literature<sup>[143]</sup>, the manufacturer, or calculated by the mixture rule) for specific heat ( $c_p$ ) and melting phase change enthalpy ( $\Delta H_m$ ). The experimental results presented variable deviations compared to the theoretical data for both water and paraffin RT44HC. Differences of the same order of magnitude appear in previous studies<sup>[144], [145]</sup>. For emulsions, both thermal properties were also experimentally measured by DSC and agreed well with the theoretical values calculated by applying the mixture rule.

In Figure 4.8 the specific heat capacity ratio is presented including error bars calculated according to Equation A.5 in Section 8.1 Uncertainty analysis, for relative values. Although an expected reduction in the sensible heat was observed (Figure 4.8) when adding paraffin, the contribution of its latent heat compensated for emulsions' total thermal energy stored ( $Q_{total}$ ).  $Q_{total}$  was calculated as the addition of the sample's SHS (within a temperature range of 15 °C) and LSH due to paraffin melting. A 16 % increase

for  $Q_{total}$  was obtained for the hybrid emulsion versus water when the experimental values were used.

**Table 4.3.** Specific heat capacity data (theoretical and experimental) at 25 °C and 60 °C and melting phase change enthalpy.

Sample	$c_{P, 25\text{ °C}}$	$c_{P, 60\text{ °C}}$	$\Delta H_m$	$c_{P, 25\text{ °C}}$	$c_{P, 60\text{ °C}}$	$\Delta H_m$
	(theor) [kJ·kg <sup>-1</sup> ·K <sup>-1</sup> ]	(theor) [kJ·kg <sup>-1</sup> ·K <sup>-1</sup> ]	(theor) [kJ·kg <sup>-1</sup> ]	(exp) [kJ·kg <sup>-1</sup> ·K <sup>-1</sup> ]	(exp) [kJ·kg <sup>-1</sup> ·K <sup>-1</sup> ]	(exp) [kJ·kg <sup>-1</sup> ]
Water	4.18	4.18	-	4.38	4.36	-
RT44HC	2	2	220	2.02	2.57	251.14
RT44HC/water	4.07	4.08	11.00	3.95	3.98	10.85
CBox-RT44HC/water	4.07	4.08	11.00	4.06	4.09	10.65



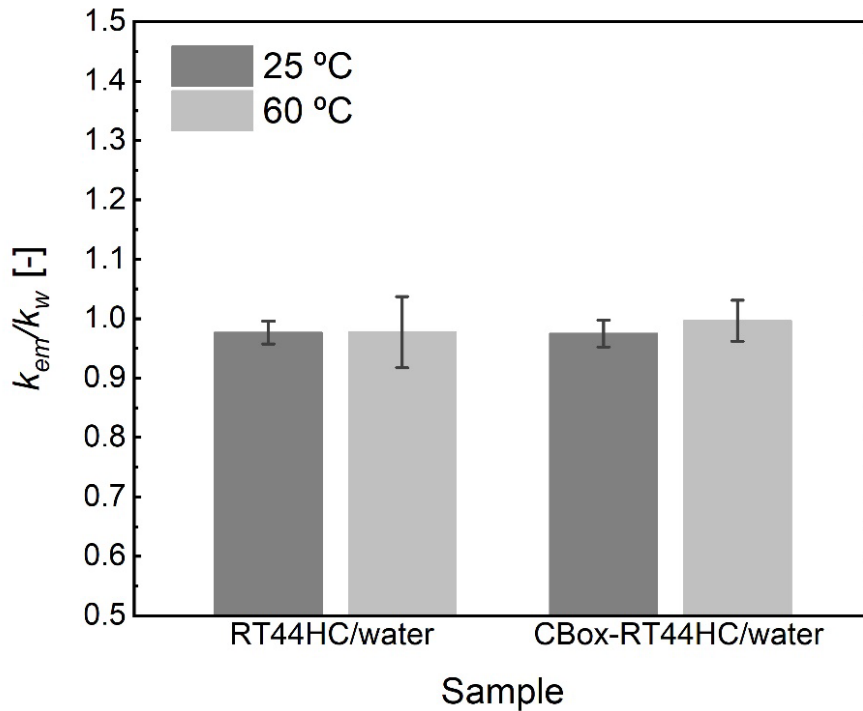
**Figure 4.8.** Experimental specific heat capacity ratio.

Table 4.4 shows the theoretical and experimental values of the thermal conductivity for the four samples at 25 °C and 60 °C. The Maxwell's equation for the effective thermal conductivity of multicomponent mixtures was applied to obtain the theoretical thermal conductivity values<sup>[19]</sup>. For this purpose, with the pure emulsion, paraffin wax was considered a solid-state particle, and the thermal conductivity value provided by the manufacturer was employed. With the emulsions with CBox NPs, these were considered to be solid-state particles with a value of  $k = 1.6 \text{ W}\cdot\text{m}^{-1}\cdot\text{K}^{-1}$  <sup>[146]</sup>.

**Table 4.4.** Thermal conductivity data (theoretical and experimental) at 25 °C and 60 °C.

Sample	$k_{25\text{ }^\circ\text{C}}$	$k_{60\text{ }^\circ\text{C}}$	$k_{25\text{ }^\circ\text{C}}$	$k_{60\text{ }^\circ\text{C}}$
	(theor) [W·m <sup>-1</sup> ·K <sup>-1</sup> ]	(theor) [W·m <sup>-1</sup> ·K <sup>-1</sup> ]	(exp) [W·m <sup>-1</sup> ·K <sup>-1</sup> ]	(exp) [W·m <sup>-1</sup> ·K <sup>-1</sup> ]
Water	0.606	0.651	0.613	0.683
RT44HC	0.2	0.2	0.258	0.172
RT44HC/water	0.603	0.611	0.599	0.667
CBox-RT44HC/water	0.603	0.611	0.598	0.681

A good agreement between the theoretical and experimental values was observed. The thermal conductivity trend followed the expected behavior for water and emulsions with increasing temperature<sup>[124]</sup>. However, as expected for addition of paraffin with lower thermal conductivity, the emulsion's effective thermal conductivity was slightly lower than that of pure water. Although the thermal conductivity of carbon was higher, the very low concentration led to a negligible effect on the emulsion's thermal conductivity. Figure 4.9 shows the experimental thermal conductivity ratio of both emulsions, and without and with CBox, in relation to water, by including error bars calculated according to Equation A.5 in Section 8.1 Uncertainty analysis, for relative values. It was concluded that differences lay in experimental uncertainty, and thermal conductivity was not affected by addition of paraffin and/or carbon NPs.



**Figure 4.9.** Experimental thermal conductivity ratio.

#### 4.4.3. Optical characterization

Figure 4.10a shows the spectral absorbance at room temperature for the base fluid (water), and for the pure and hybrid emulsions measured in a 1 mm thick cuvette. As expected, water remained almost transparent within the visible wavelength range, with water absorption bands at wavelengths around 970, 1,200 and 1,450 nm<sup>[147]–[149]</sup>. The spectral absorbance of the pure emulsion markedly increased within the range between 300 and 1,400 nm versus the base fluid. For the hybrid emulsion, absorbance further increased (on average by 225.7 % compared to the pure emulsion), which indicates that a significant increase in light absorption capacity was achieved by introducing a small amount of NPs.

In addition to absorbance, reflectance can play a key role in the sample's overall absorption because the incident light in the different sample layers can significantly lower<sup>[129]</sup>. The three samples' spectral reflectance at room temperature for a 1-mm thickness is presented in Figure 4.10b. The reflectance of water is negligible, however the direct reflection of the cuvette used in the measurements increases this value up to around

7.5 %. The addition of particles in the base fluid increased reflectance up to an average spectral value of 37.2 % with the pure emulsion and up to 16.4 % for the hybrid emulsion. In these two samples, and as similarly reported in previous studies<sup>[132]</sup>, the contribution of scattering prevailed at the lower wavelengths, and the introduction of the carbon NPs (with high absorbance capability) reduced scattering due to PCM.

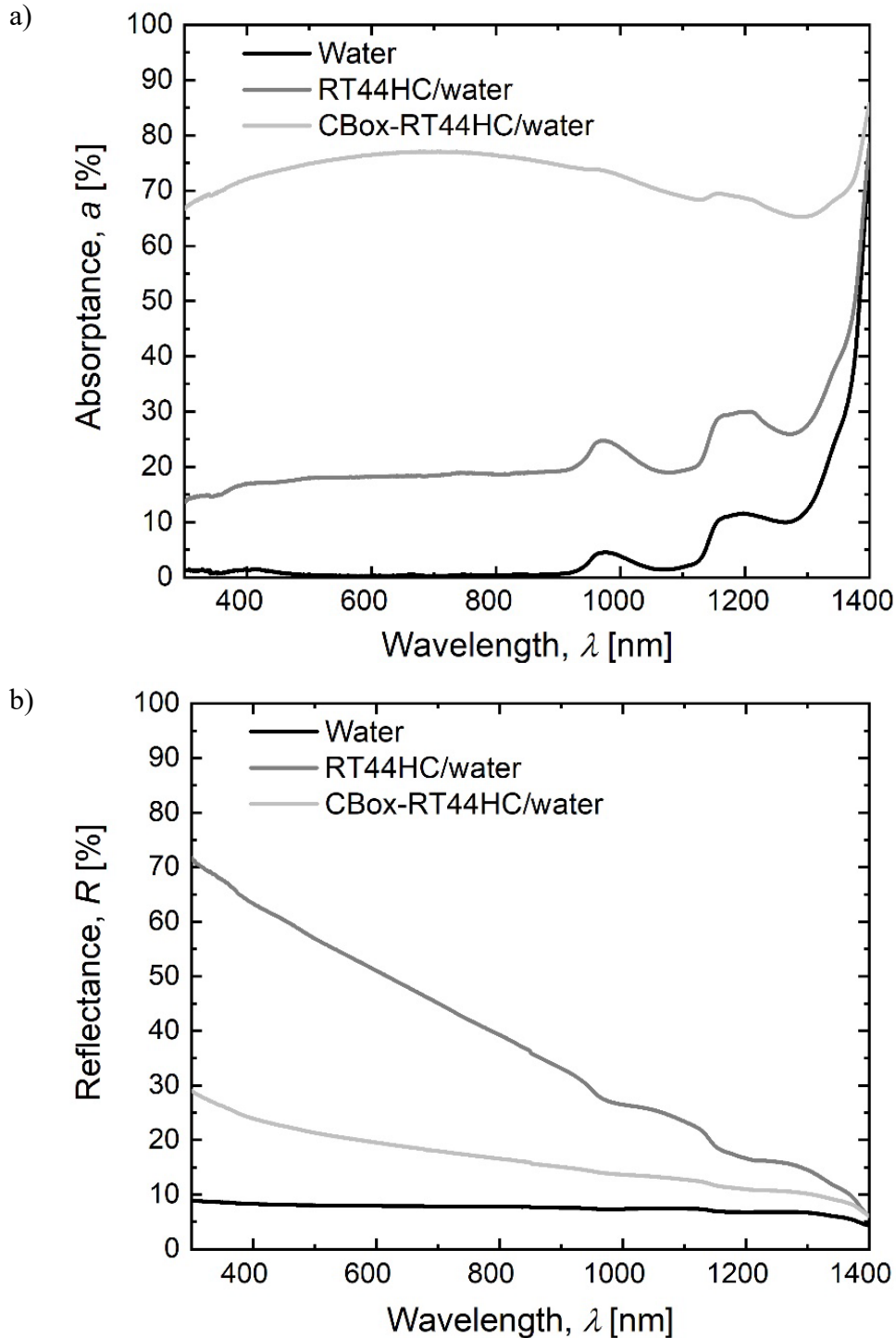


**Figure 4.10.** a) Absorbance and b) Reflectance of the base fluid (water), RT44HC/water and CBox-RT44HC/water emulsions.

As previously mentioned, due to restrictions in the available experimental equipment, samples' optical characterization was performed at room temperature with paraffin in the solid state. However, in the photothermal experiments, samples underwent different temperature evolutions and, depending on local temperatures, the paraffin of samples were in a solid or a molten state. Previous studies have reported wide variations in optical paraffin properties depending on the state. For example, *Said et al.*<sup>[150], [151]</sup> obtained a change in the transmittance of a paraffin wax (60 °C melting temperature) from totally opaque in the solid state to almost transparent when changing from the solid to the melted state. *Wang et al.*<sup>[152]</sup> obtained the transmittance of Fe<sub>3</sub>O<sub>4</sub>@graphene NPs (0.02 wt.%) in a paraffin wax sample (50 °C melting temperature) of about 80 % in the solid state, which changed to 30 % for the molten state. Therefore, in the present photothermal experiments (using 5 wt. % paraffin samples), slightly deeper light penetration for temperatures above 43 °C was expected due to the reported increase in the transmission of incident light in the molten state.

#### ***4.4.4. Photothermal conversion efficiency***

The temperature increase evolution of the three samples (water, pure and hybrid emulsions) was recorded at both experimental facilities (see Figure 4.11 and Figure 4.12).

With the solar simulator (Figure 4.3), samples were illuminated one after another, with a constant intensity of 3.5 suns and thermocouples were placed at different depths (0.2, 0.5 and 0.7 cm) from the illuminated surface. As observed by the temperature evolutions of the different thermocouples, emulsions' temperature distributions (Figure 4.11b and c) were more heterogeneous than that of water (Figure 4.11a). This temperature stratification in relation to water could be caused by greater attenuation of incoming light on deeper sample layers, caused by higher scattering for the pure emulsion and by a higher scattering and absorption for the hybrid emulsion.

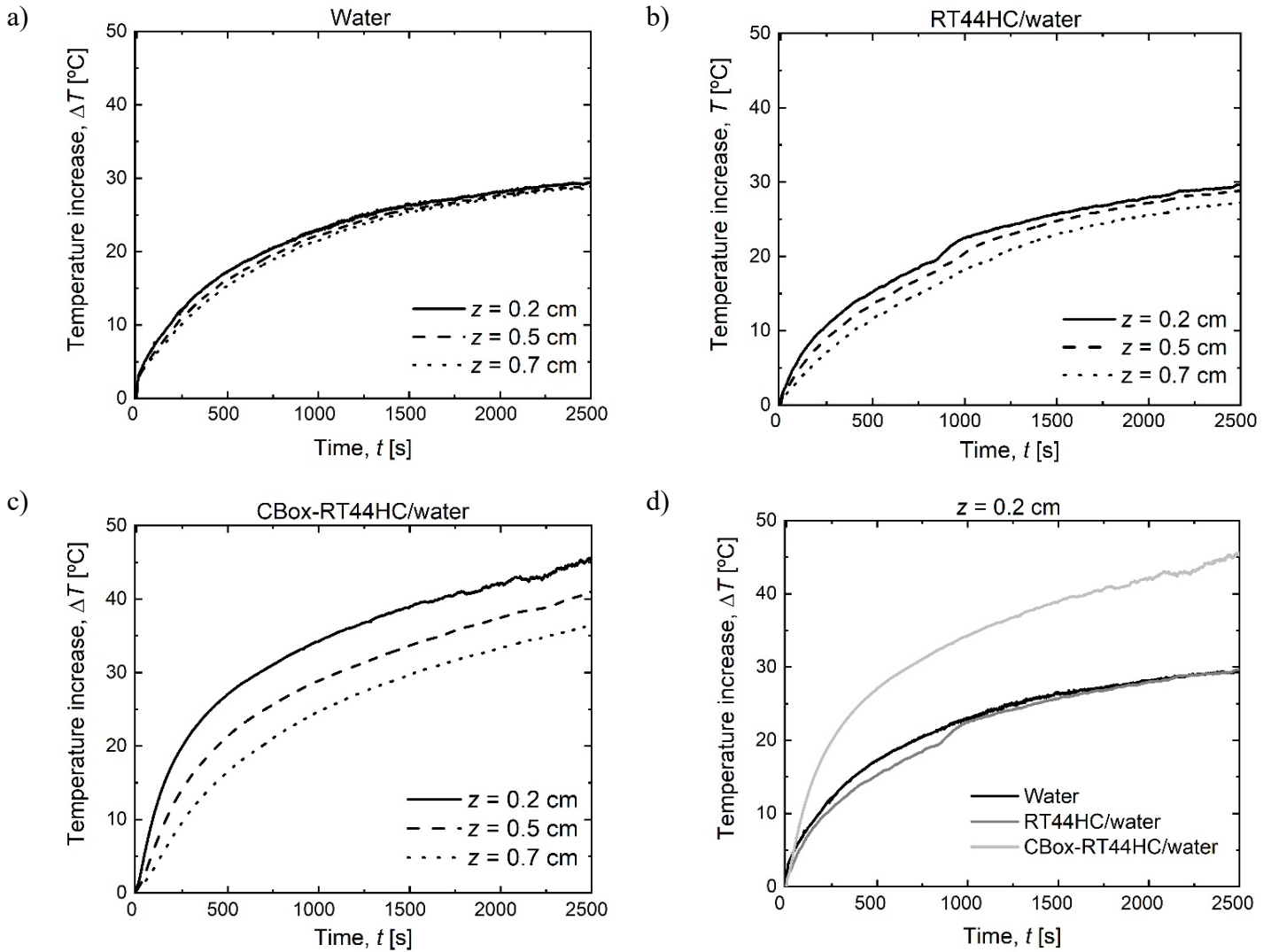


**Figure 4.11.** Temperature increase evolution for the solar simulator experiments for a) water, b) RT44HC/water emulsion and c) CBox-RT44HC/water emulsion at different depths; d) for all samples at a constant depth of  $z = 0.2$  cm.

As presented in Figure 4.11d, for a similar illumination time (2,500 s), similar temperature rises occurred for the pure emulsion and for water. Previous works have also measured similar or lower temperature increases for paraffin emulsion samples compared to water<sup>[111], [124], [125], [130], [134]</sup>. These results can be related to the optical properties measured for 1 mm and presented in Figure 4.10. Although high absorption values were observed for the pure emulsion compared to water, high reflectance was also measured for this sample. This could imply reduced incident light reaching deeper sample layers to, thus, reduce the available energy that could then be absorbed. A significant temperature rise in



the hybrid emulsion was observed compared to the other two samples. The marked higher absorption combined with lower reflection could explain this behavior.

Due to the rapid temperature rise in samples, only a small step near the paraffin melting temperature was observed for the top thermocouple in Figure 4.11b. Despite this effect not being easily noted in the figures, the use of paraffin caused the final temperature reached by the emulsion to be partially lower due to the influence of the PCM thermal charging process during its melting at around 43 °C. This effect could be important for DASC systems because it reduces heat losses, and also delays temperature reduction (due to the discharging PCM process) when solar irradiation decreases.

In the NS experimental setup (Figure 4.4), the tubes with the different samples were illuminated simultaneously under the same solar conditions. As experiments were performed under sunny conditions, the measured solar irradiance arriving at Fresnel lenses was kept constant while the experiment lasted (around 350 s). The measured intensity at the tube positions was 136 suns. In this setup, the thermocouple was placed at the central quartz tube position, which implies 1.25 cm from the illuminated surface.

As expected, Figure 4.12 shows faster temperature increases due to greater light intensity. In the SS experimental setup, it takes 2,500 s to increase the temperature of the hybrid emulsion 45 °C; however, in the NS setup this value is reached after only 165 s. A higher final temperature difference for the pure emulsion sample versus water was observed (3 °C) compared to the SS experimental setup (almost no difference). This could be related to the deeper measuring location. Also, significantly higher temperature increase for the hybrid emulsion versus the base fluid was observed for the NS setup (40 °C) when compared to the SS setup (15 °C). To better compare the results of the different setups, *PTE* values were calculated using Equation 4.2.

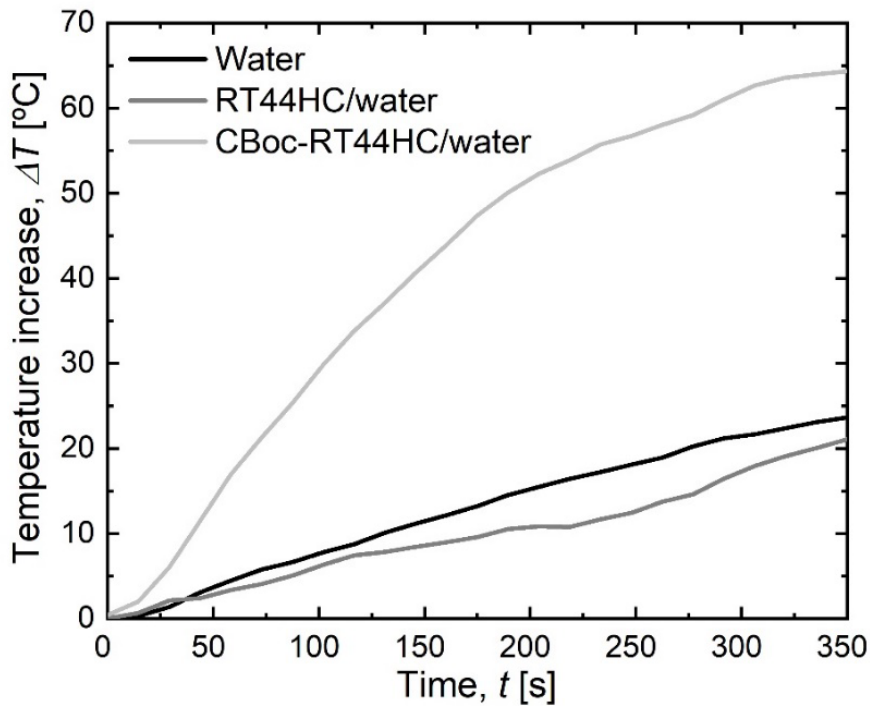


**Figure 4.12.** Temperature increase evolution for the natural sunlight experiments at depth  $z = 1.25$  cm for water, RT44HC/water and CBoc-RT44HC/water emulsions

Figure 4.13 shows the average *PTE* results for all the samples and both experimental setups, including the experimental errors calculated using Equation A.2 in Section 8.1 Uncertainty analysis.

The results for the solar simulator (Figure 4.13a) showed no *PTE* spatial stratification for water, and this *PTE* value lowered with depth for the hybrid emulsion. For both experimental setups, significant *PTE* enhancements in relation to the base fluid were achieved for the hybrid emulsion, while similar values (or even reductions) were observed when the carbon NPs were not included in emulsions.

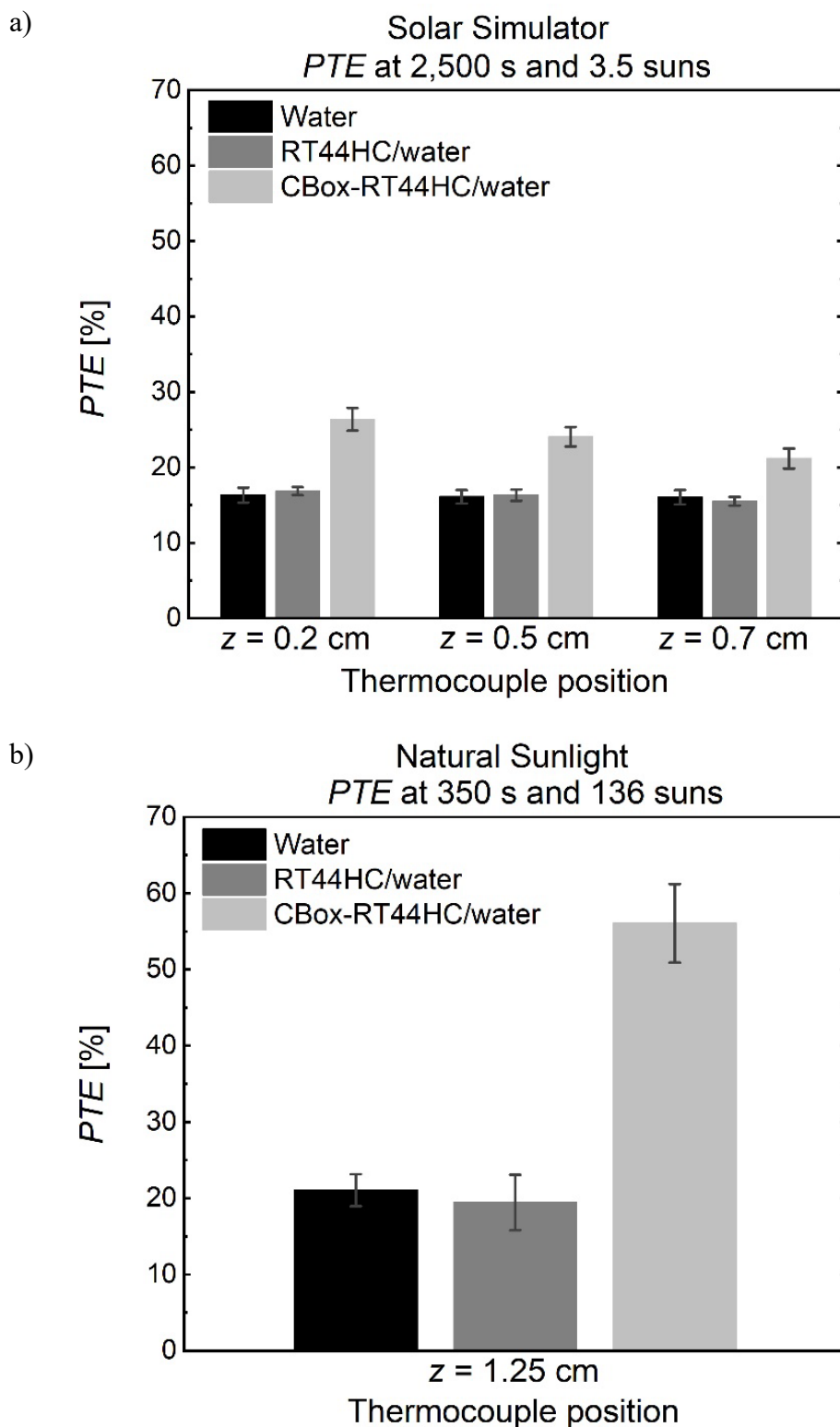


**Figure 4.13.** Photothermal conversion efficiency of samples for a) solar simulator at different depths and b) natural sunlight at depth  $z = 1.25$  cm.

The differences in the experimental setups (incident light, illumination configuration, sample holders, thermocouple position, heat losses, calculating times, etc.) did not allow

a direct comparison of the absolute  $PTE$  results obtained for both setups. Relative  $PTE$  was evaluated by normalizing the  $PTE$  of emulsions with that of the base fluid (water). The results are presented in Figure 4.14 including error bars calculated according to Equation A.5 in Section 8.1 Uncertainty analysis, for relative values. For the solar simulator data, the average value for the three measured locations was taken. Although introducing paraffin into the base fluid can provide similar  $PTE$  (due to its high reflectance), for both experimental setups, employing hybrid emulsion can considerably improve  $PTE$  (by also maintaining the benefits for DASC systems of using PCM). Better improvements were obtained for the NS experimental setup, where photothermal efficiency of the hybrid emulsion was 2.7-fold greater than that of water. A smaller  $PTE$  enhancement was observed for the same emulsion in the other setup. Differences in both experimental setup configurations (as illuminating configuration, measuring location, heat losses, etc.) could be responsible of these variations.

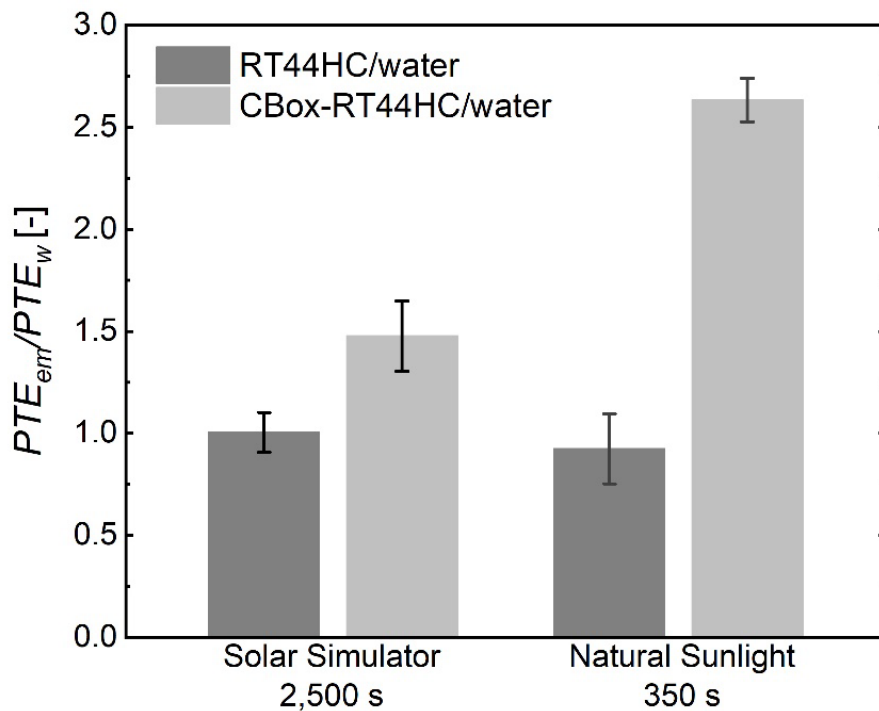


**Figure 4.14.** Relative photothermal efficiency of RT44HC/water and CBox-RT44HC/water emulsions with solar simulator and natural sunlight.

#### 4.5. Conclusions

In this study, paraffin/water (RT44HC 5 wt. %) and hybrid carbon-paraffin/water emulsions (CBox 0.01 wt. %) were synthesized and characterized. The commercial paraffin was selected from among those with a phase change temperature within water working temperature range to maximize thermal energy storage density, with a 16 % increase for a temperature range of 15 °C. Up to eight different surfactants were tested during emulsions synthesis, and SDS gave the best high temperature and thermal cycling stability results.

Phase change enthalpy, specific heat capacity and thermal conductivity of water and both pure and hybrid emulsions were measured at 25 °C and 60 °C, with paraffin remaining in the solid and the liquid state, respectively. These experimental thermal results were compared to the theoretical values by applying theoretical models (mixture rule and Maxwell's equation) and showed a good agreement.

Regarding optical characterization, both spectral absorptance and reflectance (including backward scattering) from 300 to 1,400 nm were measured at room temperature. While these optical properties remained almost negligible for water, their values increased significantly for emulsions. Spectral average values of 37.2 % and 16.4 % for reflectance and of 22.3 % and 72.6 % for absorptance were measured for the pure and the hybrid emulsions, respectively. Thus, a small quantity of carbon NPs brings about a significant increase in light absorption, which is also affected by the scattering caused by the paraffin.

Finally, photothermal behavior was investigated in two different setups: one using a solar simulator (3.5 suns) and the other under natural sunlight conditions (136 suns). Outcomes indicated that temperature spatial distribution in water (base fluid) was lower than in emulsions due to higher scattering in the pure emulsion and to higher scattering and absorption in the hybrid emulsion. Similar or even worse *PTE* results were obtained for pure emulsions compared to water, as its high reflectance reduced incident light, which can, therefore, be absorbed in different deeper layers. *PTE* enhancements of up to 1.5- and 2.7-fold than that of the base fluid (water) were obtained for the hybrid emulsion in the solar simulator setup and the natural sunlight setup, respectively. In all the measurements, the use of paraffin reduces the temperature of the emulsion, thus decreasing heat losses in DASC systems, and also can delay temperature reduction of the

emulsion when solar light is no longer available. The measured properties render the proposed hybrid carbon-paraffin/water emulsions promising candidates to be used as advanced fluid in low-temperature DASC systems with three different functions: solar absorbers, heat transfer and heat storage materials.

# **CHAPTER 5.**

## **General Discussion and Conclusions**





## **5. General discussion and conclusions**

This Thesis deals with different HTFs to be used in DASCs. In particular, this Thesis focuses on improving the solar absorption properties, storage and heat transfer capacity of the new fluids in relation to those conventionally used.

The development of two new HTFs, solar NFs and hybrid emulsions with PCMs in DASC systems allows to reduce heat losses and to increase TES density thanks to the possibility of utilizing the same fluids during the sunlight absorption, storage and heat transfer processes. The addition of low NPs concentrations also improves optical absorption properties and maintains good thermal performance, whereas PCMs increase TES capacity.

The most relevant conclusions about the development and characterization carried out on the solar NFs and hybrid emulsions fabricated in the present Thesis can be divided into three milestones, which were summarized in Table 1.2 of Section 1.4. The main results are presented below as outstanding contributions of the present doctoral Thesis:

Regarding the formulation and production of solar NFs and hybrid emulsions, it was concluded that:

- Water was selected as the base fluid for its suitability for low-temperature applications, its availability, low cost and high specific heat capacity. Au and carbon NPs were chosen for their excellent solar radiation absorption properties. Paraffin wax was selected as a PCM for its high latent heat capacity and phase change temperature within water working ranges.
- For the Au solar NFs, the influence of the particle size and concentration of the Au NPs on the *PTE* and temperature increase under solar irradiation conditions was experimentally and statistically demonstrated. The best performance was obtained for the NFs whose particle size was 5 nm at concentrations of 51.3 ppm.
- For hybrid emulsions, the effect on the colloidal stability of eight surfactants was studied. The samples with SDS as the surfactant obtained the best colloidal stability results during thermal cycling.
- The DLS particle size studies demonstrated the colloidal stability of the commercial Au NFs stabilized with PBS and of the hybrid emulsions stabilized

with the selected surfactant (SDS). Both HTFs underwent negligible particle size variations when submitted to thermal cycling.

Regarding the thermophysical characterization of solar NFs and hybrid emulsions, it was concluded that:

- The optical parameters of the Au solar NFs and hybrid emulsions were evaluated using different spectrophotometry systems. The very high potential of commercial Au NFs as light absorbers was demonstrated by the presence of a peak of maximum solar radiation absorption, which corresponded to the surface plasmon resonance at the 516 and 520 nm wavelengths for the Au NPs of 5 and 20 nm, respectively. Higher concentrations (51.3 ppm) of the Au NPs showed a spectral average increment of 632.2 % in the extinction coefficient in relation to water. The low concentrations of the oxidized carbon black NPs (0.01 wt. %) were able to increase absorptance up to 225.7 % versus the pure emulsion in spite of the fact that the presence of the dispersed paraffin wax in the base fluid increased reflectance by decreasing the maximum absorption capacity of the emulsion.
- The thermal conductivity of the Au solar NFs and hybrid emulsions was measured at 25 °C and 60 °C. The experimental results showed negligible variations in relation to the base fluid due to the low NPs concentrations, with a maximum increase of 3.9 % for the Au NFs. For the hybrid emulsions, the lower thermal conductivity values of paraffin were balanced out by the presence of the carbon NPs and by maintaining a maximum decrease of 2.5 % for the hybrid emulsions. In addition, the theoretical results calculated by Maxwell's equation for the effective thermal conductivity of the multicomponent mixtures agreed well with the experimental results.
- The phase change enthalpy and specific heat capacity of the pure and hybrid emulsions at 25 °C and 60 °C were analyzed experimentally and theoretically. The obtained experimental results agreed well with the theoretical values, and the thermal energy storage density increased by 16 % for a temperature step of 15 °C.

Finally, on the photothermal conversion efficiency in the DASC applications, it was concluded that:

- Three different experimental facilities with simulated and natural sunlight were developed to perform photothermal conversion experiments, with or without a

light concentration. The first one was used to study the performance of the Au NFs under simulated solar radiation conditions with no light concentration. The second one also applied simulated solar radiation, and included a Fresnel lens to concentrate light. It was applied to study the performance of the pure and hybrid emulsions. Finally, a third experimental setup was developed to expose samples to concentrated natural sunlight. In this new facility, up to four samples could be measured at the same time, each with its respective Fresnel lens, to study the pure and hybrid emulsions.

- The *PTE* analysis for both developed fluids was calculated as the ratio between the power of energy absorbed by the sample and the power of incident radiation. Different equations were developed based on the scenarios that took into account whether heat losses and phase change phenomena occurred during the solar to thermal conversion process.
- The best *PTE* results for the Au NFs were obtained for the NFs with a NPs size of 5 nm and a concentration of 51.3 ppm, with increments in efficiency of 121 % *versus* the base fluid when considering heat losses, and of 112 % when heat losses were not considered. Furthermore, the *PTE* analysis of the pure and hybrid emulsions was performed by not considering heat losses, but by taking into account the contribution of the latent heat included in the total thermal energy storage density. In this way, and thanks to the higher sunlight absorption capacity of the hybrid emulsions with the carbon NPs, *PTE* improved by up to 50 % *versus* water with simulated sunlight.
- Finally, the pure and hybrid emulsions were also analyzed under natural sunlight conditions. The increases recorded for the samples with the carbon NPs went up to 170 % in relation to water under the concentrated natural sunlight conditions.



# **CHAPTER 6.**

## **Gaps and Future Research Works**



## 6. Gaps and future research works

To achieve the proposed objectives to face climate change, it is necessary to develop and improve efficient technologies that make use of renewable energy sources. Solar thermal energy is one of the most promising alternatives, thanks to the great accessibility of the energy source, the Sun. The performance improvement of these systems, like direct absorption solar collectors, involves the development of heat transfer fluids such as solar nanofluids and hybrid emulsions with phase change materials capable to absorb solar radiation, transport and store heat, as advanced in the present Thesis. However, there is still much to discover and aspects to develop in this type of new materials. Some new lines of research that could be pursued are:

- To investigate new hybrid nanofluids with up to two or three different types of nanoparticles, capable of improving the performance and reducing the costs of direct absorption solar collectors.
- To increase the concentration of phase change materials up to an optimal value to ensure that the thermal energy storage increase provided by the latent heat exceeds the sensible heat decrease, while maintaining the good colloidal stability of the samples.
- To experimentally study the heat transfer processes under dynamic conditions of solar nanofluids and hybrid emulsions.
- To study the viscosity and the rheological behavior of solar nanofluids and hybrid emulsions to understand their response when flowing under dynamic conditions.
- To develop experimental facilities capable to analyze photothermal conversion efficiency, storage capacity and heat transfer under dynamic conditions closer to reality, making solar nanofluids or hybrid emulsions flowing through the experimental setups.
- To numerically formulate by the finite element method theoretical models to evaluate the temperature increases and photothermal conversion efficiency in a wide range of experimental conditions to optimize the use of these new materials in direct absorption technologies.





# **CHAPTER 7.**

## **References**



## 7. References

- [1] H. Ritchie, “How have the world’s energy sources changed over the last two centuries?,” 2021. <https://ourworldindata.org/grapher/global-energy-substitution>
- [2] J. Delbeke, A. Runge-Metzger, Y. Slingenberg, and J. Werksman, “The paris agreement,” *Toward a Clim. Eur. Curbing Trend*, pp. 24–45, 2019, doi: 10.4324/9789276082569-2.
- [3] “COP26 The Glasgow Climate Pact,” *COP26 The Glasgow Climate Pact*, 2021. <https://webarchive.nationalarchives.gov.uk/ukgwa/20230418183423/https://ukcop26.org/the-glasgow-climate-pact/>
- [4] United Nations, “The SDGs in action,” 2015. <https://www.undp.org/sustainable-development-goals>
- [5] Red Eléctrica, “Renewable generation by technology /fuel source.” <https://www.ree.es/en/datos/generation/renewable-structure>
- [6] “El entorno del sector solar térmico Marco Nacional,” *ASIT. Informe anual 2023*, 2023. [https://www.asit-solar.com/informe-anual-asit-2023/#dearflip-df\\_3236/31/](https://www.asit-solar.com/informe-anual-asit-2023/#dearflip-df_3236/31/)
- [7] M. S. Răboacă *et al.*, “Concentrating Solar Power Technologies,” *Energies*, vol. 12, no. 6, p. 1048, Mar. 2019, doi: 10.3390/en12061048.
- [8] P. Phelan, T. Otanicar, R. Taylor, and H. Tyagi, “Trends and Opportunities in Direct-Absorption Solar Thermal Collectors,” *ASME. J. Therm. Sci. Eng. Appl.*, vol. 5(2), p. 021003, 2013, doi: 10.1115/1.4023930.
- [9] H. L. Zhang, J. Baeyens, J. Degève, and G. Cacères, “Concentrated solar power plants: Review and design methodology,” *Renew. Sustain. Energy Rev.*, vol. 22, pp. 466–481, Jun. 2013, doi: 10.1016/J.RSER.2013.01.032.
- [10] R. Dobriyal, P. Negi, N. Sengar, and D. B. Singh, “A brief review on solar flat plate collector by incorporating the effect of nanofluid,” *Mater. Today Proc.*, vol. 21, pp. 1653–1658, Jan. 2020, doi: 10.1016/J.MATPR.2019.11.294.
- [11] W. Chamsa-ard, S. Brundavanam, C. Fung, D. Fawcett, and G. Poinern, “Nanofluid Types, Their Synthesis, Properties and Incorporation in Direct Solar

- Thermal Collectors: A Review,” *Nanomaterials*, vol. 7, no. 6, p. 131, May 2017, doi: 10.3390/nano7060131.
- [12] J. E. Minardi and H. N. Chuang, “Performance of a ‘black’ liquid flat-plate solar collector,” *Sol. Energy*, vol. 17, no. 3, pp. 179–183, 1975, doi: 10.1016/0038-092X(75)90057-2.
- [13] T. Hu, J. Zhang, J. Xia, X. Li, P. Tao, and T. Deng, “A Review on Recent Progress in Preparation of Medium-Temperature Solar-Thermal Nanofluids with Stable Dispersion,” *Nanomaterials*, vol. 13, no. 8, p. 1399, Apr. 2023, doi: 10.3390/nano13081399.
- [14] Robert A. Taylor; Patrick E. Phelan; Todd P. Otanicar; Chad A. Walker; Monica Nguyen; Steven Trimble; Ravi Prasher, “Applicability of nanofluids in high flux solar collectors,” *J. Renew. Sustain. Energy*, vol. 3, p. 023104, 2011, doi: doi:10.1063/1.3571565.
- [15] H. Benoit, L. Spreafico, D. Gauthier, and G. Flamant, “Review of heat transfer fluids in tube-receivers used in concentrating solar thermal systems: Properties and heat transfer coefficients,” *Renew. Sustain. Energy Rev.*, vol. 55, pp. 298–315, Mar. 2016, doi: 10.1016/J.RSER.2015.10.059.
- [16] M. Romero and A. Steinfeld, “Concentrating solar thermal power and thermochemical fuels,” *Energy Environ. Sci.*, vol. 5(11), pp. 9234–9245, 2012, doi: 10.1039/C2EE21275G.
- [17] A. Zeiny, H. Jin, L. Bai, G. Lin, and D. Wen, “A comparative study of direct absorption nanofluids for solar thermal applications,” *Sol. Energy*, vol. 161, no. January, pp. 74–82, 2018, doi: 10.1016/j.solener.2017.12.037.
- [18] H. Jin, G. Lin, L. Bai, M. Amjad, E. P. Bandarra Filho, and D. Wen, “Photothermal conversion efficiency of nanofluids: An experimental and numerical study,” *Sol. Energy*, vol. 139, pp. 278–289, Dec. 2016, doi: 10.1016/J.SOLENER.2016.09.021.
- [19] J.C. Maxwell, *A treatise on electricity and magnetism*, vol. 1. Oxford UK, 1873.
- [20] S. U. S. Choi and J. A. Eastman, “Enhancing thermal conductivity of fluids with nanoparticles,” *American Society of Mechanical Engineers, Fluids Engineering Division (Publication) FED*, 1995. <https://www.osti.gov/servlets/purl/196525>

- [21] T. P. Otanicar, P. E. Phelan, and J. S. Golden, "Optical properties of liquids for direct absorption solar thermal energy systems," *Sol. Energy*, vol. 83, no. 7, pp. 969–977, 2009, doi: 10.1016/j.solener.2008.12.009.
- [22] X. Wang and A. Mujumdar, "Heat transfer characteristics of nanofluids: a review," *Int. J. Therm. Sci.*, vol. 46, pp. 1–19, 2007, doi: doi:10.1016/j.ijthermalsci.2006.06.010.
- [23] A. Arshad, M. Jabbal, Y. Yan, and D. Reay, "A review on graphene based nanofluids: Preparation, characterization and applications," *J. Mol. Liq.*, vol. 279, pp. 444–484, Apr. 2019, doi: 10.1016/J.MOLLIQ.2019.01.153.
- [24] H. Zhang, H. J. Chen, X. Du, G. Lin, and D. Wen, "Dependence of photothermal conversion characteristics on different nanoparticle dispersions," *J. Nanosci. Nanotechnol.*, vol. 15, no. 4, pp. 3055–3060, 2015, doi: 10.1166/jnn.2015.9673.
- [25] Z. Said, R. Saidur, and N. A. Rahim, "Optical properties of metal oxides based nanofluids," *Int. Commun. Heat Mass Transf.*, vol. 59, pp. 46–54, 2014, doi: 10.1016/j.icheatmasstransfer.2014.10.010.
- [26] E. Sadeghinezhad *et al.*, "A comprehensive review on graphene nanofluids: Recent research, development and applications," *Energy Convers. Manag.*, vol. 111, pp. 466–487, 2016, doi: 10.1016/j.enconman.2016.01.004.
- [27] X. Li, G. Zeng, and X. Lei, "The stability, optical properties and solar-thermal conversion performance of SiC-MWCNTs hybrid nanofluids for the direct absorption solar collector (DASC) application," *Sol. Energy Mater. Sol. Cells*, vol. 206, no. 1, p. 110323, 2020, doi: 10.1016/j.solmat.2019.110323.
- [28] A. Kosinska, B. V. Balakin, and P. Kosinski, "Use of biodegradable colloids and carbon black nanofluids for solar energy applications," *AIP Adv.*, vol. 11, no. 5, May 2021, doi: 10.1063/5.0053258.
- [29] O. Mahian, A. Kianifar, S. A. Kalogirou, I. Pop, and S. Wongwises, "A review of the applications of nanofluids in solar energy," *Int. J. Heat Mass Transf.*, vol. 57, no. 2, pp. 582–594, Feb. 2013, doi: 10.1016/J.IJHEATMASSTRANSFER.2012.10.037.
- [30] H. Tyagi, P. Phelan, and R. Prasher, "Predicted Efficiency of a Low-Temperature

- Nanofluid-Based Direct Absorption Solar Collector,” *J. Sol. Energy Eng.*, vol. 131, no. 4, Sep. 2009, doi: 10.1115/1.3197562.
- [31] M. Q. Brewster and C. L. Tien, “Radiative Transfer in Packed Fluidized Beds: Dependent Versus Independent Scattering,” *J. Heat Transfer*, vol. 104, no. 4, pp. 573–579, Nov. 1982, doi: 10.1115/1.3245170.
- [32] T. B. Gorji and A. A. Ranjbar, “A review on optical properties and application of nanofluids in direct absorption solar collectors (DASCs),” *Renew. Sustain. Energy Rev.*, vol. 72, no. January, pp. 10–32, 2017, doi: 10.1016/j.rser.2017.01.015.
- [33] E. Sani *et al.*, “Carbon nanohorns-based nanofluids as direct sunlight absorbers,” *Opt. Express*, vol. 18, no. 5, p. 5179, 2010, doi: 10.1364/oe.18.005179.
- [34] E. Sani *et al.*, “Potential of carbon nanohorn-based suspensions for solar thermal collectors,” *Sol. Energy Mater. Sol. Cells*, vol. 95, no. 11, pp. 2994–3000, 2011, doi: 10.1016/j.solmat.2011.06.011.
- [35] “Standard tables for reference solar spectral irradiances: direct normal and hemispherical on 37° tilted surface.” ASTM International, p. G 173, 2012.
- [36] A. R. Mallah, M. N. Mohd Zubir, O. A. Alawi, K. M. Salim Newaz, and A. B. Mohamad Badry, “Plasmonic nanofluids for high photothermal conversion efficiency in direct absorption solar collectors: Fundamentals and applications,” *Sol. Energy Mater. Sol. Cells*, vol. 201, p. 110084, Oct. 2019, doi: 10.1016/J.SOLMAT.2019.110084.
- [37] M. Chen, Y. He, J. Zhu, and D. Kim, “Enhancement of photo-thermal conversion using gold nanofluids with different particle sizes,” *Energy Convers. Manag.*, vol. 112, pp. 21–30, 2016, doi: doi.org/10.1016/j.enconman.2016.01.009.
- [38] H. Duan, Y. Zheng, C. Xu, Y. Shang, and F. Ding, “Experimental investigation on the plasmonic blended nanofluid for efficient solar absorption,” *Appl. Therm. Eng.*, vol. 161, p. 114192, Oct. 2019, doi: 10.1016/J.APPLTHERMALENG.2019.114192.
- [39] M. Chen, Y. He, J. Huang, J. Z.-E. C. and Management, and U. 2016, “Synthesis and solar photo-thermal conversion of Au, Ag, and Au-Ag blended plasmonic nanoparticles,” *Energy Convers. Manag.*, vol. 127, pp. 292–300, 2016, doi:

- doi.org/10.1016/j.enconman.2016.09.015.
- [40] M. Chen, Y. He, J. Zhu, Y. Shuai, B. Jiang, and Y. Huang, “An experimental investigation on sunlight absorption characteristics of silver nanofluids,” *Sol. Energy*, vol. 115, pp. 85–94, May 2015, doi: 10.1016/J.SOLENER.2015.01.031.
- [41] L. Wang *et al.*, “Dual plasmonic Au/TiN nanofluids for efficient solar photothermal conversion,” *Sol. Energy*, vol. 184, no. April 2018, pp. 240–248, 2019, doi: 10.1016/j.solener.2019.04.013.
- [42] A. Borode, N. Ahmed, and P. Olubambi, “A review of solar collectors using carbon-based nanofluids,” *J. Clean. Prod.*, vol. 241, p. 118311, Dec. 2019, doi: 10.1016/J.JCLEPRO.2019.118311.
- [43] A. Gimeno-Furió *et al.*, “Optical characterisation and photothermal conversion efficiency of a water-based carbon nanofluid for direct solar absorption applications,” *Energy*, vol. 212, p. 118763, Dec. 2020, doi: 10.1016/J.ENERGY.2020.118763.
- [44] M. Karami, M. A. Akhavan Bahabadi, S. Delfani, and A. Ghozatloo, “A new application of carbon nanotubes nanofluid as working fluid of low-temperature direct absorption solar collector,” *Sol. Energy Mater. Sol. Cells*, vol. 121, pp. 114–118, Feb. 2014, doi: 10.1016/J.SOLMAT.2013.11.004.
- [45] S. M. Ladjevardi, A. Asnaghi, P. S. Izadkhast, and A. H. Kashani, “Applicability of graphite nanofluids in direct solar energy absorption,” *Sol. Energy*, vol. 94, pp. 327–334, Aug. 2013, doi: 10.1016/J.SOLENER.2013.05.012.
- [46] H. Tiznobaik and D. Shin, “Enhanced specific heat capacity of high-temperature molten salt-based nanofluids,” *Int. J. Heat Mass Transf.*, vol. 57, no. 2, pp. 542–548, Feb. 2013, doi: 10.1016/J.IJHEATMASSTRANSFER.2012.10.062.
- [47] B. Dudda and D. Shin, “Effect of nanoparticle dispersion on specific heat capacity of a binary nitrate salt eutectic for concentrated solar power applications,” *Int. J. Therm. Sci.*, vol. 69, pp. 37–42, Jul. 2013, doi: 10.1016/J.IJTHERMALSCI.2013.02.003.
- [48] H. Mehling and L. F. Cabeza, *Heat and Cold Storage with PCM*. Springer Berlin, Heidelberg, 2008. doi: <https://doi.org/10.1007/978-3-540-68557-9>.

- [49] M. Delgado, A. Lázaro, J. Mazo, and B. Zalba, “Review on phase change material emulsions and microencapsulated phase change material slurries: Materials, heat transfer studies and applications,” *Renew. Sustain. Energy Rev.*, vol. 16, no. 1, pp. 253–273, Jan. 2012, doi: 10.1016/J.RSER.2011.07.152.
- [50] D. Cabaleiro *et al.*, “Review on phase change material emulsions for advanced thermal management: Design, characterization and thermal performance,” *Renew. Sustain. Energy Rev.*, vol. 159, no. February, 2022, doi: 10.1016/j.rser.2022.112238.
- [51] R. Mondragón, R. Martínez-Cuenca, L. Hernández, P. Andreu-Cabedo, L. Cabedo, and E. Juliá, “Nanotechnology and Nanomaterials for Thermal Energy Storage,” in *Handbook of Clean Energy Systems*, Jinyue Yan, Ed. John Wiley & Sons, 2015.
- [52] S. Chakraborty and P. K. Panigrahi, “Stability of nanofluid: A review,” *Appl. Therm. Eng.*, vol. 174, p. 115259, Jun. 2020, doi: 10.1016/J.APPLTHERMALENG.2020.115259.
- [53] O. Ouabouch, M. Kriraa, and M. Lamsaadi, “Stability, thermophysical properties of nanofluids, and applications in solar collectors: A review,” *AIMS Mater. Sci.*, vol. 8, no. 4, pp. 659–684, 2021, doi: 10.3934/matensci.2021040.
- [54] Z. Aqachmar, H. Ben Sassi, K. Lahrech, and A. Barhdadi, “Solar technologies for electricity production: An updated review,” *Int. J. Hydrogen Energy*, vol. 46, no. 60, pp. 30790–30817, 2021, doi: 10.1016/j.ijhydene.2021.06.190.
- [55] R. A. Rasih, N. A. C. Sidik, and S. Samion, “Recent progress on concentrating direct absorption solar collector using nanofluids: A review,” *Journal of Thermal Analysis and Calorimetry*, vol. 137, no. 3. Springer Netherlands, pp. 903–922, Aug. 15, 2019. doi: 10.1007/s10973-018-7964-6.
- [56] M. M. Tawfik, “Experimental studies of nanofluid thermal conductivity enhancement and applications: A review,” *Renew. Sustain. Energy Rev.*, vol. 75, no. July 2016, pp. 1239–1253, 2017, doi: 10.1016/j.rser.2016.11.111.
- [57] E. C. Okonkwo, I. Wole-Osho, I. W. Almanassra, Y. M. Abdullatif, and T. Al-Ansari, “An updated review of nanofluids in various heat transfer devices,” *J. Therm. Anal. Calorim.*, no. March, 2020, doi: 10.1007/s10973-020-09760-2.



- [58] R. Taylor *et al.*, “Small particles, big impacts: A review of the diverse applications of nanofluids,” *J. Appl. Phys.*, vol. 113, no. 1, Jan. 2013, doi: 10.1063/1.4754271.
- [59] E. P. Bandarra Filho, O. S. H. Mendoza, C. L. L. Beicker, A. Menezes, and D. Wen, “Experimental investigation of a silver nanoparticle-based direct absorption solar thermal system,” *Energy Convers. Manag.*, vol. 84, pp. 261–267, 2014, doi: 10.1016/j.enconman.2014.04.009.
- [60] H. Zhang, H. Chen, X. Du, and D. Wen, “Photothermal conversion characteristics of gold nanoparticle dispersions,” *Sol. Energy*, vol. 100, pp. 141–147, 2014, doi: 10.1016/j.solener.2013.12.004.
- [61] H. Jin, G. Lin, L. Bai, A. Zeiny, and D. Wen, “Steam generation in a nanoparticle-based solar receiver,” *Nano Energy*, vol. 28, pp. 397–406, 2016, doi: 10.1016/j.nanoen.2016.08.011.
- [62] M. Chen, Y. He, J. Huang, and J. Zhu, “Investigation into Au nanofluids for solar photothermal conversion,” *Int. J. Heat Mass Transf.*, vol. 108, pp. 1894–1900, 2017, doi: 10.1016/j.ijheatmasstransfer.2017.01.005.
- [63] X. Wang, Y. He, X. Liu, L. Shi, and J. Zhu, “Investigation of photothermal heating enabled by plasmonic nanofluids for direct solar steam generation,” *Sol. Energy*, vol. 157, pp. 35–46, 2017, doi: doi.org/10.1016/j.solener.2017.08.015.
- [64] Y. He, M. Chen, X. Wang, and Y. Hu, “Plasmonic multi-thorny Gold nanostructures for enhanced solar thermal conversion,” *Sol. Energy*, vol. 171, pp. 73–82, 2018.
- [65] T. Yousefi, F. Veysi, E. Shojaeizadeh, and S. Zinadini, “An experimental investigation on the effect of Al<sub>2</sub>O<sub>3</sub>-H<sub>2</sub>O nanofluid on the efficiency of flat-plate solar collectors,” *Renew. Energy*, vol. 39, no. 1, pp. 293–298, 2012, doi: 10.1016/j.renene.2011.08.056.
- [66] H. K. Gupta, G. Das Agrawal, and J. Mathur, “An experimental investigation of a low temperature Al<sub>2</sub>O<sub>3</sub>-H<sub>2</sub>O nanofluid based direct absorption solar collector,” *Sol. Energy*, vol. 118, pp. 390–396, 2015, doi: 10.1016/j.solener.2015.04.041.
- [67] D. Han, Z. Meng, D. Wu, C. Zhang, and H. Zhu, “Thermal properties of carbon black aqueous nanofluids for solar absorption,” *Nanoscale Res. Lett.*, vol. 6, pp. 1–

- 7, 2011, doi: 10.1186/1556-276X-6-457.
- [68] S. Delfani, M. Karami, and M. A. Akhavan-Behabadi, “Performance characteristics of a residential-type direct absorption solar collector using MWCNT nanofluid,” *Renew. Energy*, vol. 87, pp. 754–764, 2016, doi: 10.1016/j.renene.2015.11.004.
- [69] T. Aguilar, E. Sani, L. Mercatelli, I. Carrillo-Berdugo, E. Torres, and J. Navas, “Exfoliated graphene oxide-based nanofluids with enhanced thermal and optical properties for solar collectors in concentrating solar power,” *J. Mol. Liq.*, vol. 306, p. 112862, 2020, doi: 10.1016/j.molliq.2020.112862.
- [70] X. Wang, Y. He, M. Chen, and Y. Hu, “ZnO-Au composite hierarchical particles dispersed oil-based nanofluids for direct absorption solar collectors,” *Sol. Energy Mater. Sol. Cells*, vol. 179, no. November 2017, pp. 185–193, 2018, doi: 10.1016/j.solmat.2017.11.012.
- [71] H. Wang, W. Yang, L. Cheng, C. Guan, and H. Yan, “Chinese ink: High performance nanofluids for solar energy,” *Sol. Energy Mater. Sol. Cells*, vol. 176, no. June 2017, pp. 374–380, 2018, doi: 10.1016/j.solmat.2017.10.023.
- [72] X. Zuo *et al.*, “Experimental investigation on photothermal conversion properties of lampblack ink nanofluids,” *Sol. Energy*, vol. 218, pp. 1–10, 2021, doi: 10.1016/j.solener.2021.02.016.
- [73] M. Rycenga *et al.*, “Controlling the synthesis and assembly of silver nanostructures for plasmonic applications,” *Chem. Rev.*, vol. 111, no. 6, pp. 3669–3712, Jun. 2011, doi: 10.1021/CR100275D.
- [74] B. Kamenik *et al.*, “Numerical analysis of performance uncertainty of heat exchangers operated with nanofluids,” *Int. J. Thermofluids*, vol. 14, p. 100144, 2022, doi: 10.1016/j.ijft.2022.100144.
- [75] J. Buongiorno *et al.*, “A benchmark study on the thermal conductivity of nanofluids,” *J. Appl. Phys.*, vol. 106, p. 094312, 2009, doi: 10.1063/1.3245330.
- [76] W. H. Lee *et al.*, “Round-robin test on thermal conductivity measurement of zno nanofluids and comparison of experimental results with theoretical bounds,” *Nanoscale Res. Lett.*, vol. 6, no. 1, pp. 1–11, 2011, doi: 10.1186/1556-276X-6-258.

- [77] B. Muñoz-Sánchez *et al.*, “Round robin test on the measurement of the specific heat of solar salt,” *AIP Conf. Proc.*, vol. 1850, pp. 080017–1–080017–8, 2017, doi: 10.1063/1.4984438.
- [78] M. Hernaiz *et al.*, “The contact angle of nanofluids as thermophysical property,” *J. Colloid Interface Sci.*, vol. 547, pp. 393–406, 2019, doi: 10.1016/j.jcis.2019.04.007.
- [79] A. A. Minea *et al.*, “NanoRound: A benchmark study on the numerical approach in nanofluids’ simulation,” *Int. Commun. Heat Mass Transf.*, vol. 108, p. 104292, 2019, doi: 10.1016/j.icheatmasstransfer.2019.104292.
- [80] N. M. Razali and Y. B. Wah, “Power comparisons of Shapiro-Wilk, Kolmogorov-Smirnov, Lilliefors and Anderson-Darling tests,” *J. Stat. Model. Anal.*, vol. 2, no. 1, pp. 21–33, 2011.
- [81] P. Mishra, U. Singh, C. M. Pandey, P. Mishra, and G. Pandey, “Application of Student’s t-test, Analysis of Variance, and Covariance,” *Ann Card Anaesth*, vol. 22, pp. 407–412, 2019, doi: 10.4103/aca.ACA.
- [82] D. J. Sheskin, “Parametric Versus Nonparametric Tests,” in *Lovric M. (eds) International Encyclopedia of Statistical Science*, Springer, Berlin, Heidelberg, 2011. doi: 10.1007/978-3-642-04898-2\_465.
- [83] S. B. Gerber and K. V. Finn, *Using SPSS For Windows Data Analysis and Graphics*, Second Edi. New York: Springer Science + Business Media, Inc., 2005.
- [84] H. M. Ali, “Phase change materials based thermal energy storage for solar energy systems,” *J. Build. Eng.*, vol. 56, p. 104731, Sep. 2022, doi: 10.1016/J.JOBE.2022.104731.
- [85] IRENA, “Global Energy Transformation: A Roadmap to 2050,” *International Renewable Energy Agency*, 2019. <https://www.irena.org/publications/2019/Apr/Global-energy-transformation-A-roadmap-to-2050-2019Edition>
- [86] Y. Lu, Z. A. Khan, M. S. Alvarez-Alvarado, Y. Zhang, Z. Huang, and M. Imran, “A critical review of sustainable energy policies for the promotion of renewable energy sources,” *Sustain.*, vol. 12, no. 12, pp. 1–30, 2020, doi:

- 10.3390/su12125078.
- [87] H. S. Moghaieb *et al.*, “Efficient solar-thermal energy conversion with surfactant-free Cu-oxide nanofluids,” *Nano Energy*, vol. 108, p. 108112, Apr. 2023, doi: 10.1016/J.NANOEN.2022.108112.
- [88] L. Mercatelli, E. Sani, D. Fontani, G. Zaccanti, F. Martelli, and P. di Ninni, “Scattering and absorption properties of carbon nanohorn-based nanofluids for solar energy applications,” *J. Eur. Opt. Soc.*, vol. 6, p. 36, 2011, doi: 10.2971/jeos.2011.11025.
- [89] L. Mercatelli *et al.*, “Absorption and scattering properties of carbon nanohorn-based nanofluids for direct sunlight absorbers,” *Nanoscale Res. Lett.*, vol. 6, no. 1, 2011, doi: 10.1186/1556-276X-6-282.
- [90] B. Koçak, A. I. Fernandez, and H. Paksoy, “Review on sensible thermal energy storage for industrial solar applications and sustainability aspects,” *Sol. Energy*, vol. 209, pp. 135–169, Oct. 2020, doi: 10.1016/J.SOLENER.2020.08.081.
- [91] P. Gadhave, F. Pathan, S. Kore, and C. Prabhune, “Comprehensive review of phase change material based latent heat thermal energy storage system,” <https://doi.org/10.1080/01430750.2021.1873848>, 2021, doi: 10.1080/01430750.2021.1873848.
- [92] A. J. Carrillo, J. González-Aguilar, M. Romero, and J. M. Coronado, “Solar Energy on Demand: A Review on High Temperature Thermochemical Heat Storage Systems and Materials,” *Chem. Rev.*, vol. 119, no. 7, pp. 4777–4816, Apr. 2019, doi: 10.1021/ACS.CHEMREV.8B00315/ASSET/IMAGES/MEDIUM/CR-2018-00315F\_0001.GIF.
- [93] I. Sarbu, “A Comprehensive Review of Thermal Energy Storage,” 2018, doi: 10.3390/su10010191.
- [94] B. A. A. Yousef, K. Elsaid, and M. A. Abdelkareem, “Potential of nanoparticles in solar thermal energy storage,” *Therm. Sci. Eng. Prog.*, vol. 25, p. 101003, Oct. 2021, doi: 10.1016/J.TSEP.2021.101003.
- [95] S. Danehkar and H. Yousefi, “A comprehensive overview on water-based energy storage systems for solar applications,” *Energy Reports*, vol. 8, pp. 8777–8797,

- Nov. 2022, doi: 10.1016/J.EGYR.2022.06.057.
- [96] M. Imran Khan, F. Asfand, and S. G. Al-Ghamdi, “Progress in research and development of phase change materials for thermal energy storage in concentrated solar power,” *Appl. Therm. Eng.*, vol. 219, p. 119546, Jan. 2023, doi: 10.1016/J.APPLTHERMALENG.2022.119546.
- [97] L. Liu, J. Niu, and J. Y. Wu, “Preparation of Stable Phase Change Material Emulsions for Thermal Energy Storage and Thermal Management Applications: A Review,” *Mater. 2022, Vol. 15, Page 121*, vol. 15, no. 1, p. 121, Dec. 2021, doi: 10.3390/MA15010121.
- [98] J. Singh, S. Parvate, J. R. Vennapusa, T. K. Maiti, P. Dixit, and S. Chattopadhyay, “Facile method to prepare 1-dodecanol@poly(melamine-paraformaldehyde) phase change energy storage microcapsules via surfactant-free method,” *J. Energy Storage*, vol. 49, May 2022, doi: 10.1016/j.est.2022.104089.
- [99] S. Shoeibi, H. Kargarsharifabad, S. A. A. Mirjalily, M. Sadi, and A. Arabkoohsar, “A comprehensive review of nano-enhanced phase change materials on solar energy applications,” *Journal of Energy Storage*, vol. 50. Elsevier Ltd, Jun. 01, 2022. doi: 10.1016/j.est.2022.104262.
- [100] G. Zhou, M. Hou, Y. Ren, Z. Jiang, and N.-C. Lai, “Full-spectrum photo-thermal conversion enabled by plasmonic titanium carbide modified phase change microcapsules,” *J. Energy Storage*, vol. 72, p. 108458, Nov. 2023, doi: 10.1016/J.EST.2023.108458.
- [101] Q. Wang, L. Yang, and J. Song, “Preparation, thermal conductivity, and applications of nano-enhanced phase change materials (NEPCMs) in solar heat collection: A review,” *Journal of Energy Storage*, vol. 63. Elsevier Ltd, Jul. 01, 2023. doi: 10.1016/j.est.2023.107047.
- [102] A. K. Mishra, B. B. Lahiri, and J. Philip, “Superior thermal conductivity and photo-thermal conversion efficiency of carbon black loaded organic phase change material,” *J. Mol. Liq.*, vol. 285, pp. 640–657, Jul. 2019, doi: 10.1016/J.MOLLIQ.2019.04.132.
- [103] M. Chen, Y. He, Q. Ye, Z. Zhang, and Y. Hu, “Solar thermal conversion and thermal energy storage of CuO/Paraffin phase change composites,” *Int. J. Heat*

- Mass Transf.*, vol. 130, pp. 1133–1140, Mar. 2019, doi: 10.1016/J.IJHEATMASSTRANSFER.2018.11.026.
- [104] P. K. S. Rathore, K. K. Gupta, B. Patel, R. K. Sharma, and N. K. Gupta, “Beeswax as a potential replacement of paraffin wax as shape stabilized solar thermal energy storage material: An experimental study,” *J. Energy Storage*, vol. 68, Sep. 2023, doi: 10.1016/j.est.2023.107714.
- [105] E. T. Iacob-Tudose, I. Mamaliga, and A. V. Iosub, *Tes nanoemulsions: A review of thermophysical properties and their impact on system design*, vol. 11, no. 12. 2021. doi: 10.3390/nano11123415.
- [106] T. Morimoto and H. Kumano, “Nucleation promoting effect of fat shell on phase change material particles dispersed in an emulsion for thermal energy storage medium,” *J. Energy Storage*, vol. 31, Oct. 2020, doi: 10.1016/j.est.2020.101637.
- [107] M. A. Kibria, M. R. Anisur, M. H. Mahfuz, R. Saidur, and I. H. S. C. Metselaar, “A review on thermophysical properties of nanoparticle dispersed phase change materials,” *Energy Convers. Manag.*, vol. 95, pp. 69–89, May 2015, doi: 10.1016/J.ENCONMAN.2015.02.028.
- [108] T. Sakai, Y. Nakagawa, and K. Iijima, “Hexadecane-in-water emulsions as thermal-energy storage and heat transfer fluids: Connections between phase-transition temperature and period of hexadecane droplets dispersed in hexadecane-in-water emulsions and characteristics of surfactants,” *Colloids Surfaces A Physicochem. Eng. Asp.*, vol. 529, pp. 394–402, Sep. 2017, doi: 10.1016/J.COLSURFA.2017.06.015.
- [109] F. Wang, C. Zhang, J. Liu, X. Fang, and Z. Zhang, “Highly stable graphite nanoparticle-dispersed phase change emulsions with little supercooling and high thermal conductivity for cold energy storage,” *Appl. Energy*, vol. 188, pp. 97–106, Feb. 2017, doi: 10.1016/J.APENERGY.2016.11.122.
- [110] F. Wang, X. Fang, and Z. Zhang, “Preparation of phase change material emulsions with good stability and little supercooling by using a mixed polymeric emulsifier for thermal energy storage,” *Sol. Energy Mater. Sol. Cells*, vol. 176, pp. 381–390, Mar. 2018, doi: 10.1016/J.SOLMAT.2017.10.025.
- [111] G. Gao, T. Zhang, S. Jiao, and C. Guo, “Preparation of reduced graphene oxide

- modified magnetic phase change microcapsules and their application in direct absorption solar collector,” *Sol. Energy Mater. Sol. Cells*, vol. 216, p. 110695, Oct. 2020, doi: 10.1016/J.SOLMAT.2020.110695.
- [112] Z. Chang *et al.*, “Review on the preparation and performance of paraffin-based phase change microcapsules for heat storage,” *Journal of Energy Storage*, vol. 46. Elsevier Ltd, Feb. 01, 2022. doi: 10.1016/j.est.2021.103840.
- [113] G. Abdeali and A. R. Bahramian, “A comprehensive review on rheological behavior of phase change materials fluids (slurry and emulsion): The way toward energy efficiency,” *J. Energy Storage*, vol. 55, p. 105549, Nov. 2022, doi: 10.1016/J.EST.2022.105549.
- [114] S. Puupponen, A. Seppälä, O. Vartia, K. Saari, and T. Ala-Nissilä, “Preparation of paraffin and fatty acid phase changing nanoemulsions for heat transfer,” *Thermochim. Acta*, vol. 601, pp. 33–38, Feb. 2015, doi: 10.1016/J.TCA.2014.12.020.
- [115] K. Golemanov, S. Tcholakova, N. D. Denkov, and T. Gurkov, “Selection of Surfactants for Stable Paraffin-in-Water Dispersions, undergoing Solid–Liquid Transition of the Dispersed Particles,” *Langmuir ACS J. surfaces colloids.*, vol. 22, no. 8, pp. 3560–3569, 2006, doi: 10.1021/la053059y.
- [116] X. Zhang, J. Niu, S. Zhang, and J.-Y. Wu, “PCM in water emulsions: Supercooling reduction effects of nano-additives, viscosity effects of surfactants and stability,” *Adv. Eng. Mater.*, vol. 17, no. 2, pp. 181–188, 2015, doi: 10.1002/adem.201300575.
- [117] D. Cabaleiro *et al.*, “Development of paraffinic phase change material nanoemulsions for thermal energy storage and transport in low-temperature applications,” *Appl. Therm. Eng.*, vol. 159, p. 113868, Aug. 2019, doi: 10.1016/J.APPLTHERMALENG.2019.113868.
- [118] B. Sivapalan, M. Neelesh Chandran, S. Manikandan, M. K. Saranprabhu, S. Pavithra, and K. S. Rajan, “Paraffin wax–water nanoemulsion: A superior thermal energy storage medium providing higher rate of thermal energy storage per unit heat exchanger volume than water and paraffin wax,” *Energy Convers. Manag.*, vol. 162, pp. 109–117, Apr. 2018, doi: 10.1016/J.ENCONMAN.2018.01.073.

- [119] T. Shi, M. Zhang, H. Liu, and X. Wang, “Phase-change nanofluids based on n-octadecane emulsion and phosphorene nanosheets for enhancing solar photothermal energy conversion and heat transportation,” *Sol. Energy Mater. Sol. Cells*, vol. 248, p. 112016, Dec. 2022, doi: 10.1016/J.SOLMAT.2022.112016.
- [120] B. M. Tripathi, S. K. Shukla, and P. K. S. Rathore, “A comprehensive review on solar to thermal energy conversion and storage using phase change materials,” *J. Energy Storage*, vol. 72, p. 108280, Nov. 2023, doi: 10.1016/j.est.2023.108280.
- [121] Z. A. Nawsud, A. Altouni, H. S. Akhijahani, and H. Kargarsharifabad, “A comprehensive review on the use of nano-fluids and nano-PCM in parabolic trough solar collectors (PTC),” *Sustain. Energy Technol. Assessments*, vol. 51, Jun. 2022, doi: 10.1016/j.seta.2021.101889.
- [122] B. Kalidasan, A. K. Pandey, S. Shahabuddin, M. Samykano, M. Thirugnanasambandam, and R. Saidur, “Phase change materials integrated solar thermal energy systems: Global trends and current practices in experimental approaches,” *Journal of Energy Storage*, vol. 27. Elsevier Ltd, Feb. 01, 2020. doi: 10.1016/j.est.2019.101118.
- [123] K. Yuan, H. Wang, J. Liu, X. Fang, and Z. Zhang, “Novel slurry containing graphene oxide-grafted microencapsulated phase change material with enhanced thermo-physical properties and photo-thermal performance,” *Sol. Energy Mater. Sol. Cells*, vol. 143, pp. 29–37, Dec. 2015, doi: 10.1016/J.SOLMAT.2015.06.034.
- [124] F. Wang, J. Liu, X. Fang, and Z. Zhang, “Graphite nanoparticles-dispersed paraffin/water emulsion with enhanced thermal-physical property and photo-thermal performance,” *Sol. Energy Mater. Sol. Cells*, vol. 147, pp. 101–107, 2016, doi: 10.1016/j.solmat.2015.12.013.
- [125] J. Liu, L. Chen, X. Fang, and Z. Zhang, “Preparation of graphite nanoparticles-modified phase change microcapsules and their dispersed slurry for direct absorption solar collectors,” *Sol. Energy Mater. Sol. Cells*, vol. 159, pp. 159–166, 2017, doi: 10.1016/j.solmat.2016.09.020.
- [126] F. Wang, Z. Ling, X. Fang, and Z. Zhang, “Optimization on the photo-thermal conversion performance of graphite nanoplatelets decorated phase change material emulsions,” *Sol. Energy Mater. Sol. Cells*, vol. 186, pp. 340–348, Nov. 2018, doi:



- 10.1016/J.SOLMAT.2018.07.005.
- [127] K. Yuan, J. Liu, X. Fang, and Z. Zhang, “Novel facile self-assembly approach to construct graphene oxide-decorated phase-change microcapsules with enhanced photo-to-thermal conversion performance,” *J. Mater. Chem. A*, vol. 6, no. 10, pp. 4535–4543, Mar. 2018, doi: 10.1039/C8TA00215K.
- [128] Z. Liu, Z. Chen, and F. Yu, “Enhanced thermal conductivity of microencapsulated phase change materials based on graphene oxide and carbon nanotube hybrid filler,” *Sol. Energy Mater. Sol. Cells*, vol. 192, pp. 72–80, Apr. 2019, doi: 10.1016/J.SOLMAT.2018.12.014.
- [129] Z. Wang, J. Qu, R. Zhang, X. Han, and J. Wu, “Photo-thermal performance evaluation on MWCNTs-dispersed microencapsulated PCM slurries for direct absorption solar collectors,” *J. Energy Storage*, vol. 26, p. 100793, Dec. 2019, doi: 10.1016/J.EST.2019.100793.
- [130] S. T. Latibari, J. Eversdijk, R. Cuypers, V. Drosou, and M. Shahi, “Preparation of phase change microcapsules with the enhanced photothermal performance,” *Polymers (Basel)*, vol. 11, no. 9, 2019, doi: 10.3390/polym11091507.
- [131] Q. Zhao *et al.*, “Graphene oxide Pickering phase change material emulsions with high thermal conductivity and photo-thermal performance for thermal energy management,” *Colloids Surfaces A Physicochem. Eng. Asp.*, vol. 575, pp. 42–49, Aug. 2019, doi: 10.1016/J.COLSURFA.2019.05.007.
- [132] F. Agresti *et al.*, “Nano-encapsulated PCM emulsions prepared by a solvent-assisted method for solar applications,” *Sol. Energy Mater. Sol. Cells*, vol. 194, no. July 2018, pp. 268–275, 2019, doi: 10.1016/j.solmat.2019.02.021.
- [133] G. Zhang, Z. Yu, G. Cui, B. Dou, W. Lu, and X. Yan, “Fabrication of a novel nano phase change material emulsion with low supercooling and enhanced thermal conductivity,” *Renew. Energy*, vol. 151, pp. 542–550, 2020, doi: 10.1016/j.renene.2019.11.044.
- [134] G. Gao, T. Zhang, C. Guo, S. Jiao, and Z. Rao, “Photo-thermal conversion and heat storage characteristics of multi-walled carbon nanotubes dispersed magnetic phase change microcapsules slurry,” *Int. J. energy Res.*, vol. 44, no. 8, pp. 6873–6884, 2020, doi: 10.1002/er.5436.

- [135] S. Barison, D. Cabaleiro, S. Rossi, A. Kovtun, M. Melucci, and F. Agresti, “Paraffin–graphene oxide hybrid nano emulsions for thermal management systems,” *Colloids Surfaces A Physicochem. Eng. Asp.*, vol. 627, no. June, 2021, doi: 10.1016/j.colsurfa.2021.127132.
- [136] S. K. Hazra, S. Ghosh, and T. K. Nandi, “Photo-thermal conversion characteristics of carbon black-ethylene glycol nanofluids for applications in direct absorption solar collectors,” *Appl. Therm. Eng.*, vol. 163, Dec. 2019, doi: 10.1016/j.applthermaleng.2019.114402.
- [137] E. T. Ulset, P. Kosinski, and B. V. Balakin, “Solar steam in an aqueous carbon black nanofluid,” *Appl. Therm. Eng.*, vol. 137, pp. 62–65, Jun. 2018, doi: 10.1016/j.applthermaleng.2018.03.038.
- [138] X. Zuo *et al.*, “Experimental investigation on photothermal conversion properties of collagen solution-based carbon black nanofluid,” *Case Stud. Therm. Eng.*, vol. 38, Oct. 2022, doi: 10.1016/j.csite.2022.102371.
- [139] J. Burgos, M. Ayora-Fernández, R. Mondragón, U. Nithiyantham, F. Fabregat-Santiago, and L. Hernández, “Characterization of hybrid carbon - paraffin/water nanoemulsions for DASC: stability, thermal energy storage and optical properties,” *IMPRES. The Sixth International Symposium on Innovative Materials and Processes in Energy Systems*, 2022. <https://impres2022.com/>
- [140] J. Burgos, R. Mondragón, E. B. Elcioglu, F. Fabregat-Santiago, and L. Hernández, “Experimental Characterization and Statistical Analysis of Water-Based Gold Nanofluids for Solar Applications: Optical Properties and Photothermal Conversion Efficiency,” *Sol. RRL*, vol. 6, no. 7, p. 2200104, 2022, doi: 10.1002/solr.202200104.
- [141] N. Navarrete *et al.*, “Nanofluid based on self-nanoencapsulated metal/metal alloys phase change materials with tuneable crystallisation temperature,” *Sci. Rep.*, vol. 7, pp. 1–10, 2017, doi: 10.1038/s41598-017-17841-w.
- [142] E. Günther, L. Huang, H. Mehling, and C. Dötsch, “Subcooling in PCM emulsions – Part 2: Interpretation in terms of nucleation theory,” *Thermochim. Acta*, vol. 522, no. 1–2, pp. 199–204, Aug. 2011, doi: 10.1016/J.TCA.2011.04.027.
- [143] W. M. Haynes, David R. Lide, and Thomas J. Bruno, Eds., *Handbook of Chemistry*

- and Physics*, 95th ed. Boca Raton, FL: CRC Press, 2014.
- [144] L. Colla, L. Fedele, S. Mancin, B. Buonomo, D. Ercole, and O. Manca, “Nano-PCMs for passive electronic cooling applications”, doi: 10.1088/1742-6596/655/1/012030.
- [145] A. Martínez, M. Carmona, C. Cortés, and I. Arauzo, “Characterization of Thermophysical Properties of Phase Change Materials Using Unconventional Experimental Technologies”, doi: 10.3390/en13184687.
- [146] R.H.Perry and D.W.Green, *Perry’s Chemical Engineering*, 7th ed. New York: McGraw-Hill.
- [147] G. A. Carter and D. C. McCain, “Relationship of leaf spectral reflectance to chloroplast water content determined using NMR microscopy,” *Remote Sens. Environ.*, vol. 46, no. 3, pp. 305–310, Dec. 1993, doi: 10.1016/0034-4257(93)90050-8.
- [148] R. A. Viscarra Rossel and A. B. McBratney, “Laboratory evaluation of a proximal sensing technique for simultaneous measurement of soil clay and water content,” *Geoderma*, vol. 85, no. 1, pp. 19–39, Jul. 1998, doi: 10.1016/S0016-7061(98)00023-8.
- [149] S. Jacquemoud, S and Ustin, “Application of radiative transfer models to moisture content estimation and burned land mapping,” in *4th International Workshop on Remote Sensing and GIS Applications to Forest Fire Management*, 2003, pp. 3–12.
- [150] A. Said, A. Salah, and G. A. Fattah, “Enhanced thermo-optical switching of paraffin-wax composite spots under laser heating,” *Materials (Basel)*, vol. 10, no. 5, 2017, doi: 10.3390/ma10050525.
- [151] A. Said, A. Salah, and G. Abdel Fattah, “Thermo-optic switching properties of paraffin-wax hosting carbon fillers,” *J. Energy Storage*, vol. 19, pp. 260–271, Oct. 2018, doi: 10.1016/J.EST.2018.07.016.
- [152] Z. Wang *et al.*, “Dynamic tuning of optical absorbers for accelerated solar-thermal energy storage,” *Nat. Commun. 2017 81*, vol. 8, no. 1, pp. 1–9, Nov. 2017, doi: 10.1038/s41467-017-01618-w.



# **CHAPTER 8.**

## **Annex**



## 8. Annex

### 8.1. Uncertainty analysis

For the different thermophysical properties measured ( $D$ ,  $c_p$ ,  $\Delta H$ ,  $k$  and  $PTE$ ) several tests were carried out in order to obtain an average value and a statistical error. Equation A.1 was used as a general expression for a measured property ( $\chi$ ), in terms of its average value ( $\bar{\chi}$ ), and the experimental statistical error ( $\varepsilon_{\bar{\chi}}$ ):

$$\chi = \bar{\chi} \pm \varepsilon_{\bar{\chi}} \quad (\text{A.1})$$

The experimental statistical error was obtained from the standard deviation,  $\sigma$ , of the taken  $n$  measurements, according to Equation A.2.

$$\varepsilon_{\bar{\chi}} = t_{n-1,0.025} \frac{\sigma}{\sqrt{n}} \quad (\text{A.2})$$

where  $t_{n-1,0.025}$  is student's t-distribution for  $n-1$  degrees of freedom at a 95 % confidence level.

Relative variables of a measured properties ( $\chi_{rel}$ ) were calculated as the ration between the average emulsion property ( $\bar{\chi}_{em}$ ) and the average water property ( $\bar{\chi}_{water}$ ):

$$\chi_{rel} = \frac{\bar{\chi}_{em}}{\bar{\chi}_{water}} \quad (\text{A.3})$$

Propagation of errors was used to calculate the experimental statistical error of the relative values ( $\varepsilon_{\chi_{rel}}$ ) as follows:

$$\varepsilon_{\chi_{rel}} = \left| \frac{\partial \chi_{rel}}{\partial \bar{\chi}_{em}} \right| \varepsilon_{\bar{\chi}_{em}} + \left| \frac{\partial \chi_{rel}}{\partial \bar{\chi}_{water}} \right| \varepsilon_{\bar{\chi}_{water}} \quad (\text{A.4})$$

$$\varepsilon_{\chi_{rel}} = \frac{1}{\bar{\chi}_{water}} \varepsilon_{\bar{\chi}_{em}} + \frac{\bar{\chi}_{em}}{\bar{\chi}_{water}^2} \varepsilon_{\bar{\chi}_{water}} \quad (\text{A.5})$$

where  $\bar{\chi}_{em}$  and  $\bar{\chi}_{water}$  are the average values of emulsion and water properties respectively, and  $\varepsilon_{\bar{\chi}_{em}}$  and  $\varepsilon_{\bar{\chi}_{water}}$  are the experimental statistical bars of emulsion of water properties calculated with Equation A.2.



## 8.2. Scientific production

### Journal contributions

- J. Burgos, R. Mondragón, E. Begum Elcioglu, F. Fabregat-Santiago and L. Hernández. Experimental characterization and statistical analysis of water-based gold nanofluids for solar applications: optical properties and photothermal conversion efficiency. *Solar RRL*. Vol. 6, no. 7, 2200104, pp.1-10. 2022.  
DOI: [10.1002/solr.202200104](https://doi.org/10.1002/solr.202200104)  
Impact factor: 7.9
- J. Burgos, R. Mondragón, R. Martínez-Cuenca, U. Nithiyantham, S. Barison, S. Mancin, F. Fabregat-Santiago and L. Hernández. Photothermal properties and performance of hybrid carbon-paraffin/water emulsions. *Journal of Energy Storage*. Vol. 73, no. 12, 109136, pp. 1-14. 2023.  
DOI: [10.1016/j.est.2023.109136](https://doi.org/10.1016/j.est.2023.109136)  
Impact factor: 9.4

### Contributions to international conferences

- J. Burgos, R. Mondragón, A. Gimeno, A. Galan and L. Hernández. Experimental characterisation of gold nanofluids for solar applications: optical properties and photothermal efficiency. 15<sup>th</sup> International conference on heat transfer, fluid mechanics and thermodynamics ([HEFAT2021](#)). Virtual (Amsterdam, Netherlands). ISBN 9781775922162.
- J. Burgos, M. Ayora-Fernández, R. Mondragón, U. Nithiyantham, Fabregat-Santiago and L. Hernández. Characterization of hybrid carbon-paraffin/water nanoemulsions for DASC: stability, thermal energy storage and optical properties. The Sixth International Symposium on Innovative Materials and Processes in Energy Systems ([IMPRES 2022](#)). Barcelona, Spain.
- J. Burgos, R. Mondragón, S. Barison, F. Agresti, S. Mancin, G. Rigueti, S. Rossi and L. Hernández. Paraffin/water nanoemulsions with reduced supercooling for thermal management systems. 8th Micro and nano flows conference ([MNF2023](#)). Padova, Italy.



**8.2.1. *Experimental characterization and statistical analysis of water-based gold nanofluids for solar applications: optical properties and photothermal conversion efficiency.***

Authors: J. Burgos, R. Mondragón, E. Begum Elcioglu, F. Fabregat-Santiago and L. Hernández

Journal: Solar RRL

ISSN: 2367-198X

Year:2022

Volume: 6

Page: 1-10

DOI: [10.1002/solr.202200104](https://doi.org/10.1002/solr.202200104)

Quality index (Source: Journal Citation Report)

2022 Journal Impact Factor: 7.9

5-Year Journal Impact Factor: 7.6

Number of citation of the paper: 5

Category	Rank	Quartile	Percentile
Materials science, multidisciplinary	71/342	Q1	79.4
Energy and fuels	29/115	Q2	75.2



# Experimental Characterization and Statistical Analysis of Water-Based Gold Nanofluids for Solar Applications: Optical Properties and Photothermal Conversion Efficiency

Jorge Burgos, Rosa Mondragón, Elif Begum Elcioglu, Francisco Fabregat-Santiago, and Leonor Hernández\*

Optimizing optical and photothermal properties of the solar nanofluids (NFs) to be used in direct absorption solar collectors is a key issue to maximize efficiencies in these collector types. This work both experimentally and statistically analyzes the influence of the size (5 and 20 nm) and concentration (5.1, 28.2, and 51.3 ppm) of gold nanoparticles (NPs) on several important variables for collector performance: NF stability, extinction coefficient, photothermal efficiency, etc. The research work shows that the addition of small amounts of gold NPs, whose surface plasmon resonance has wavelengths close to 520 nm, greatly improves the light absorption capacity of the base fluid (water). The statistical analysis confirms the influence of NP size and concentration on photothermal conversion efficiency (PTE), which lead to an increase of up to 121% for the smallest-sized NF with the highest concentration.

While recent trends indicate that the implementation of environment-conscious energy systems is an accompanist to alternative fossil fuel use, it is becoming increasingly clear that a paradigm change is required to make clean energy processes dominant to not exceed the global warming limit.

In recent decades, solar energy has been regarded as the most promising source of inexhaustible clean energy. The two main ways of collecting and transforming solar energy are photovoltaic solar energy and solar thermal energy,<sup>[2]</sup> of which the latter is the basis of this work. In solar thermal energy, solar radiation is collected by an absorption material and transferred as heat

energy to a transfer medium, usually a heat transfer fluid (HTF). Solar collectors are the devices used for solar-to-thermal energy conversion. They can be classified as concentrating and non-concentrating solar collectors. Non-concentrating solar collectors are used at low-to-medium temperatures, while the concentrating collectors that employ mirrors to concentrate incident solar energy are employed at higher temperatures.

The absorption material in conventional collectors is a dark surface that heats up and transfers heat to the HTF flowing through pipes. Although these collectors offer good energy conversion efficiency, a series of thermal losses appear to lower the possible maximum efficiency limit. In the 1970s, directly exposing HTF to incident radiation was proposed as an alternative to avoid such losses in conventional collectors.<sup>[3]</sup> This concept, in which heat is absorbed volumetrically by the working fluid instead of the surface, is known as direct absorption solar collectors (DASC). However, commonly used HTFs (water, oils, molten salts, etc.) are transparent in most of the solar spectrum, possess low solar radiation absorption capacity and, hence, offer low solar-to-thermal conversion efficiency. To overcome this issue, nanofluids (NFs) used as HTFs have been proposed in the literature.<sup>[4]</sup>

NFs were first postulated by Choi in 1995<sup>[5]</sup> as suspensions of nanoparticles (NPs, with sizes ranging from 1 to 100 nm) homogeneously dispersed in a base fluid to achieve improved thermal properties, mainly thermal conductivity and heat transfer performance. A wide variety of materials of different natures can be employed in these NFs to improve thermal characteristics. Some examples are metals (Ag, Au, Cu, Al, etc.), metal oxides (SiO<sub>2</sub>, Al<sub>2</sub>O<sub>3</sub>, TiO<sub>2</sub>, CuO, Fe<sub>2</sub>O<sub>3</sub>, etc.), and carbon-based materials (carbon nanotubes, graphene, graphene oxide, graphite, etc.).<sup>[6–9]</sup>

## 1. Introduction

The 2015 Paris Agreement was motivated to obtain a global response to climate change by keeping the rise in global temperature well below 2 °C and pursuing efforts to limit it to 1.5 °C.<sup>[1]</sup> European Union and United Nations Member States intend to address different strategies in relation to the energy system: improving energy efficiency and decarbonizing energy production systems by implementing renewable energy sources.

J. Burgos, R. Mondragón, L. Hernández  
Departamento de Ingeniería Mecánica y Construcción  
Universitat Jaume I  
12071 Castellón de la Plana, Spain  
E-mail: lhernand@uji.es

E. B. Elcioglu  
Department of Mechanical Engineering  
Eskisehir Technical University  
26555 Eskisehir, Turkey

F. Fabregat-Santiago  
Institute of Advanced Materials (INAM)  
Universitat Jaume I  
12071 Castellón de la Plana, Spain

 The ORCID identification number(s) for the author(s) of this article can be found under <https://doi.org/10.1002/solr.202200104>.

© 2022 The Authors. Solar RRL published by Wiley-VCH GmbH. This is an open access article under the terms of the Creative Commons Attribution-NonCommercial-NoDerivs License, which permits use and distribution in any medium, provided the original work is properly cited, the use is non-commercial and no modifications or adaptations are made.

DOI: 10.1002/solr.202200104



**8.2.2. *Photothermal properties and performance of hybrid carbon-paraffin/water emulsions.***

Authors: J. Burgos, R. Mondragón, R. Martínez-Cuenca, U. Nithiyantham, S. Barison, S. Mancin, F. Fabregat-Santiago and L. Hernández.

Journal: Journal of Energy Storage

ISSN: 2352-152X

Year: 2023

Volume: 73

Page: 1-14

DOI: [10.1016/j.est.2023.109136](https://doi.org/10.1016/j.est.2023.109136)

Quality index (Source: Journal Citation Report)

2022 Journal Impact Factor: 9.4

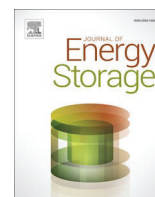
5-Year Journal Impact Factor: 9.1

Number of citation of the paper: 0

Category	Rank	Quartile	Percentile
Energy and fuels	19/115	Q1	83.9







## Research papers

# Photothermal properties and performance of hybrid carbon-paraffin/water emulsions

Jorge Burgos<sup>a</sup>, Rosa Mondragón<sup>a</sup>, Raúl Martínez-Cuenca<sup>a</sup>, Udayashankar Nithiyantham<sup>a</sup>,  
Simona Barison<sup>b</sup>, Simone Mancin<sup>c</sup>, Francisco Fabregat-Santiago<sup>d</sup>, Leonor Hernández<sup>a,\*</sup>

<sup>a</sup> Departamento de Ingeniería Mecánica y Construcción, Universitat Jaume I, 12071 Castellón de la Plana, Spain

<sup>b</sup> CNR ICMATE, Padova, Italy

<sup>c</sup> Department of Management and Engineering, University of Padova, Vicenza, Italy

<sup>d</sup> Institute of Advanced Materials (INAM), Universitat Jaume I, 12071 Castellón de la Plana, Spain



## ARTICLE INFO

## Keywords:

Solar nanofluid  
Phase change materials  
Emulsions  
Photothermal conversion efficiency  
Direct absorption solar collector

## ABSTRACT

Solar thermal energy has attracted renewed research interest for its excellent energy efficiency among different types of solar technologies. However, the limiting factor of them all is the intermittent nature of solar radiation. To overcome this drawback, it is possible to store absorbed light in form of heat using emulsions with phase-change materials (PCMs) dispersed in solar nanofluids by combining the advantage of solar thermal storage characteristics of PCMs and the higher light absorption capacity of solar nanofluids. In this study, paraffin/water and hybrid carbon-paraffin/water emulsions with 5 wt% paraffin wax RT44HC as PCM are proposed. Low-cost emulsions with proven colloidal stability were successfully produced, with and without small amounts of oxidized carbon black nanoparticles (0.01 wt%) dispersed in the emulsion. Thermal energy storage capacity improved up to 16 %, while maintaining good thermal conductivity properties. Optical properties were evaluated by means of a spectrophotometer with an integrating sphere, including both spectral absorbance and reflectance of the samples. Two experimental setups were developed with concentrated light, to evaluate the photothermal conversion efficiency under simulated and natural sunlight. The improvement of the light to heat conversion properties provided by the oxidized carbon black nanoparticles was confirmed, with PTE values of 1.5- and 2.7-fold better than the base fluid (water) using a solar simulator and natural sunlight, respectively.

## 1. Introduction

The global climate emergency has forced society to look for alternatives to produce sustainable clean energy. A variety of renewable energy sources is being proposed to replace or minimize the use of fossil fuels, including biomass, geothermal, hydropower, solar and wind [1]. Of them, solar energy has become an effective and potential way to achieve sustainable human development. Taking the leap from conventional fossil fuel energy production to renewable energy sources, such as solar, also implies an imbalance between production and demand. For this reason, thermal energy storage (TES) is one of the most promising ways to improve the efficiency and energy demand faced by society mainly due to industrial revolution [2,3].

Solar collectors in which solar radiation is absorbed directly on a dark surface and then thermal energy is transferred to a heat transfer fluid (HTF) are the commonest technology used to convert solar

radiation into heat. This collector type offers good efficiencies. However, during the process of transferring heat from the surface to fluid, losses that limit systems' efficiency occur. To improve this collector type, in the 1970s [4] the alternative of exposing HTF directly to incident radiation to, thus, absorb heat volumetrically, but not superficially, was proposed. These systems are now known as direct absorption solar collectors (DASC). In DASC systems, the possible effect of heat losses by conduction and convection processes is neglected compared to conventional collectors through direct absorption. However, the HTFs traditionally used in these systems (i.e. water, alcohols, oils, molten salts, etc.) [5] are mostly transparent over most of the solar spectrum, which makes them inefficient in absorbing light and, thus, reduces the heat conversion efficiency ability of light [6].

To solve the issue raised by these HTFs, employing nanofluids (NFs), consisting of the dispersion of nanoparticles (NPs) with a size range from 1 to 100 nm in a base fluid, was proposed. These NFs, capable of improving solar radiation absorption with very low concentrations of

\* Corresponding author.

E-mail address: [lhermand@uji.es](mailto:lhermand@uji.es) (L. Hernández).



### 8.2.3. *Contributions to international conferences*

- J. Burgos, R. Mondragón, A. Gimeno, A. Galan and L. Hernández. Experimental characterisation of gold nanofluids for solar applications: optical properties and photothermal efficiency. 15<sup>th</sup> International conference on heat transfer, fluid mechanics and thermodynamics ([HEFAT2021](#)). Virtual (Amsterdam, Netherlands). ISBN 9781775922162.
- J. Burgos, M. Ayora-Fernández, R. Mondragón, U. Nithiyantham, Fabregat-Santiago and L. Hernández. Characterization of hybrid carbon-paraffin/water nanoemulsions for DASC: stability, thermal energy storage and optical properties. The Sixth International Symposium on Innovative Materials and Processes in Energy Systems ([IMPRES 2022](#)). Barcelona, Spain.
- J. Burgos, R. Mondragón, S. Barison, F. Agresti, S. Mancin, G. Rigueti, S. Rossi and L. Hernández. Paraffin/water nanoemulsions with reduced supercooling for thermal management systems. 8th Micro and nano flows conference ([MNF2023](#)). Padova, Italy.



## EXPERIMENTAL CHARACTERISATION OF GOLD NANOFUIDS FOR SOLAR APPLICATIONS: OPTICAL PROPERTIES AND PHOTOTHERMAL EFFICIENCY

Burgos J., Mondragón R., Gimeno-Furió A., Galan A. and Hernández L.\*

\*Author for correspondence

Department of Mechanical Engineering and Construction

Universitat Jaume I

Castellón de la Plana, 12071.

Spain

E-mail : lhernand@uji.es

### ABSTRACT

Noble metal nanoparticles are introduced in solar applications to improve the photothermal efficiency of solar fluids used in direct solar absorption collectors. These metallic particles are interesting due to the effect of surface plasmon resonance (SPR), which usually occurs in the visible light spectrum, range weakly absorbed by most of the heat transfer fluids. When these nanoparticles are irradiated with the appropriate wavelength, the free charge carriers are perturbed and begin to oscillate with the same resonance as the irradiated energy. For this reason, particles able to interact with solar radiation can offer advantages in direct photothermal conversion processes, increasing the efficiency of solar collectors. In the present work, gold nanoparticles were introduced into water to be tested as a solar radiation absorber. Some studies confirm that with low concentrations of these nanoparticles in a base fluid, it is possible to increase the absorption capacity, obtaining a notable improvement in the efficiency of solar energy conversion to thermal energy. Three commercial nanofluids were tested, which contain gold nanoparticles with different sizes of 5, 20 and 50 nm. The particle size distribution was studied by measuring particles at different temperatures (25, 40, 60 and 85 °C) using the Dynamic Light Scattering (DLS) technique. The extinction coefficient of all samples was obtained by measurements with the help of a spectrophotometer. Finally, the temperature change achieved when lighting the samples with an artificial sunlight simulator was measured and photothermal conversion efficiencies were evaluated, with important increases when comparing the nanofluids with the base fluid. These results provide evidence of the improvement that occurs when nanoparticles are introduced into direct absorption solar collectors.

### INTRODUCTION

The consumption of energy worldwide and mainly in industrialised countries continues to grow at an unstoppable rate. Society today is highly dependent on the consumption of fossil fuel sources, used to produce energy both industrially and domestically. The development and use of renewable energy sources are the optimal solution to tackle the growing problem of increasing energy demand on the one hand, and the need to reduce emissions of polluting gases due to the burning of fossil fuels on the other. Solar energy is one of the best candidates to replace these energy sources, as it is clean, cheap and inexhaustible. Systems based on direct absorption solar collectors (DASC) are a good alternative to improve the

efficiency of systems used in the conversion of solar energy into thermal energy [1, 2]. This type of collector is based on the direct absorption of solar radiation by the working fluid in the system, this heat transfer fluid (HTF) can be water, oils, molten salts, ionic liquids, etc; which are transparent to most of the solar spectrum.

The suspension of certain nanoparticles (NPs) like metals (such as Ag, Au, Cu and Al) [3], metal oxides (such as CuO, TiO<sub>2</sub>, Al<sub>2</sub>O<sub>3</sub> and Fe<sub>2</sub>O<sub>3</sub>) [4] or carbon-based (such as graphite, graphene, carbon nanotubes, etc.) [5], form what is known as nanofluid (NF) defined in 1995 by Choi et al [6] as a stable suspension of dilute particles with sizes smaller than 100 nm. They present several thermal and optical advantages over the usual HTFs used for energy production, however, due to the large variety of particles mentioned above, a detailed analysis is necessary to obtain as much information as possible about their specific properties. Optical phenomena in nanofluids are produced by the two media, the base fluid and the nanoparticles. Due to the unusual behaviour of nanoparticles observed in some cases, the optical properties cannot be described as in the case of a macroscopic system. The corresponding linear response of a nanoparticle system is therefore the result of many factors that must be taken into account: particle size, shape, material, base fluid and the distance between the individual particles in the medium [7].

In the particular case of plasmonic NPs, such as Au and Ag, they have a great interest due to the surface plasmon resonance (SPR) effect, which is the collective oscillation of electrons stimulated by incident light, which is an effective way of converting solar energy into thermal energy. The resonance is established when the frequency of the light photons matches the natural frequency of the surface electrons oscillating against the restoring force of the positive nuclei. In addition to modifying the absorption capacity of the fluid, plasmonic particles can effectively convert light into heat [8]. Therefore, particles able to interact with this radiation have a great interest for application in direct photothermal conversion processes.

Zhang et al [9], demonstrated that low concentrations (0.15 ppm) of gold nanoparticles (GNP) resulted in an increase in photothermal conversion efficiency (PTE) of 20%, compared to the pure base fluid and a specific absorption rate (SAR) of  $\approx 10$  kW/g. The PTE increased with increasing nanoparticle concentration, in contrast to the SAR, which showed an inverse trend. Filho et al [8], found that the photothermal properties of Ag particles nanofluids were good for small particle concentrations between 1.65 and 6.5 ppm. An almost constant

SAR value of 0.6 kW/g was obtained at initial heating for concentrations up to 6.5 ppm, with a clear reduction in performance at higher concentrations, associated with an increase in particle-particle interactions.

In the present work, three commercial nanofluids with different sizes of gold nanoparticles dispersed in water as the based fluid were analysed in terms of particle size, colloidal stability under high temperature conditions, optical properties and photothermal conversion efficiency.

## NOMENCLATURE

$A$	[m <sup>2</sup> ]	Area
$\beta$	[kJ/s°C]	Loss Coefficient
$c_p$	[kJ/kg°C]	Specific Heat
$I$	[W/m <sup>2</sup> ]	Incident radiation
$I_0$	[W/m <sup>2</sup> ·nm]	Incident intensity
$I_T$	[W/m <sup>2</sup> ·nm]	Transmitted intensity
$\lambda$	[nm]	Wavelength
$\mu_{ext}$	[cm <sup>-1</sup> ]	Extinction Coefficient
$m$	[kg]	Mass
$D_{50}$	[nm]	Mean diameter
$t$	[s]	Time
$T$	[°C]	Ambient Temperature
$\tau$	[-]	Transmission
$W$	[W]	Power
$x$	[cm]	Sample Thickness

### Subscripts

$0$	Initial
$a$	Ambient
$abs$	Absorbed
$loss$	Loss
$measured$	Measured
$n$	Nanoparticles
$sample$	Sample
$w$	Water

### Abbreviations

DASC	Direct Absorption Solar Collector
DLS	Dynamic Light Scattering
GNP	Gold Nanoparticle
HTF	Heat Transfer Fluid
ICP-MS	Inductively Coupled Plasma Mass Spectrometer
NF	Nanofluid
NP	Nanoparticle
PBS	Phosphate Buffered Saline
PTE	Photothermal Conversion Efficiency
SPR	Surface Plasmon Resonance
SAR	Specific Absorption Rate

## MATERIALS AND METHODS

### Nanofluids

To study the effect of NP size and concentration on photothermal conversion efficiency, three commercial water-based NFs, provided by Sigma Aldrich, were used. These contain nanoparticles of different sizes (5, 20 and 50 nm, according to the manufacturer), all of them are stabilized in 0.1 mM PBS (Phosphate Buffered Saline), reactant free and have an optical density of one. Finally, the results were compared with the ones obtained for ultrapure water Milli-Q.

### Experimental techniques

The inductively coupled plasma mass spectrometer technique, which allows the elemental analysis of the gold nanofluid solutions, was used to measure the gold concentration of the three nanofluids with the ICAP-RQ equipment (ThermoFisher Scientific). Argon was used as carrier gas while Helium was used for removal of interferences. The sample volume was of 10-15 ml and a certified gold standard was used to measure the concentration.

The size distribution of the NPs in the nanofluids was analysed using the DLS technique with a Zetasizer Nano ZS instrument (Malvern Instruments Ltd.). It measures the light scattered by the particles in suspension due to their Brownian motion and the intensity of the signal is related to their size. The instrument consists of a laser centred at 532 nm and the hydrodynamic diameter is calculated based on the intensity of the scattered light at 173°. The system allows the samples to be heated by means of a Peltier system, so each NF was measured at four temperatures: 25, 40, 60 and 85 °C in a quartz cuvette.

The commercial spectrophotometer Cary 500 (Varian) UV-Vis-NIR was used to determine the optical properties. This device can analyse the electromagnetic spectrum and thus determine the properties of light. The system consists of a Xenon lamp as light source, which shines a double beam into the reference cell and into the cell containing the sample, allowing the detector to compare the two signals. The wavelength range used by the spectrophotometer in the measurement is from 400 to 1100 nm, a range that comprises 76.7% of the total radiation incident on the earth's surface [10]. The system first operates by passing the light beam, with incident intensity,  $I_0$ , allowing a fraction of radiation to pass through the medium, thus acquiring the transmitted intensity,  $I_T$ . With these two values the extinction coefficient ( $\mu_{ext}(\lambda)$ ) was obtained as a function of wavelength. When the light beam is incident, it is scattered and absorbed by the particles in the medium. However, as the nanoparticles are highly dispersed in the nanofluid, it was considered multiple scattering a phenomenon that can be neglected, thus obtaining the *Beer-Lambert law* relating transmittance and extinction presented in equation 1:

$$\mu_{ext}(\lambda) = -\frac{\log(I_T/I_0)}{x} \quad (1)$$

where  $x$  is the sample thickness (1 cm in the measurement).

Photothermal conversion tests were carried out using a commercial Mercury-Xenon lamp (Oriel Instruments Light Source, Mercury-Xenon, 1000 W) as a light source. The spectrum of the source is represented in Figure 1, showing how the solar simulator reproduces to some extent the spectral behaviour of the solar irradiation at ground level. The way of preparation and measurement of the experimental setup for photothermal characterisation was carried out in the same way as in previous work [10]. The experiment was carried out in a closed and insulated room to avoid the thermal effects of the environment and to work under more controlled conditions. A

potentiometer (Ophir 1Z01500, Nova Display) was used to measure the power of the solar simulator in place of the glass tube ( $W_{measured}$ ). Afterwards, the tube with the NF was put in place.

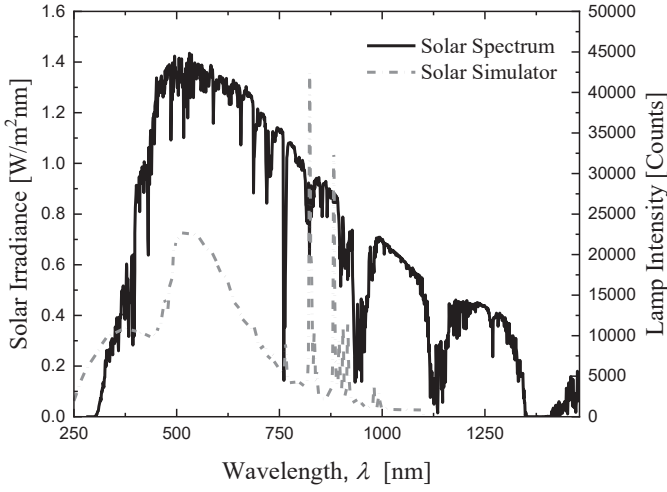


**Figure 1** Solar and artificial sunlight simulator spectra

In this work, the photothermal conversion efficiency (PTE) was calculated in two different ways. As a first approach, the PTE was defined as the ratio between the power of energy absorbed by the fluid ( $W_{abs}$ ) and the power of the radiation incident on the sample ( $W_{sample}$ ) as shown in the equation (2):

$$PTE(\%) = \frac{W_{abs}}{W_{sample}} \cdot 100 \quad (2)$$

$W_{sample}$  can be calculated from  $W_{measured}$  by applying a correction that considers the losses caused by the propagation of light through media with different refractive indices between the glass of the tube and liquid, using the equation (3):

$$W_{sample} = W_{measured} \cdot \tau \quad (3)$$

where  $\tau$  is the transmission rate and has a value of 0.86 in this experiment [10].

The PTE was calculated during the heating process of the NF, between the starting period of the experiment and the first 6000 s of the measurement, which is sufficient time for the temperature to stabilise. To obtain the power absorbed by the fluid,  $W_{abs}$ , it is necessary to make a power balance including the  $W_{sample}$  and the losses due to convection and radiation ( $W_{loss}$ ), through the following equations:

$$W_{sample} = W_{abs} - W_{loss} \quad (4)$$

$$m_w \cdot c_{p,w} \cdot \frac{dT}{dt} = W_{abs} - \beta(T - T_a) \quad (5)$$

where  $m_w$  is the mass of the water,  $c_{p,w}$  is the specific heat of the water,  $T$  is the fluid temperature,  $T_a$  is the ambient temperature

and  $\beta$  is the loss coefficient. Data of water are taken into account in the equation instead of that of the nanofluid due to the small contribution of the low nanoparticle concentration. By operating and applying the boundary equations at the beginning of the experiment, the equation of the heating process can be obtained:

$$T = \left[ \frac{W_{abs}}{\beta} + T_a \right] + [T_0 - T_a - \frac{W_{abs}}{\beta}] e^{-\frac{\beta}{m_w c_{p,w}} t} \quad (6)$$

where  $T_0$  is the initial temperature of the NF and  $t$  is the time. By fitting to an exponential curve to obtain the value of  $W_{abs}$ , the photothermal conversion efficiency defined in equation (2) can be calculated.

As a second approach, the PTE can be defined as the ratio between the energy stored in the nanofluid and the total incident radiation in an interval of time [9, 11-13]. Therefore, another method was used to calculate the PTE in the different nanofluids by means of the equation (7):

$$PTE = \frac{(c_{p,w} m_w + c_{p,n} m_n) \cdot \Delta T}{I \cdot A} \cdot \frac{\Delta T}{\Delta t} \sim \frac{(c_{p,w} m_w) \cdot \Delta T}{I \cdot A} \cdot \frac{\Delta T}{\Delta t} \quad (7)$$

Where  $c_{p,w}$  and  $c_{p,n}$  are the specific heat of water and nanoparticles,  $m_w$  and  $m_n$  are the mass of water and nanoparticles,  $\Delta T$  is the overall temperature increase of the system in a time interval  $\Delta t$ ,  $A$  is the area of the nanofluid illuminated during the experiment and  $I$  is the incident radiation. In this case the intensity value is also multiplied by a reduction factor of 0.86 due to changes in the refractive indices of the glass and the fluid. As the concentration of the nanoparticles in the fluid is very small, the term  $c_{p,n} m_n \sim 0$  and it can be disregarded for the calculation of efficiency.

In order to compare the experimental PTE obtained, a maximum theoretical photothermal efficiency is calculated, which is the maximum value that the ratio between the absorbed and incident intensity could theoretically reach, through the following equation [13]:

$$PTE_{max} = \frac{\int_{400}^{1100} I_{\lambda,i} (1 - e^{-\mu_{ext} x}) d\lambda}{\int_{400}^{1100} I_{\lambda,i} d\lambda} \quad (8)$$

where  $x$  is the length travelled by the light (2.5 cm in this case).

## RESULTS AND DISCUSSION

To ensure equal optical density for each nanofluid containing nanoparticles with different size, it is necessary to modify their concentration. As this information was not provided by the manufacturer, ICP-MS was used to experimentally measure the gold concentration. In Table 1 the results are shown and it can be observed how higher concentrations are obtained for the samples with smaller particle size.

**Table 1** Concentrations of gold NFs measured by ICP-MS

Nanofluid	Concentration [mg/l]
5 nm	59.6
20 nm	41.6
50 nm	23.9

The DLS measurements of the three NFs were performed at temperatures between 25 and 85 °C. Figure 2a. shows the particle size distribution for the three samples at 40 °C, in which it can be observed that the curves of the three nanofluids are monomodal and present the maximum frequency peak at values very close to those provided by the manufacturer. These peaks indicate a mean particle size of 7.25, 18.87 and 46.63 nm, which deviate slightly from the theoretical values of 5, 20 and 50 nm, respectively.

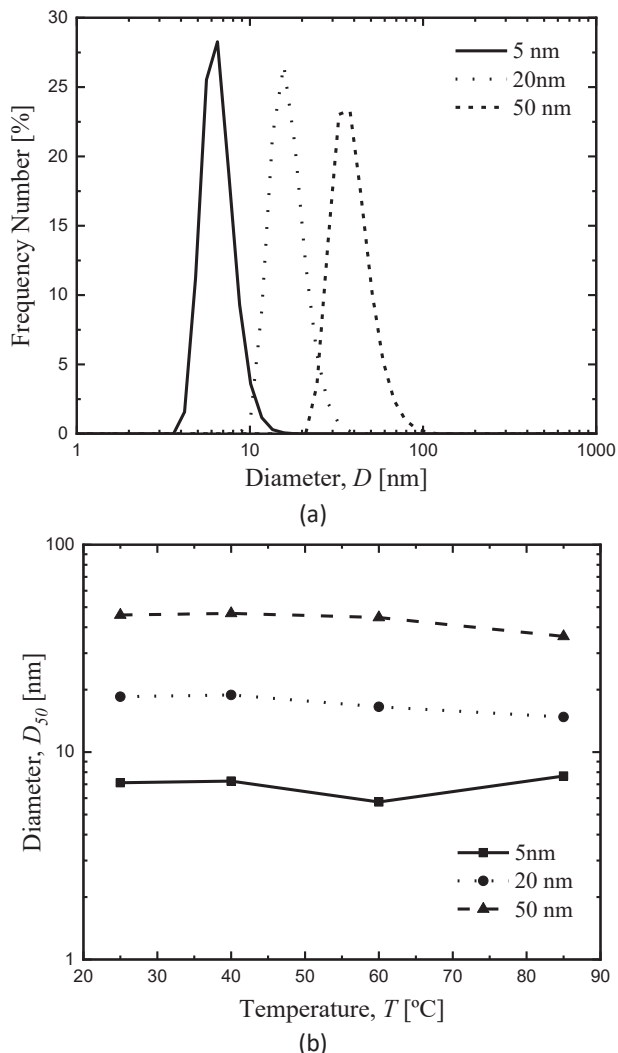


**Figure 2** (a) Particle size distribution of the NFs at 40 °C (b) Mean diameter ( $D_{50}$ ) of NFs at 25, 40, 60 and 85 °C

Figure 2b. shows the mean diameter ( $D_{50}$ ) values for the three samples measured at temperatures of 25, 40, 60 and 85 °C. The values in the graph indicate the variation of the particle diameters with temperature, showing that no significant changes were observed. The highest size decrease was measured for the 50 nm at 85 °C. In spite of this, the results indicate that increasing the temperature within this range does not significantly affect the stability of the nanofluids.

Figure 3 shows the extinction coefficients of the base fluid (water) and the three nanofluids with different particle sizes and concentrations (5, 20 and 50 nm). It can be seen how water does not present the SPR peak in the wavelength range of the visible spectrum, where the gold nanofluids do around 520-540 nm, following the behaviour of water in the rest of the wavelengths. All three NFs have an optical density value  $\sim 1$ , which is expected and is in good agreement with the values provided by the manufacturer. At the same time and as expected a blue shift of the SPR peak is observed with increasing particle size [14]. It is possible to see the direct relationship between the concentration values of nanoparticles of different sizes and the extinction coefficients: the higher the concentration of nanoparticles, the higher the value of the extinction coefficient. This behaviour has been observed both in previous experimental and theoretical studies [13] [15].

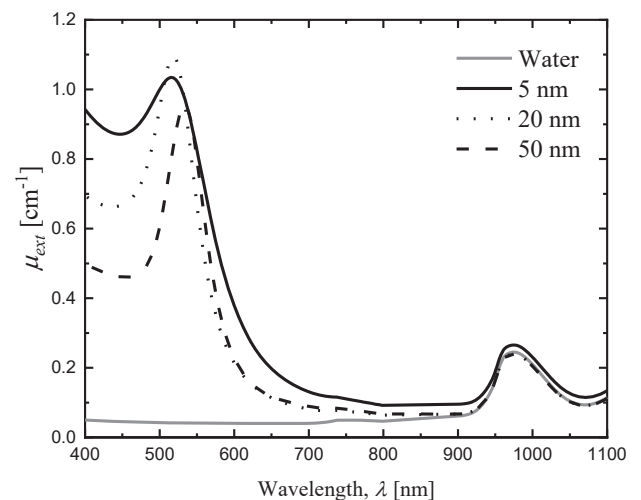


**Figure 3** Extinction coefficients of the base fluid (grey) and the base fluid with gold nanoparticles with different particle sizes

Figure 4 shows the temperature variation of the water and the three nanofluids with respect to the initial ambient temperature. After an irradiation time of 6000 s, water shows a temperature increase of  $\sim 9$  °C with respect to  $T_a$ , while nanofluids with particles sizes of 5, 20 and 50 nm increase up to 18, 15 and 14 °C, respectively. The trend observed in Figure 4 is related with the results in Figure 3 as the increase in the temperature rise of nanofluids with respect to water is in accordance with the higher absorption in the visible range of nanofluids.



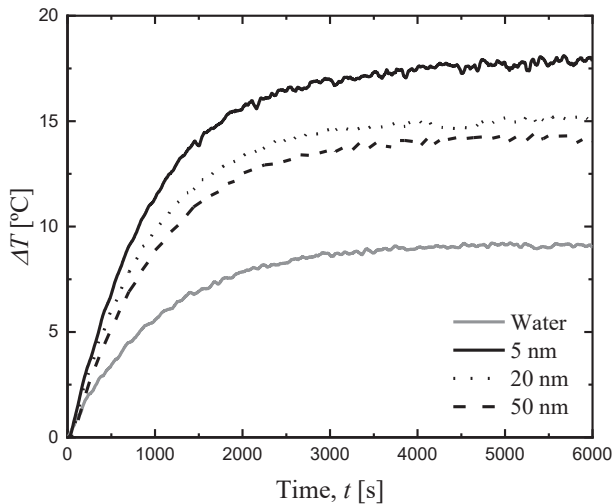


**Figure 4** Temperature profiles of base fluid (water) and the water-based gold nanofluids with different particle sizes

Based on the obtained temperature increases, using equation (2) and the average value over the measurement time for the first 6000 s calculated with the equation (7), the experimental PTE values were calculated. At the same time, the maximum values that the NFs could theoretically reach were calculated using equation (8). The ratios obtained between the efficiency values of the nanofluids with respect to water ( $PTE_{NF}/PTE_{water}$ ) for the three different PTE calculations are presented in Table 2. The efficiency values for the three nanoparticle sizes are directly connected to the extinction coefficient values, related in turn with the nanoparticle concentrations. Therefore, as the particle size decreases (and concentration increases), the efficiency value improves. Values higher than 1 means an improvement with respect to the efficiency of the base fluid, showing the better performance of the nanofluids.

The efficiency values for water are not presented, because in the wavelength range in which the measurement is made, water is mostly transparent to incident irradiation, so it is assumed that the value of the increase in efficiency is due to the presence of the gold nanoparticles [13].

**Table 2** Photothermal conversion efficiency ratios between the nanofluids and water with different calculation methods

Nanofluid	$PTE_{NF}/PTE_{water}$		
	Eq. (2)	Eq. (7)	Eq. (8)
5 nm	1.97	1.97	6.00
20 nm	1.92	1.65	5.19
50 nm	1.71	1.55	4.99

It is possible to see how the results obtained from the two types of experimental calculations (Eq. 2 and Eq. 7) and the maximum theoretical value (Eq. 8) follow the same trend, proving that there are large increases in efficiency with respect to water. The same or very similar results are seen in the case

of the calculations for the experimental results, the most efficient being the nanofluid with 5 nm nanoparticles, which almost doubles the efficiency value with respect to water. If the experimental results are compared with the theoretical ones, it is also possible to see how there is a big difference between the different values, this may be due to heat losses in the system.

## CONCLUSION

In this work, three water-based nanofluids with gold nanoparticles of similar optical depth with different sizes (5, 20 and 50 nm) and concentrations were characterised. Nanofluids were demonstrated to be colloidally stable up to 85 °C with no significant change in the particle size with temperature.

Regarding the optical characterisation, the extinction coefficient was measured confirming the higher absorption of the nanofluids due to the SPR of gold NPs ( $\lambda = 520\text{-}545$  nm). This increase leads to an enhancement in the photothermal conversion efficiency with respect to the base fluid as expected.

Different experimental PTE calculations were performed, obtaining similar results. These data were also compared to maximum theoretical PTE, that presented similar trends but with higher values, indicating heat losses in the measuring system. From the evolution of optical properties and efficiency with the particle size it can be concluded that the higher the concentration (smaller diameter), the higher the overall solar radiation absorption and therefore the photothermal conversion efficiency. As a main result, an enhancement of 97% in the PTE can be obtain with the 5 nm gold NPs dispersed in water.

## ACKNOWLEDGMENTS

This research was partially funded by Generalitat Valenciana through the project PROMETEO/2020/029 and by the Universitat Jaume I through the project UJI-B2020-32.

## REFERENCES

- [1] Rasih R. A., Sidik N. A. C., and Samion, S., Recent progress on concentrating direct absorption solar collector using nanofluids, *Journal of Thermal Analysis and Calorimetry*, Vol. 137, 2019, pp. 903-922
- [2] Chamsa-Ard W., Brundavanam S., Fung C. C., Fawcett D., and Poinern G., Nanofluid types, their synthesis, properties and incorporation in direct solar thermal collectors: A review, *Nanomaterials*, Vol. 7, 2017, pp. 131
- [3] Chen M., He Y., Zhu J., Shuai Y., Jiang B., and Huang, Y., An experimental investigation on sunlight absorption characteristics of silver nanofluids, *Solar Energy*, Vol.115, 2015, pp. 85-94
- [4] Gupta H. K., Agrawal G. D., and Mathur, J., An experimental investigation of a low temperature Al<sub>2</sub>O<sub>3</sub>-H<sub>2</sub>O nanofluid based direct absorption solar collector, *Solar Energy*, Vol 118, 2015, pp. 390-396
- [5] Mesgari S., Coulombe S., Hordy N., and Taylor, R. A., Thermal stability of carbon nanotube-based nanofluids for solar thermal collectors, *Materials Research*

- Innovations*, Vol. 19, 2015, S5-650
- [6] Choi S. U., and Eastman J. A., Enhancing thermal conductivity of fluids with nanoparticles, *International mechanical engineering congress and exhibition*, San Francisco, CA (United States), 12-17 Nov 1995.
- [7] Otanicar T. P., DeJarnette D., Hewa-kuruppu Y., and Taylor R. A., Filtering light with nanoparticles: a review of optically selective particles and applications, *Advances in Optics and Photonics*, Vol. 8, 2016, pp. 541-585
- [8] Bandarra Filho E. P., Mendoza O. S. H., Beicker C. L. L., Menezes A., and Wen D., Experimental investigation of a silver nanoparticle-based direct absorption solar thermal system, *Energy conversion and Management*, Vol. 84, 2014, pp. 261-267
- [9] Zhang H., Chen H. J., Du X., and Wen D., Photothermal conversion characteristics of gold nanoparticle dispersions, *Solar Energy*, Vol. 100, 2014, pp.141-147
- [10] Gimeno-Furió A., Martínez-Cuenca R., Mondragón R., Gasulla A. F. V., Doñate-Buendía C., Mínguez-Vega G., and Hernández L., Optical characterisation and photothermal conversion efficiency of a water-based carbon nanofluid for direct solar absorption applications, *Energy*, Vol. 212, 2020, pp. 118763
- [11] Jin H., Lin G., Bai L., Amjad M., Bandarra Filho E. P., and Wen D., Photothermal conversion efficiency of nanofluids: An experimental and numerical study *Solar Energy*, Vol. 139, 2016, pp.278-289
- [12] Zhang H., Chen H. J., Du X., Lin G., and Wen D. Dependence of photothermal conversion characteristics on different nanoparticle dispersions, *Journal of nanoscience and nanotechnology*, Vol. 15, 2015, pp. 3055-3060
- [13] Zeiny A., Jin H., Bai L., Lin G., and Wen D., A comparative study of direct absorption nanofluids for solar thermal applications, *Solar Energy*, Vol. 161, 2018, pp. 74-82
- [14] Chen M., He Y., Zhu J., and Kim D. R., Enhancement of photo-thermal conversion using gold nanofluids with different particle sizes, *Energy Conversion and Management*, Vol. 112, 2016, pp. 21-30
- [15] Taylor R. A., Phelan P. E., Otanicar T. P., Adrian R., and Prasher R., Nanofluid optical property characterization: towards efficient direct absorption solar collectors, *Nanoscale research letters*, Vol 6, 2011, pp. 1-11

---

## 193: Characterization of hybrid carbon - paraffin/water nanoemulsions for DASC: stability, thermal energy storage and optical properties

---

J. Burgos<sup>1</sup>, M. Ayora-Fernández<sup>1</sup>, R. Mondragón<sup>1</sup>, U. Nithiyantham<sup>1</sup>, F. Fabregat-Santiago<sup>2</sup>, L. Hernández<sup>1</sup>

<sup>1</sup>Departamento de Ingeniería Mecánica y Construcción, Universitat Jaume I, 12071 Castellón de la Plana  
<sup>2</sup>Institute of Advanced Materials (INAM), Universitat Jaume I, 12071 Castellón de la Plana

**KEYWORDS:** Paraffin/water nanoemulsion, carbon nanoparticles, optical properties, thermal energy storage

The combined use of solar nanofluids and phase change materials (PCMs) makes them good candidates as working fluids in direct absorption solar collectors (DASCs). Therefore, in this work, thermal energy storage densities of different paraffins were studied to fabricate hybrid carbon-paraffin/water nanoemulsions, incorporating small amounts of carbon nanoparticles. The effect of different surfactants on the stability of the nanoemulsions and the improvement in light absorption produced by the incorporation of carbon nanoparticles was studied.

Materials and experimental techniques: Three commercial paraffin waxes, RT<sub>35</sub>HC, RT<sub>44</sub>HC and RT<sub>54</sub>HC (Rubitherm Technologies GmbH) were used as PCMs. The selected carbon nanoparticles were carbon black (CB) (ELFTEX 570, Cabot Corporation) and oxidised carbon black (CBox). The surfactants studied (Sigma Aldrich, Ltd.) were PVP, Triton X-100, DS, SDBS, SDS, BAC, CTAB and CTPB .. Emulsions of paraffins in distilled water and nanoemulsion of PCMs with nanoparticles were prepared with an ultrasound probe (Sonopuls, HD2200, Bandelin) for 3 minutes at medium input energy (50%) and then cooled. The concentrations were set to 5 wt.% for the paraffin, 1:8 weight fraction for surfactant:paraffin and 0.01 wt.% for carbon nanoparticles. These values were also used in previous studies. The size distributions of the samples were analysed by the dynamic light scattering (DLS) technique with a Zetasizer Nano ZS instrument (Malvern Instruments Ltd.). Thermal data as specific heat ( $C_p$ ) and phase change enthalpy ( $\Delta H$ ) were obtained by Differential Scanning Calorimetry analysis (DSC, DSC2 Mettler Toledo). The areas method was used to study  $C_p$  at 25 °C and 60 °C. The optical absorbance of the samples was measured with a Lambda 1050+ UV/Vis/NIR (PerkinElmer) spectrophotometer between 200-1500 nm. As the samples were opaque, the reflectance of the samples was measured using an integrating sphere. The absorbance was calculated as  $A = -\log_{10} \left[ \frac{I_{R\_cuvette}}{I_0} \right]$ , where  $I_R$  and  $I_{R\_cuvette}$  are the intensities reflected by the sample and the sample holder, respectively and  $I_0$  is the incident intensity.

Discussion and Results: The optimization process to obtain the optimum carbon-paraffin/water nanoemulsion was performed in three steps:

Selection of paraffin maximizing thermal energy storage density. The best result was obtained for RT<sub>44</sub>HC, for both theoretical and experimental data, being hence this paraffin selected for the further stages of the research.

Preselection of surfactant maximizing stability. From the initial visual inspection surfactants PVP, Triton, DS and CTPB were eliminated as sedimentations were observed in any of the two processed samples during 3 days after fabrication. From the DSL results SDBS and BAC were also discarded and finally carbon-paraffin/water nanoemulsions were synthesised using SDS and CTAB.

SDS provided better stability results with temperature cycling for both carbon nanoparticles (especially for CBox), so this was the surfactant selected for the following step.

Selection de carbon nanoparticles optimizing spectral absorption. A slight increase in the absorbance of CBox samples can be seen with respect to CB nanoemulsions, and therefore this carbon nanoparticle was chosen.

Conclusion. The combination of water+SDS+RT<sub>44</sub>+CBox was selected as the optimal nanoemulsion with enhanced thermal energy storage density (improvement of 5.63% for water+5% RT<sub>44</sub>), as well as good thermal stability and highest solar radiation absorption capacity, with respect to the nanoemulsion with CB nanoparticles.

Acknowledgments: This research was partially funded by the Generalitat Valenciana through Project PROMETEO/2020/029 and by the Universitat Jaume I through Project UJI-B2020-32.

# Paraffin/water nanoemulsions with reduced supercooling for thermal management systems

Jorge BURGOS<sup>1</sup>, Rosa MONDRAGÓN<sup>1</sup>, Simona BARISON<sup>2</sup>, Filippo AGRESTI<sup>2</sup>, Simone MANCIN<sup>3</sup>,  
Giulia RIGHETTI<sup>3</sup>, Stefano ROSSI<sup>4</sup>, Leonor HERNANDEZ<sup>1,\*</sup>

1: Department of Mechanical Engineering and Construction, Universitat Jaume I, Castellón de la Plana, Spain

2: CNR ICMATE, Padova, Italy

3: Department of Management and Engineering, University of Padova, Vicenza, IT

4: CNR ITC, Padova, Italy

\* Corresponding author: Email: lhernand@uji.es

**Abstract:** Phase change material nanoemulsions were synthesised and characterised to be used as possible storage and heat transfers fluids in low temperature thermal management. Thermal energy storage densities of different paraffin / water nanoemulsions were studied, and RT44HC was selected as the optimized PCM. Seven different nucleating agents, including paraffin waxes with higher melting point, nanoparticles and other organic materials, have been experimentally tested. It was found that 5% paraffin nanoemulsions with 1-octadecanol as nucleating agent (weight fraction 1:10 with respect to PCM), reduced supercooling up to 32 % over samples without nucleating agent, while maintaining the thermal properties of the sample under thermal cycling. Good stability (for both high temperatures and thermal cycling) of the nanoemulsions were observed, while an increase in the viscosity was measured.

**Keywords:** Paraffin/water nanoemulsion, supercooling, thermal management systems

## 1. Introduction

Thermal management systems (TMS) are crucial in the present context of heating and cooling energy demands. TMS with water as working fluid is one of the most commonly used. However, water can only use sensible heat to store thermal energy. Latent heat from phase change materials (PCM) can improve this thermal energy storage density, so different paraffin/water nanoemulsions have been previously studied. Some practical applications of these nanoemulsions could be for electronic cooling or for solar thermal systems. Nevertheless, three important challenges for the applications of these nanoemulsions are high supercooling, poor stability and increased viscosity. The addition of nucleating agents (NA) is the most common approach to reduce supercooling. In this study, different NA have been used when synthesizing paraffin/water nanoemulsions (PCMEs) with 5% of optimized PCM. Stability and viscosity measurements have been performed for the sample with the best supercooling behaviour.

## 2. Materials and synthesis

Three commercial paraffin waxes in the temperature range of water applications, RT35HC, RT44HC and RT54HC (Rubitherm Technologies GmbH) were evaluated as PCMs for the PCME. Sodium dodecyl sulphate (SDS) was used as surfactant, as provided the highest nanoemulsion stability in previous studies [1]. Seven NA were tested to reduce supercooling: RT70HC, palmitic acid, functionalized TiO<sub>2</sub>, myristic acid, 1-octadecanol, 1-hexadecanol and docosanol.

The paraffin and the NA were pre-melted in a temperature controlled oil bath under magnetic stirring, while SDS was dissolved in deionised water and then mixed with the melted paraffin/NA mixture. This mixture was dispersed with the ultrasound probe (Sonics VCX130, Sonics and Material, Inc., operating at 20 kHz and 130 W), firstly at 50% power for 5 minutes in on-off steps of 5 seconds in the oil bath between 50-60 °C, and then the same process was carried out at room temperature at 75% power. To prepare 20 g of sample the

concentrations were set to 5 wt.% for the paraffin, 1:8 weight fraction for SDS:PCM and 1:10 for NA:PCM, except for functionalized TiO<sub>2</sub> nanoparticles, where 0.5:10 was used. These values were also used in previous studies [1].

## 2. Results

The first step was to select the paraffin to be used in the nanoemulsion by maximizing their resulting thermal energy storage density (TESD). TESD was calculated as the addition of sensible heat storage of the emulsion (in a temperature step of 15°C) and the latent heat storage due to the paraffin melting. Theoretical (provided by manufacturer) and experimental (measured in DSC3 Mettler Toledo) datasets were used for these calculations. The best result was obtained for the RT44HC nanoemulsion, for both theoretical and experimental data, with 14.9% and 16.1% of TESD increase with respect to water. Hence this paraffin was selected for the further stages of the research. The supercooling of PCME using different types of NA was evaluated. It was remarkable the 32.4% supercooling improvement when using 1-octadecanol, reducing the initial supercooling of the nanoemulsion from 14.9 to 10.1 °C. Figure 1 shows the DSC heat flow curves for the RT44HC paraffin, and the PCME without and with 1-Octadecanol as NA. The melting point is maintained for both nanoemulsions. However, while supercooling is low for pure paraffin, significantly increases for the nanoemulsion, although an important reduction is observed when using 1-octadecanol as NA.

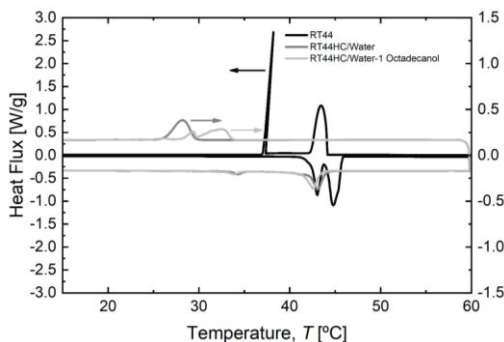


Fig 2. Heat flow curves of different samples.

Once the optimized nanoemulsions were

developed (RT44HC/water-1 octadecanol), their colloidal stability and rheological behaviour was evaluated. High temperature colloidal stability of the sample was measured with DLS (Malvern Zetasizer Nano ZS) at different temperatures: first at 25°C, then at 70°C and then at 25°C again. The resulting Z-average values for each of these temperatures were 189.2 nm, 180.5 nm and 202.1 nm respectively, showing a good stability with only small changes in the size distribution. Thermal cycling stability was evaluated applying ten temperature cycles between 0 and 60 °C in DSC. Negligible changes in crystallization temperature (0.5%) and latent heat (0.6%) of the nanoemulsion were observed. The apparent viscosity of PCME at different temperatures was measured with a rotational rheometer (AR G2, TA Instruments) in the 0-1200 s<sup>-1</sup> shear rate range. Viscosities of 1.31 mPa·s and 0.57 mPa·s were obtained for 25 °C and 70 °C respectively, which represents an increase of about 44% with respect to water.

## 3. Conclusions

The use of 5 wt.% of RT44HC in PCME increased by 16% TESD while the addition of 1-octadecanol as NA reduced its supercooling by 32%. The resulting nanoemulsions showed good results for stability (both high temperature and thermal cycling), however an increase in the viscosity (around 44%) was observed.

## Acknowledgments:

This research was partially funded by projects UJI-B2020-32, PROMETEO/2020/029, PCM Cool Project@CNR and research stay CIBAFP/2021/10.

## References

- [1] Burgos, J., Ayora-Fernández, M., Mondragón, R., Nithiyantham, U., Fabregat-Santiago, F., Hernández, L., 2022 October. Characterization of hybrid carbon-paraffin/water nanoemulsions for DASC: stability, thermal energy storage and optical properties. In 6th Int. Symposium on IMPRES.

### 8.3. Co-authors letters

- Experimental characterization and statistical analysis of water-based gold nanofluids for solar applications: optical properties and photothermal conversion efficiency.
  - Leonor Hernández López (Universitat Jaume I, Castellón de la Plana, Spain).
  - Rosa Mondragón Cazorla (Universitat Jaume I, Castellón de la Plana, Spain).
  - Elif Begum Elcioglu (Eskisehir Technical University, Eskisehir, Turkey).
  - Francisco Fabregat-Santiago (Institute of Advanced Materials, Castellón de la Plana, Spain).
- Photothermal properties and performance of hybrid carbon-paraffin/water emulsions.
  - Leonor Hernández López (Universitat Jaume I, Castellón de la Plana, Spain).
  - Rosa Mondragón Cazorla (Universitat Jaume I, Castellón de la Plana, Spain).
  - Raúl Martínez-Cuenca (Universitat Juame I, Castellón de la Plana, Spain).
  - Udayashankar Nithiyantham (Universitat Juame I, Castellón de la Plana, Spain).
  - Simona Barison (CNR ICMATE, Padova, Italy).
  - Simone Mancin (University of Padova, Vicenza, Italy).
  - Francisco Fabregat-Santiago (Institute of Advanced Materials, Castellón de la Plana, Spain).





Castelló de la Plana, 16<sup>th</sup> October 2023

I, Leonor Hernández López, hereby authorise Jorge Burgos Rodríguez to include the publications listed below in his doctoral thesis. In addition, I waive the right to use those articles as part of any other doctoral thesis.

List of articles:

- J. Burgos, R. Mondragón, E. Begum Elcioglu, F. Fabregat-Santiago and L. Hernández. Experimental characterization and statistical analysis of water-based gold nanofluids for solar applications: optical properties and photothermal conversion efficiency. *Solar RRL*. Vol. 6, no. 7, 2200104, pp.1-10. 2022.  
DOI: 10.1002/solr.202200104
- J. Burgos, R. Mondragón, R. Martínez-Cuenca, U. Nithiyantham, S. Barison, S. Mancin, F. Fabregat-Santiago and L. Hernández. Photothermal properties and performance of hybrid carbon-paraffin/water emulsions. *Journal of Energy Storage*. Vol 73, no. 12, 109136, pp. 1-14. 2023.  
DOI: 10.1016/j.est.2023.109136

Signed,

LEONOR|  
HERNANDEZ|  
LOPEZ

Firmado digitalmente  
por LEONOR|  
HERNANDEZ|LOPEZ  
Fecha: 2023.10.16  
09:41:32 +02'00'

*In accordance with article 28 of the Regulations on doctoral studies of the Universitat Jaume I in Castelló, regulated by RD 99/2011, at the Universitat Jaume I (Approved by the Governing Council at its meeting no. 8/2020 held on 2 October 2020):*

"(...)

*4. In the case of joint publications, all the co-authors must explicitly state their approval that the doctoral student presented the work as part of her/his thesis and the express waiver of presenting this same work as part of another doctoral thesis. This authorisation must be attached as documentation when the evaluation of the thesis begins."*

Castelló de la Plana, 16<sup>th</sup> October 2023

I, Rosa Mondragón Cazorla, hereby authorise Jorge Burgos Rodríguez to include the publications listed below in his doctoral thesis. In addition, I waive the right to use those articles as part of any other doctoral thesis.

List of articles:

- J. Burgos, R. Mondragón, E. Begum Elcioglu, F. Fabregat-Santiago and L. Hernández. Experimental characterization and statistical analysis of water-based gold nanofluids for solar applications: optical properties and photothermal conversion efficiency. *Solar RRL*. Vol. 6, no. 7, 2200104, pp.1-10. 2022.  
DOI: 10.1002/solr.202200104
- J. Burgos, R. Mondragón, R. Martínez-Cuenca, U. Nithiyantham, S. Barison, S. Mancin, F. Fabregat-Santiago and L. Hernández. Photothermal properties and performance of hybrid carbon-paraffin/water emulsions. *Journal of Energy Storage*. Vol 73, no. 12, 109136, pp. 1-14. 2023.  
DOI: 10.1016/j.est.2023.109136

Signed,



Firmado por MONDRAGON  
CAZORLA, ROSA (FIRMA) el  
día 16/10/2023 con un  
certificado emitido por  
AC DNIE 006

*In accordance with article 28 of the Regulations on doctoral studies of the Universitat Jaume I in Castelló, regulated by RD 99/2011, at the Universitat Jaume I (Approved by the Governing Council at its meeting no. 8/2020 held on 2 October 2020):*

*"(...)*

*4. In the case of joint publications, all the co-authors must explicitly state their approval that the doctoral student presented the work as part of her/his thesis and the express waiver of presenting this same work as part of another doctoral thesis. This authorisation must be attached as documentation when the evaluation of the thesis begins."*

Castelló de la Plana, 16<sup>th</sup> October 2023

I, Francisco Fabregat-Santiago, hereby authorise Jorge Burgos Rodríguez to include the publications listed below in his doctoral thesis. In addition, I waive the right to use those articles as part of any other doctoral thesis.

List of articles:

- J. Burgos, R. Mondragón, E. Begum Elcioglu, F. Fabregat-Santiago and L. Hernández. Experimental characterization and statistical analysis of water-based gold nanofluids for solar applications: optical properties and photothermal conversion efficiency. *Solar RRL*. Vol. 6, no. 7, 2200104, pp.1-10. 2022.  
DOI: 10.1002/solr.202200104
- J. Burgos, R. Mondragón, R. Martínez-Cuenca, U. Nithiyantham, S. Barison, S. Mancin, F. Fabregat-Santiago and L. Hernández. Photothermal properties and performance of hybrid carbon-paraffin/water emulsions. *Journal of Energy Storage*. Vol 73, no. 12, 109136, pp. 1-14. 2023.  
DOI: 10.1016/j.est.2023.109136

Signed,

FRANCISCO|  
FABREGAT|SANTIAGO

Firmado digitalmente por FRANCISCO|FABREGAT|  
SANTIAGO  
Nombre de reconocimiento (DN): cn=FRANCISCO|  
FABREGAT|SANTIAGO, serialNumber=XXXXXX96G,  
givenName=FRANCISCO, sn=FABREGAT SANTIAGO,  
ou=CIUDADANOS, o=ACCV, c=ES  
Fecha: 2023.10.16 17:45:21 +02'00'

*In accordance with article 28 of the Regulations on doctoral studies of the Universitat Jaume I in Castelló, regulated by RD 99/2011, at the Universitat Jaume I (Approved by the Governing Council at its meeting no. 8/2020 held on 2 October 2020):*

"(...)

*4. In the case of joint publications, all the co-authors must explicitly state their approval that the doctoral student presented the work as part of her/his thesis and the express waiver of presenting this same work as part of another doctoral thesis. This authorisation must be attached as documentation when the evaluation of the thesis begins."*

Eskisehir/Turkey, 29<sup>th</sup> March 2022

I, Elif Begum Elcioglu, hereby authorise Jorge Burgos Rodríguez to include the publications listed below in his doctoral thesis. In addition, I waive the right to use those articles as part of any other doctoral thesis.

List of articles:

- J. Burgos, R. Mondragón, E. Begum Elcioglu, F. Fabregat-Santiago and L. Hernández. Experimental characterization and statistical analysis of water-based gold nanofluids for solar applications: optical properties and photothermal conversion efficiency. *Solar RRL*. Vol. 6, no. 7, 2200104, pp.1-10. 2022.  
DOI: 10.1002/solr.202200104

Signed,



*In accordance with article 28 of the Regulations on doctoral studies of the Universitat Jaume I in Castelló, regulated by RD 99/2011, at the Universitat Jaume I (Approved by the Governing Council at its meeting no. 8/2020 held on 2 October 2020):*

*"(...)*

*4. In the case of joint publications, all the co-authors must explicitly state their approval that the doctoral student presented the work as part of her/his thesis and the express waiver of presenting this same work as part of another doctoral thesis. This authorisation must be attached as documentation when the evaluation of the thesis begins."*

Castelló de la Plana, 12<sup>th</sup> October 2023

I, Udayashankar Nithiyantham, hereby authorise Jorge Burgos Rodríguez to include the publications listed below in his doctoral thesis. In addition, I waive the right to use those articles as part of any other doctoral thesis.

List of articles:

- J. Burgos, R. Mondragón, R. Martínez-Cuenca, U. Nithiyantham, S. Barison, S. Mancin, F. Fabregat-Santiago and L. Hernández. Photothermal properties and performance of hybrid carbon-paraffin/water emulsions. *Journal of Energy Storage*. Vol 73, no. 12, 109136, pp. 1-14. 2023.

DOI: 10.1016/j.est.2023.109136

Signed, 

*In accordance with article 28 of the Regulations on doctoral studies of the Universitat Jaume I in Castelló, regulated by RD 99/2011, at the Universitat Jaume I (Approved by the Governing Council at its meeting no. 8/2020 held on 2 October 2020):*

*"(...)*

*4. In the case of joint publications, all the co-authors must explicitly state their approval that the doctoral student presented the work as part of her/his thesis and the express waiver of presenting this same work as part of another doctoral thesis. This authorisation must be attached as documentation when the evaluation of the thesis begins."*

Castelló de la Plana, 16<sup>th</sup> October 2023

I, Raúl Martínez-Cuenca, hereby authorise Jorge Burgos Rodríguez to include the publications listed below in his doctoral thesis. In addition, I waive the right to use those articles as part of any other doctoral thesis.

List of articles:

- J. Burgos, R. Mondragón, R. Martínez-Cuenca, U. Nithiyantham, S. Barison, S. Mancin, F. Fabregat-Santiago and L. Hernández. Photothermal properties and performance of hybrid carbon-paraffin/water emulsions. *Journal of Energy Storage*. Vol 73, no. 12, 109136, pp. 1-14. 2023.  
DOI: 10.1016/j.est.2023.109136

Signed,

Firmado digitalmente por  
MARTINEZ CUENCA RAUL -  
XXXXXX33Y  
Fecha: 2023.10.16 08:35:19  
'+02'00



*In accordance with article 28 of the Regulations on doctoral studies of the Universitat Jaume I in Castelló, regulated by RD 99/2011, at the Universitat Jaume I (Approved by the Governing Council at its meeting no. 8/2020 held on 2 October 2020):*

"(...)

*4. In the case of joint publications, all the co-authors must explicitly state their approval that the doctoral student presented the work as part of her/his thesis and the express waiver of presenting this same work as part of another doctoral thesis. This authorisation must be attached as documentation when the evaluation of the thesis begins."*

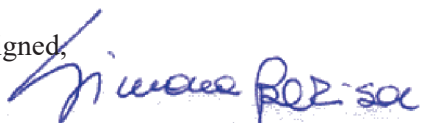
Padova, 12<sup>th</sup> October 2023

I, Simona Barison, hereby authorise Jorge Burgos Rodríguez to include the publications listed below in his doctoral thesis. In addition, I waive the right to use those articles as part of any other doctoral thesis.

List of articles:

- J. Burgos, R. Mondragón, R. Martínez-Cuenca, U. Nithiyantham, S. Barison, S. Mancin, F. Fabregat-Santiago and L. Hernández. Photothermal properties and performance of hybrid carbon-paraffin/water emulsions. *Journal of Energy Storage*. Vol 73, no. 12, 109136, pp. 1-14. 2023.  
DOI: 10.1016/j.est.2023.109136

Signed,



*In accordance with article 28 of the Regulations on doctoral studies of the Universitat Jaume I in Castelló, regulated by RD 99/2011, at the Universitat Jaume I (Approved by the Governing Council at its meeting no. 8/2020 held on 2 October 2020):*

*"(...)*

*4. In the case of joint publications, all the co-authors must explicitly state their approval that the doctoral student presented the work as part of her/his thesis and the express waiver of presenting this same work as part of another doctoral thesis. This authorisation must be attached as documentation when the evaluation of the thesis begins."*

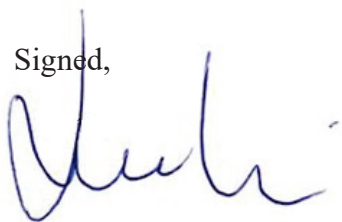
Vicenza, 13<sup>th</sup> October 2023

I, Simone Mancin, hereby authorise Jorge Burgos Rodríguez to include the publications listed below in his doctoral thesis. In addition, I waive the right to use those articles as part of any other doctoral thesis.

List of articles:

- J. Burgos, R. Mondragón, R. Martínez-Cuenca, U. Nithiyantham, S. Barison, S. Mancin, F. Fabregat-Santiago and L. Hernández. Photothermal properties and performance of hybrid carbon-paraffin/water emulsions. *Journal of Energy Storage*. Vol 73, no. 12, 109136, pp. 1-14. 2023.  
DOI: 10.1016/j.est.2023.109136

Signed,



*In accordance with article 28 of the Regulations on doctoral studies of the Universitat Jaume I in Castelló, regulated by RD 99/2011, at the Universitat Jaume I (Approved by the Governing Council at its meeting no. 8/2020 held on 2 October 2020):*

*"(...)*

*4. In the case of joint publications, all the co-authors must explicitly state their approval that the doctoral student presented the work as part of her/his thesis and the express waiver of presenting this same work as part of another doctoral thesis. This authorisation must be attached as documentation when the evaluation of the thesis begins."*